Elucidation of Metal-Carbon Bond Characters in CO_2 Multi-Electron Reduction on Metals

Kiyotsuna Toyohara

Doctor of Philosophy

Department of Structural Molecular Science
School of Mathematical and Physical Science
The Graduate University for Advanced Studies

1995

List of Publications

1) Comparison of Ru-C Bond Characters Involved in Successive Reduction of Ru-CO_2 to Ru-CH_2OH

Kiyotsuna Toyohara, Kiyoshi Tsuge, Koji Tanaka

Organometallics **1995**, *14*, 5099-5103

2) Ruthenium Formyl Complexes as the Branch Point in Two- and Multi-Electron Reduction of CO_2

Kiyotsuna Toyohara, Hirotaka Nagao, Tetsunori Mizukawa, Koji Tanaka

Inorganic Chemistry **1995**, *34*, 5399-5400

3) Crystal Structure of $[Ru(bpy)_2(CO)(\eta^1\text{-}C(O)OH)]^+$ (bpy = 2,2'-bipyridine) as a Key Intermediate in CO_2/CO Conversion

Kiyotsuna Toyohara, Hirotaka Nagao, Tomohiro Adachi, Toshikatsu Yoshida, and Koji Tanaka

Chemistry Letters **1996**, 27-28

Abstract

Carbon dioxide is a potential C1 source for the synthesis of future fuels and chemicals. A variety of metal complexes have proven to be active as precursors to CO and/or HC(O)OH generations in electro- and photochemical reductions of CO_2. From the viewpoint of the utilization of CO_2, however, multi-electron reduction of CO_2 accompanied with C-C bond formation is much more important than the two electron reduction of CO_2. Recently, highly reduced products containing C-C bonds are obtained in a few photo- and electrochemical CO_2 reductions mediated by transition metal complexes in both homogeneous and heterogeneous reactions. Elucidation of the reaction mechanism including M-C bond formation of CO_2 to metals would serve to construct a strategy for the design of catalysts, which effectively catalyze the reduction of CO_2 accompanied with C-C bond formation. In this connection, knowledge concerning the binding modes of CO_2 to metals is a fundamental importance to understand the reactivity of CO_2 ligated to metals. Among a various metal CO_2 complexes reported so far, metal complexes with an η^1-CO_2 ligand are generally accepted as reaction intermediates for CO generation in photo- and electrochemical CO_2 reductions, since metal-η^1-CO_2 complexes ([M-η^1-CO_2]) are subject to protonation in protic media to form metal-hydroxycarbonyls ([M-C(O)OH]) and -carbonyls ([M-CO]) as precursors to $HC(O)O^-$ and CO, respectively. The molecular structures of M-η^1-CO_2 and the conjugated acid M-η^1-C(O)OH, therefore, are of interest in the elucidation of the CO_2/CO conversion on metals because of the lack of the data concerning the structural difference in those two complexes. Furthermore, the elucidation of the role of an M-C(O)H in the reduction of CO_2 is also interested on the basis of the proposal as the key intermediate in the multi-electron reduction of CO_2 accompanying by C-C bond formation.

The purpose of this study is to elucidate the main factor which controls the selectivity of two- and multi-electron reduction of CO_2. This would afford a strategy for designing of effective catalysts directed toward multi-electron reduction of CO_2 accompanied by C-C bond formation.

Interconversion of CO_2 and CO on metals requires an intramolecular 2-electron transfer between metals and CO_2 or CO through the metal-C bond. The two electron transfer from and to metal centered orbitals may cause serious configurational changes of metal complexes, which would strongly hamper the smooth CO_2/CO conversion. Such the structural change of complexes in the metal centerd redox reaction would be effectively depressed by participation of π-orbitals of ligands as well as d-orbitals of metals in the intramolecular electron transfer, and that would accelerate the CO_2/CO conversion. Hydroxycarbonyl complexes (M-η^1-C(O)OH) as the intermediate in the CO_2/CO conversion, therefore, may afford the fundamental knowledge about the intramolecular electron transfer by the comparison of the deprotonated complexes, M-η^1-CO_2. In the Chapter 2, the molecular structure of $[Ru(bpy)_2(CO)(\eta^1\text{-}C(O)OH)]^+$ is determined as the first example of a hydroxycarbonyl intermediate in CO_2 reduction. The comparison in the molecular structures between $[Ru(bpy)_2(CO)(\eta^1\text{-}C(O)OH)]^+$ and $[Ru(bpy)_2(CO)(\eta^1\text{-}CO_2)]$ revealed that not only the Ru-CO_2 but also the Ru-N (trans to CO_2) bond distance is largely influenced by a protonation of $[Ru(bpy)_2(CO)(\eta^1\text{-}CO_2)]$. Thus, σ- donor and π- acceptor abilities of bpy play the role in the electron reservoir to facilitate the smooth interconversion among $[Ru(bpy)_2(CO)(\eta^1\text{-}CO_2)]$, $[Ru(bpy)_2(CO)(\eta^1\text{-}C(O)OH)]^+$ and $[Ru(bpy)_2(CO)_2]^{2+}$ in protic media.

The adjustment of the electron density of the CO_2 moiety in M-η^1-CO_2 complexes would serve the control of the reactivities of the CO_2 intermediate in the reduction of CO_2. In the Chapter 3, stabilization of $[Ru(bpy)_2(CO)(\eta^1\text{-}CO_2)]$ in non protic media is described. In solid state, $[Ru(bpy)_2(CO)(\eta^1\text{-}CO_2)]$ forms three hydrogen bonds between the oxygens of the η^1-CO_2 moiety and three hydrate water molecules. The complex dissociates CO_2 to form $[Ru(bpy)_2(CO)H]^+$ in CH_3CN in the presence of a small amount of H_2O. Furthermore, $[Ru(bpy)_2(CO)(\eta^1\text{-}CO_2)]$ also reacted with O_2 with evolving CO_2 in dry CH_3CN to give $[Ru(bpy)_2(O_2CO)]$ possibly through an O_2 adduct intermediate ($[Ru(bpy)_2(CO)(O_2)]$). On the other hand, $[Ru(bpy)_2(CO)(\eta^1\text{-}CO_2)]$ is quite stable in alcohol even in air. Thus, hydrogen bondings formed between $[Ru(bpy)_2(CO)(\eta^1\text{-}CO_2)]$

and alcohol effectively stabilizes the complex by depression of the accumulation of excess electrons in the η^1-CO_2 moiety. Otherwise [Ru(bpy)$_2$(CO)(η^1-CO_2)] dissociates CO_2, and the resulting [Ru(bpy)$_2$(CO)]^0 undergoes an electrophilic attack of a proton and O_2. Stabilization of [Ru(bpy)$_2$(CO)(η^1-CO_2)] in dry CH_3CN is also achieved by the presence of Li^+. The ^{13}C NMR of an CD_3CN solution of the carbon-13 enriched [Ru(bpy)$_2$(CO)(η^1-CO_2)] in the presence of Li^+ showed a broad and a sharp signal at δ 215 and 203 ppm assignable to CO_2 and CO groups, respectively. Furthermore a low $\nu_{asym}(CO_2)$ band appeared at 1467 cm^{-1} in the solution IR spectra in CD_3CN in the presence of Li^+. The observations that the shift of the $^{13}CO_2$ signal from δ 210 ppm in CH_3OH to δ 215 in CH_3CN and the missing of the $\nu_{asym}(CO_2)$ band in the IR spectra in CD_3CN in the presence of Li^+, are reasonably explained by the formation of a carbene like structure (I) in the medium .

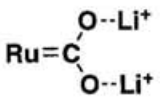

I

Thus, the bond character of a M-η^1-CO_2 complex is controlled by the intermolecular bondings. Hydrogen bonding and association of Li^+ to the oxygen atoms of the η^1-CO_2 group cause inclination of electrons to the CO_2 moiety and stabilize [Ru(bpy)$_2$(CO)(η^1-CO_2)]. Destruction of those intermolecular bondings results in the shift of electrons to metal centers, which gives rise to dissociation of CO_2 to form unstable [Ru(bpy)$_2$(CO)]^0.

In the Chapter 4, reactivities of [Ru(bpy)$_2$(CO)(CHO)]$^+$ and [Ru(bpy)$_2$(CO)(CH_2OH)]$^+$ as models of reaction intermediates in multi-electron reduction of CO_2 are studied. Electrochemical reduction of CO_2 by [Ru(bpy)(trpy)(CO)]$^{2+}$ in EtOH/H_2O produces not only CH_2O and CH_3OH but also HO(O)CCHO and HO(O)CCH_2OH together with HC(O)OH as the main product. Both [Ru(bpy)(trpy)(CHO)]$^+$ and [Ru(bpy)(trpy)(CH_2OH)]$^+$, which are generated by two- and four-electron reduction of [Ru(bpy)(trpy)(CO)]$^{2+}$, are proposed as the precursors to those highly reduced products.

In order to elucidate the role of $[Ru(bpy)(trpy)(CHO)]^+$ in the multi-electron reduction of CO_2, the reactivity of $[Ru(bpy)_2(CO)(CHO)]^+$ instead of $[Ru(bpy)(trpy)(CHO)]^+$ toward CO_2 was examined due to the extremely thermal lability of the latter. In CH_3CN, $[Ru(bpy)_2(CO)(CHO)]^+$ is stable below -20°C. Even such a low temperature, $[Ru(bpy)_2(CO)(CHO)]^+$ smoothly reacted with CO_2 to form $HC(O)O^-$ with generation of $[Ru(bpy)_2(CO)_2]^{2+}$. A strong hydride donor ability of $[Ru(bpy)_2(CO)(CHO)]^+$ well explains the generation of HC(O)OH as the main product in the multi-electron reduction of CO_2 by $[Ru(bpy)(trpy)(CO)]^{2+}$. Taking into account of the formation of $HC(O)O^-$ and $[Ru(bpy)_2(CO)_2]^{2+}$ in the reaction of $[Ru(bpy)_2(CO)(CHO)]^+$ with CO_2, where the reaction pass strongly interferes the multi-electron reduction, a decrease in a hydride ability of a formyl complex would overcome the difficulty in multi-electron reduction of CO_2 by metal complexes. Thus, a metal-formyl complex is the key intermediate as for the two- and multi-electron reductions of CO_2. Furthermore, the observation that protonation and carboxylation of $[Ru(bpy)_2(CO)(CH_2OH)]^+$ as a model of $[Ru(bpy)(trpy)(CH_2OH)]^+$ produced CH_3OH and $HO(O)CCH_2OH$ under electrolysis conditions reasonably elucidates the function of Ru-CH_2OH in the six-electron reduction of CO_2.

The multi-step conversion from Ru-CO_2, Ru-C(O)OH, Ru-CO, Ru-C(O)H to Ru-CH_2OH is inevitably accomplished by variation in the carbon orbital of the Ru-C bonds (sp^2, sp, and sp^3), which would also give crucial influence on the formation energy of HC(O)OH, CO, CH_2O, CH_3OH, and CH_4 in multi-electron reduction of CO_2 by metal complexes. Vibrational spectroscopy may provide useful information about the Ru-C bond characters in the conversion from Ru-CO_2 to Ru-CH_2OH. In the Chapter 5, comparisons of raman spectra of a series of *cis*-$[Ru(bpy)_2(CO)X]^{n+}$ (X = CO, C(O)OH, $C(O)OCH_3$, CO_2, CHO, and CH_2OH; n = 0, 1, 2) and their ^{18}O or deuterium substituted analogs permit reasonable assignments of ν(Ru-X) and ν(Ru-CO) bands around 500 and 470 cm^{-1}, respectively. The validity of the assignments of those bands led to identification of two configurational isomers of *cis*-$[Ru(bpy)_2(CO)(CH_2OH)]^+$ with respect to the orientation of the CH_2-OH bond. The ν(Ru-X) bands shift to higher wavenumbers with lengthening

the Ru-X bond distances (d(Ru-X)). Such unusual dependence of ν(Ru-X) upon d(Ru-X) may be associated with multi-bond characters of the C≡O, C=O, and C-O bonds in the Ru-X moieties.

Contents

Chapter 1

General Introduction

Chemical simulation of the biosynthesis of organic materials from carbon dioxide is highly desired from the viewpoints of not only utilization of carbon dioxide as the starting material for organic compounds but also the origin of the lives on the earth. Recent development of the chemistry of carbon dioxide will lead us to the new area of science for the understanding of the nature. To achieve the recycling of atmospheric CO_2 for fuels and chemicals as an ultimate goal is required the deeper understanding for the catalytic processes, particularly electrocatalysis whereby redox transformations are expected to serve for interfaces between solar and electronic energy input. The purpose of this paper is to present a general concept for the mechanism and design of electrochemically-driven processes for the reduction of carbon dioxide.

1. Outline

We have a serious environmental problem concerning the concentration of CO_2 in the air, so called "Green House Effect". Because of expansion of economic activities and too much deforestation, the increase in the CO_2 concentration is accelerating in recent years, and which may cause serious problem for the earth unless the adequate measures are taken to cope with the situation. Nature stores carbon mainly as organic materials in organisms by photosynthesis and inorganic carbonates in minerals in the sea and rocks. Although disposal of CO_2 exhausted from big power plants and factories into the deep sea has been proposed, utilization of CO_2 directed toward synthesis of fuels and chemicals would be of much more important in near future. [1] So, we have to search for new methodology for the utilization of CO_2 as a possible feedstock. Carbon dioxide has been used for urea synthesis in industrial scale since 1920, [2] for salicylic acid preparations by the Kolbe-Schmitt reaction, [3] and for a number of carboxylation of organic compounds on a small scale. In general, CO_2 as an electrophile is allowed to react with organic fragments activated on catalysts.

On the other hand, activation of CO_2 is required in photo-[4] and electrochemical reduction of CO_2 in aqueous media. Methodologies which enable to produce highly reduced products such as CH_2O, CH_3OH, CH_4, and C2 compounds in the reduction of CO_2 may have good prospects for practical use. A variety of metal complexes have proven to be active in the reduction of CO_2, and some of them have been shown to produce not only CO and HC(O)OH but also higher reduced products. The efficiency of the reduction of CO_2 is also largely influenced by the overpotential or reaction rates, the materials of electrodes, solvents, proton sources and so on. Thus, various problems for the efficient reduction of CO_2 still remain unsolved.

2. General character of carbon dioxide

Carbon dioxide is the ultimate oxidation product of carbon materials and regarded as the extremely thermodynamically stable form. Taking advantage of some reactivities of CO_2, however, it is possible thermodynamically to enable the conversion of CO_2 into more useful organic compounds by chemical processes.

Carbon dioxide is a linear molecule with overall nonpolar nature. The qualitative MO energy level diagram is shown in Figure1-1.[5] The HOMO is non-bonding $n\pi$ orbital on the p orbital of the oxygen atom. The LUMO is π^* orbital which is contributed with the central carbon atom. The level of the lowest unoccupied antibonding orbital (ca. 3.8eV) indicates a high electron affinity, so that the elctrophilicity of the carbon is anticipated as the predominant reactivity. On the other hand, the first ionization potential is high (13.7eV), which indicates low nucleophilicity of terminal oxygens.

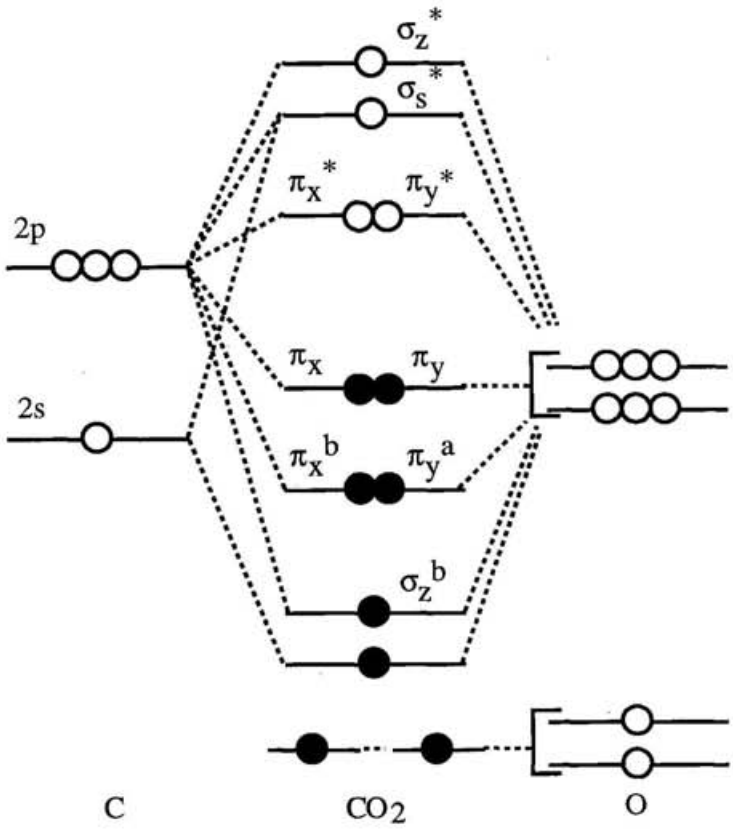

Figure 1-1 MO energy level diagram for the linear triatomic molecule CO_2.

3. Electrochemical potential of carbon dioxide

The standard redox potentials of carbon dioxide is determined as follows:

$CO_2 + e^- \rightarrow CO_2^{\cdot -}$ -2.1V(vs.SCE)

$CO_2^{\cdot -} + e^- \rightarrow CO_2^{2-}$ -1.4V(vs.SCE)

The first reduction causes the structural change from the linear structure of CO_2 to a bent one of $CO_2^{\cdot -}$. The serious configurational change is associated with a very slow self-exchange rate for $CO/CO_2^{\cdot -}$ couple and a significant overpotential in the reduction of CO_2. The bent structure of the mono anion radical (<OCO=135°) substantially stabilizes the π^* orbital but slightly destabilizes the $n\pi$ orbital of CO_2. In Figure 1-2, [6] illustrations of the π, $n\pi$ and π^* orbitals in the linear and a bent geometry show that the bonding-character appears on the π^* orbital in bent geometry. The bent structure of CO_2 on metals beforehand would be effective for the smooth reduction.

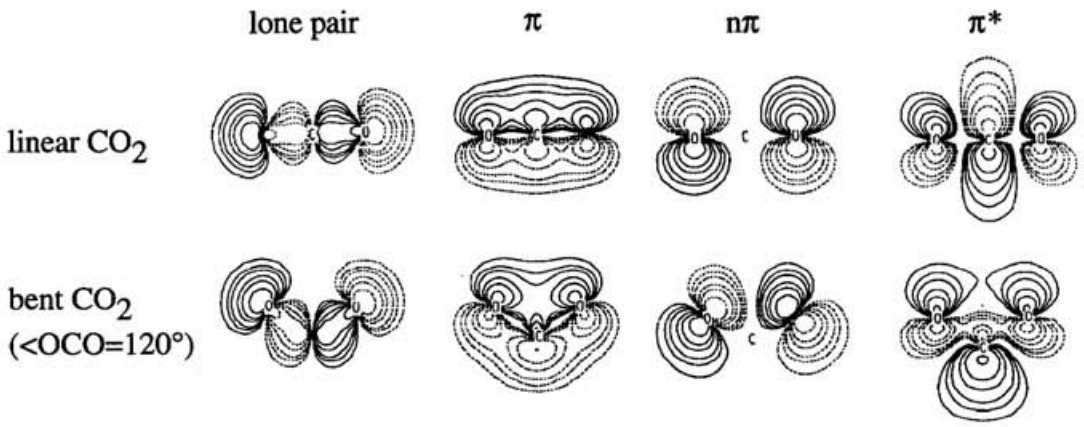

Figure 1-2 The shapes of orbitals in CO_2 molecule

4. Electrochemical reduction of CO_2

Electrochemical reduction of CO_2 on electrodes have been investigated by many researchers. [5-7] In 1914, Fischer et al. reported that the reduction of CO_2 on Zn-amalgam electrode produced HC(O)OH with a current efficiency of 100 %. [8] Electrodes with high hydrogen overvoltages have widely been used for the reduction of CO_2 in aqueous solution to prevent hydrogen evolution. Most of CO_2 reduction on those electrodes gave CO, HC(O)OH and oxalate, except for a Cu electrode on which CO_2 is reduced to CH_4, C_2H_6, and some higher reduced species. [9] Hori et al. summarized the property of metal for electrodes into four types; (1) Cu which mainly generates hydrocarbons. (2) Au, Ag, Zn which generate CO. (3) In, Pb, Sn, Cd which generate HC(O)OH. (4) Pt, Fe, Ni, Mo, Ti which generate H_2 without CO_2 reduction. [10]

Recently much attention has been paid to the photoelectrochemical reduction of CO_2 using semiconductor electrodes. Under light irradiation, semiconductor electrodes effectively convert incident photon energy into electric energy required for the reduction of CO_2 on the electrodes. In 1978, Halmann et al. reported for the first time the CO_2 reduction on a p-type GaP electrode polarized at -1.0 V vs. SCE under illumination of visible light (λ >366 nm) and formate, formaldehyde and methanol were identified as the reduction

products. [11] Similarly, CH_3OH and CH_2O were also obtained in the photoelectrochemical reduction of CO_2 on the metal supported TiO_2 electrode. [12] Reduction of CO_2 by photoinduced polaron on the semiconductor is well studied in recent years. The reaction path to give higher reduced products, however, has not been revealed yet.

Carbon dioxide reduction using homogeneous catalysts has been also extensively investigated by many researchers. Sauvage et al. showed that $Ni(cyclam)^{2+}$ (cyclam = 1,4,8,11-tetraazacyclooctadecane) was an efficient catalyst for the selective CO generation in the reduction of CO_2 in acidic (pH 4) aqueous solution. [13] Rodgers et al. determined the binding constant of CO_2 to $[Ni(cyclam)]^+$ as the intermediate of the reduction. [14] The selective CO formation without H_2 evolution would be associated with the large binding constant ($[Ni(cyclam)(CO_2)]^+ \rightleftharpoons [Ni(cyclam)]^{2+} + CO_2^{\cdot-}$; K = 0.062 M) compared with that (for Co complexes ; $K \cong 1.7 \cdot 10^{-7}$) of other metal complexes. In fact, H_2 evolution becomes the main reaction in the reduction of CO_2 catalyzed by Co complexes in H_2O. In contrast to the reduction of CO_2 on metal electrode, many efforts have been paid to the elucidation of the activation of CO_2 on catalysts in homogeneous reactions. Fujita et al. have demonstrated that CO_2 bound to $[Co(L)]^+$ (L = tetraazamacrocycle) with an η^1(C)-CO_2 mode to Co, and a hydrogen bond between NH on the ligand and oxygen of CO_2 stabilizes the 1:1 adduct. [15] The Co-η^1-CO_2 complex is protonated in an acidic condition (pKa = 3.1), but the conversion to the Co-CO derivative has not been elucidated so far. Both electrochemical and photochemical CO_2 reductions are effectively mediated by $[Ru(bpy)_2(CO)X]^{n+}$ (n = 1, 2 ; X = CO, H, CH_3CN, Cl) under homogeneous conditions. [16] The Ru complex has two functional sites for catalytic reaction; π acceptable ligands play a role in an electron reservoir and the metal center has an ability to bind CO_2. Tanaka et al. found the reversible conversion from CO_2 to CO due to the equilibria among $u(bpy)_2(CO)(CO_2)]$, $[Ru(bpy)_2(CO)(C(O)OH)]^+$ and $[Ru(bpy)_2(CO)_2]^{2+}$ in aqueous media . [17]

$$[Ru(bpy)_2(CO)_2]^{2+} \underset{H^+}{\overset{OH^-}{\rightleftharpoons}} [Ru(bpy)_2(CO)(C(O)OH)]^{+} \underset{H^+}{\overset{OH^-}{\rightleftharpoons}} [Ru(bpy)_2(CO)(CO_2)]$$

colorless yellow red

The equilibrium constants are 1.32×10^5 $mol^{-1}dm^3$ and 2.27×10^4 for K_1 and K_2, respectively. Thus, $[Ru(bpy)_2(CO)_2]^{2+}$ becomes as the main species in an acidic condition (pH 6). As a result, CO was mainly produced in contrast to the favorable generation of HC(O)OH in a basic condition (pH 9). On the other hand, Meyer et al. proposed another mechanism for HC(O)OH formation through $[Ru(bpy)_2(CO)(H)]^0$ in organic media containing small amount of water. [16c] Thus there is still a controversy concerning the mechanism for the HC(O)OH formation in electro- and photochemical CO_2 reductions.

5. Why is multi-electron reduction of CO_2?

Energy consumption for CO_2 reduction is one of the most important factor for utilization of CO_2 as a C1 resource. The standard free energy and redox potentials of 2-, 4, 6-, and 8-electron reduction of CO_2 are shown below; [5]

	E^0 (V vs NHE)
$2CO_2 + 2H^+ + 2e^- \rightarrow H_2C_2O_4$	-0.475
$CO_2 + 2H^+ + 2e^- \rightarrow HC(O)OH$	-0.199
$CO_2 + 2H^+ + 2e^- \rightarrow CO(g) + H_2O$	-0103
$CO_2 + 4H^+ + 4e^- \rightarrow CH_2O(aq) + H_2O$	-0.071
$CO_2 + 6H^+ + 6e^- \rightarrow CH_3OH(aq) + H_2O$	+0.030
$CO_2 + 8H^+ + 8e^- \rightarrow CH_4(g) + 2H_2O$	+0.169

This clearly shows that multi-electron reductions are thermodynamically more favorable processes than two electron reduction ones. Although the difficulty in the multi-electron reduction of CO_2 was ascribed to the transfer of multiple electrons to the reduction site, the electrochemical reduction of CO_2 by $[Ru(trpy)(bpy)(CO)]^{2+}$ has been shown to afford

CH_2O, CH_3OH and C2 products such as glyoxylic acid and glycolic acid together with HC(O)OH. [18] Taking into account the difficulty in the elucidation of the reaction mechanism for the formation of methanol on semiconductors, the discovery of the multiple electron reduction of CO_2 in homogeneous reactions would greatly serve for the understanding the reaction mechanism.

6. Summary

This paper is consisted of four chapters, mainly describing about the mechanisms of two- and multi-electron reduction of CO_2. The chapter 2 shows the structure of a hydroxycarbonyl complex (Ru-C(O)OH) as the first structural characterization of an intermediate in the reduction of CO_2, and revealed the driving force for the smooth interconversion between the Ru-CO_2 and Ru-C(O)OH moieties. The chapter 3 describes the stability of a Ru-η^1-CO_2 intermediate and the reactivity depending on media. A multi-bond character between Ru and CO_2 is substantially influenced by the existence of an additional Lewis acid. The stabilization of the M-CO_2 intermediate is discussed based on spectral investigations. The chapter 4 describes the chemical property of the formyl intermediate, which plays not only an intermediate of the multielectron reduction of CO_2 but also a strong hydride donor to CO_2 affording HC(O)OH. In addition to these reactions, a disproportionation reaction of the formyl complex gives a hydroxymethyl complex, the latter of which smoothly reacts with CO_2 to form glycolic acid under electrolysis conditions. Thus these intermediates are the key compounds for C-C bond formation in CO_2 reduction. The chapter 5 describes the evaluation of the Ru-C bond character in the series of $[Ru(bpy)_2(CO)X]^{n+}$ (X = CO_2, C(O)OH, CO, CHO CH_2OH; n = 0, 1, 2) in Raman spectra. The assignment of the ν(Ru-C) based on the isotope shifts clearly revealed that the shifts of the bands were closely related with the multi-bond character and configuration of the carbon orbitals.

Chapter 2

Crystal Structure and Reactivity of $[Ru(bpy)_2(CO)(\eta^1\text{-}C(O)OH)]^+$ (bpy = 2,2' bipyridine) as a Key Intermediate in CO_2/CO Conversion

Introduction

Metal hydroxycarbonyls (M-C(O)OH) have been proposed as key intermediates in not only Water-Gas-Shift-Reaction (WGSR) but also electro- and photochemical CO_2 reduction catalyzed by metal complexes. A few complexes with η^1-,η^2-,μ^2-, and μ^3- C(O)OH have been characterized so far, and the reactivities of the M-C(O)OH group are classified into three types; dissociation of H^+, OH^-, and CO_2 affording M-CO_2, M-CO, and M-H complexes. [5] The selectivity of those reactions would be controlled by the degree of charge transfer interaction from d-orbitals of the metals to the π^* orbital of the hydroxycarbonyls. It has been reported that $[Ru(bpy)_2(CO)(\eta^1\text{-}C(O)OH)]^+$ (**1**) exists as an equilibrium mixture with its dehydroxy species $[Ru(bpy)_2(CO)_2]^{2+}$ (**3**) and deprotonated species $[Ru(bpy)_2(CO)(\eta^1\text{-}CO_2)]$ (**2**) with equilibrium constants, K_1 and K_2 , of 1.32×10^5 and 2.27×10^4 mol^{-1} dm^3, respectively, in an aqueous solution. [17] The diffusion controlled conversion from **2** to **1** in aqueous solutions has the fundamental importance in electro- and photochemical CO_2 reductions. On the basis of preferential formation of CO and HC(O)OH in high and low concentrations of proton, respectively, in the reduction of CO_2, our research group proposed that **2** and **1** resulting from **3** are the precursors to CO and HC(O)OH generations. As for HC(O)OH generation in the electrochemical reduction of CO_2 in the presence of $[Ru(bpy)_2(CO)(NCCH_3)]^{2+}$, Meyer et al. reported another path through $[Ru(bpy)_2(CO)(OC(O)H)]^+$ formed by CO_2 insertion of the Ru-H bond of $[Ru(bpy)_2(CO)(H)]^+$ (**4**). [16c] Furthermore, **4** is produced by protonation of $[Ru(bpy)_2(CO)(NCCH_3)]^0$ and decarboxylation of **1**. The controversy concerning the precursor to HC(O)OH in the reduction of CO_2, therefore, may result from the uncertainty of the formation path of **4** and of the reactivity of **1** under the electrolysis conditions. To

clarify the role of **1** in the reduction of CO_2, the author has focused on the chemical and physical properties of **1**.

Despite much attention to hydroxycarbonyl complexes as the key intermediates of the reductive CO_2 conversion to HC(O)OH/CO, there has been only one report concerning the molecular structure. Bennett et al. reported a crystal structure of $[Pt(C_6H_5)(PEt_3)_2(\eta^1\text{-}C(O)OH)]$, which, however, does not dissociate the proton even in the presence of tertiary amines in organic solvents. [19] The lack of the crystal data on hydroxycarbonyl complexes may be associated with a tendency of a disproportionation reaction ($2(M\text{-}C(O)OH) \rightleftharpoons M\text{-}CO + M\text{-}CO_2 + H_2O$). Such a disproportionation reaction of $[Ru(bpy)_2(CO)(\eta^1\text{-}C(O)OH)]^+$ in solutions was successfully depressed by choosing a counter ion and single crystals of $[Ru(bpy)_2(CO)(\eta^1\text{-}C(O)OH)]^+$ were obtained. The comparison of the molecular structures of $[Ru(bpy)_2(CO)(\eta^1\text{-}C(O)OH)]^+$ and $[Ru(bpy)_2(CO)(\eta^1\text{-}CO_2)]$ [20] would give fundamental information with respect to the smooth conversion between C(O)OH and CO_2.

Experiments

1. Preparation of $[Ru(bpy)_2(CO)(\eta^1\text{-}C(O)OH)](CF_3SO_3)\cdot H_2O$ (**1**).

Hydroxycarbonyls are synthesized by the following eq. 1

$$[M\text{-}CO] + OH^- \longrightarrow [M\text{-}C(O)OH]^- \qquad (1)$$

In this study, powder of basic alumina as hydroxide source was applied for the synthesis of $[Ru(bpy)_2(CO)(\eta^1\text{-}C(O)OH)](CF_3SO_3)\cdot H_2O$. Pure product could be given in a good yield without contamination of excess hydroxide. $[Ru(bpy)_2(CO)_2](CF_3SO_3)_2$ dissolved into acetonitrile was adsorbed on the top of basic alumina, and then developed with benzene/acetonitrile (50/50 vol. %). The color of the top part of the column changed into yellow as the reaction of $[Ru(bpy)_2(CO)_2]^{2+}$ with basic alumina proceeded. The yellow portion eluted by acetonitrile/ethanol/water (50/45/5 vol. %) was evaporated under reduced pressure. The resulting orange solid was recrystalized from acetonitrile/water (70/30 vol.%). Anal. Found: C, 42.28; H, 2.96; N, 8.63. Calcd for $C_{23}H_{18}N_4O_6F_3SRu\cdot H_2O$: C,

42.27; H, 2.93; N, 8.57. IR (KBr): ν(OH) 3416 and 3073 cm^{-1}, ν(C≡O) 1952.2 cm^{-1}, ν(C=O) 1583.7 cm^{-1}.

2. X-ray crystallography of **1**

All measurements were made on a Rigaku AFC5R diffractometer with graphite monochromated Mo-Kα radiation. All calculations were carried out with TEXSAN. Hydrogen atoms were placed in idealized positions and included in the structure factor calculation. The final cycle of full-matrix least-squares refinement was based on 3861 observed reflections ($I > 3.00\sigma(I)$) and 352 variable parameters and converged with R = 0.058, Rw = 0.042. Crystal data for **1**: $C_{23}H_{19}O_7N_4F_3SRu$, triclinic, $\overline{P}_1$, a = 11.988(3) Å, b = 13.424(2) Å, c = 8.700(1) Å, α = 96.90(1)°, β = 110.43(1)°, γ = 72.02(2)°, V = 1247.9(5) $Å^3$, Z = 2, crystal size 0.20 × 0.20 × 0.10 mm. 7599 reflections ($6° < \theta < 60°$), 7275 independent ($Rini$ = 0.061). (Structural parameters are summarized in Table S1a - S5a.)

3. Cyclic voltammogram of **1**

The cyclic voltammograms of **1** (1.0 $mmoldm^{-3}$) were measured in CH_3CN containing n-Bu_4NBF_4 as a supporting electrolyte after N_2 was bubbled for 10 minutes or CO_2 for 30 seconds.

4. Controlled potential electrolysis of **1**

(1) Under CO_2

Controlled potential electrolysis of **1** (15.8 mg, 25 μmol) in CO_2 saturated CH_3CN (5 ml) containing 0.05 M tetramethylammonium tetrafluoroborate as a supporting electrolyte was carried out by using a glassy carbon electrode at -1.4 V ~ -1.5V (vs. Ag/AgCl). After 5.5 C (2 electron for **1**) passed in the electrolysis, 2.5 μmol of CO was evolved without H_2 and HC(O)OH formations.

(2) Under N_2

The electrolysis of **1** (32 mg, 50 μmol) in dry acetonitrile (10 ml) containing 0.05 M tetramethylammonium tetrafluoroborate as a supporting electrolyte under N_2 atmosphere was carried out at -1.4 V~-1.5V (vs. Ag/AgCl) electrode on a glassy carbon electrode. After 11C (2 electron for **1**) passed, neither CO, HC(O)OH nor H_2 was detected in the electrolysis cell. The electrolyte solution was allowed to stand in air, and then evaporated under vacuo. The residue was washed with dichloromethane (15 ml). An addition of ether (30 ml) into the yellow solution resulted in a yellow precipitate (16 mg).

Result

1. Structure of $[Ru(bpy)_2(CO)(\eta^1\text{-}C(O)OH)](CF_3SO_3)(H_2O)$

The molecular structure of $[Ru(bpy)_2(CO)(\eta^1\text{-}C(O)OH)](CF_3SO_3)(H_2O)$ (**1**) together with selected bond angles and distances is shown in Figure 2-1. The C=O, C-O bond distances (1.242 and 1.345 Å, respectively) and the O-C-O angle (114°) of **1** are close to those of *trans*-$[Pt(\eta^1\text{-}C(O)OH)(C_6H_5)(PEt_3)_2]$, which exists as a dimeric form through two hydrogen bonds between the hydroxycarbonyl moieties. On the other hand, the hydroxycarbonyl of **1** binds to hydrated water (O1-O5: 2.822(8) Å) which is also connected to triflate (O5-O4: 2.769(8) Å) with another hydrogen bond (Figure 2-2). Furthermore, the hydrate water molecule is located in the neighborhood of the carbonyl oxygen of the hydroxycarbonyl group in another molecule of **1** (O5-O2': 3.040(8) Å), suggesting a weak interaction between them. As a result, two molecules of **1** are related to an inversion center in a triclinic unit cell through a weak hydrogen bond. On the basis of Nakamoto's diagram of hydrogen bond lengths vs. ν(OH) bands, [21] two strong bands observed at 3416 and 3073 cm^{-1} in the IR spectrum of **1** in KBr disk are reasonably assigned to the ν(OH) bands of the strong hydroxycarbonyl-water (2.82 Å) and water-triflate (2.77 Å) hydrogen bonds, respectively, while no ν(OH) band assignable to the weak hydrogen bond with the atomic distance of 3.04 Å appeared in the spectrum.

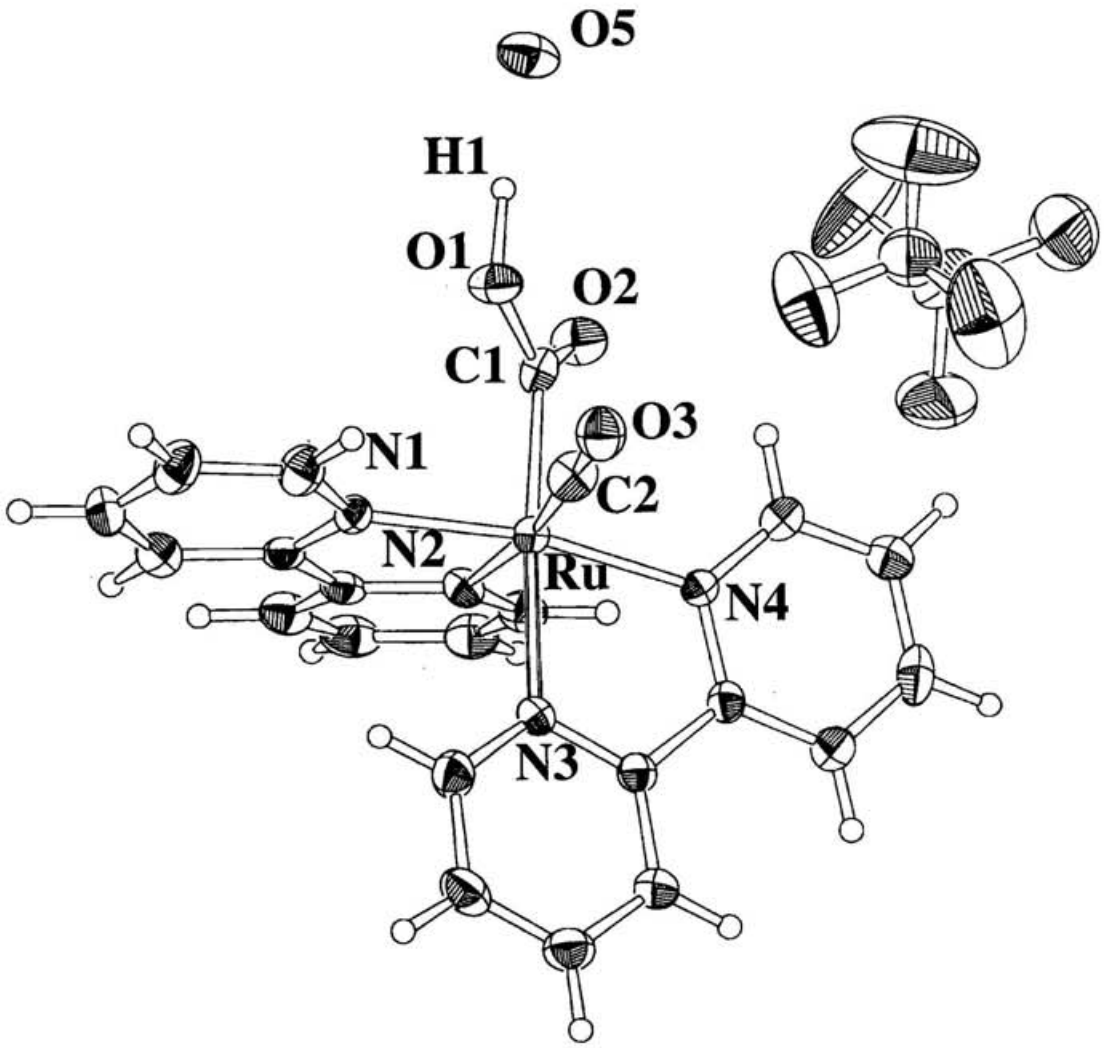

Figure 2-1 Molecular structure of $[Ru(bpy)_2(CO)(C(O)OH)](CF_3SO_3)\cdot H_2O$ (**1**).

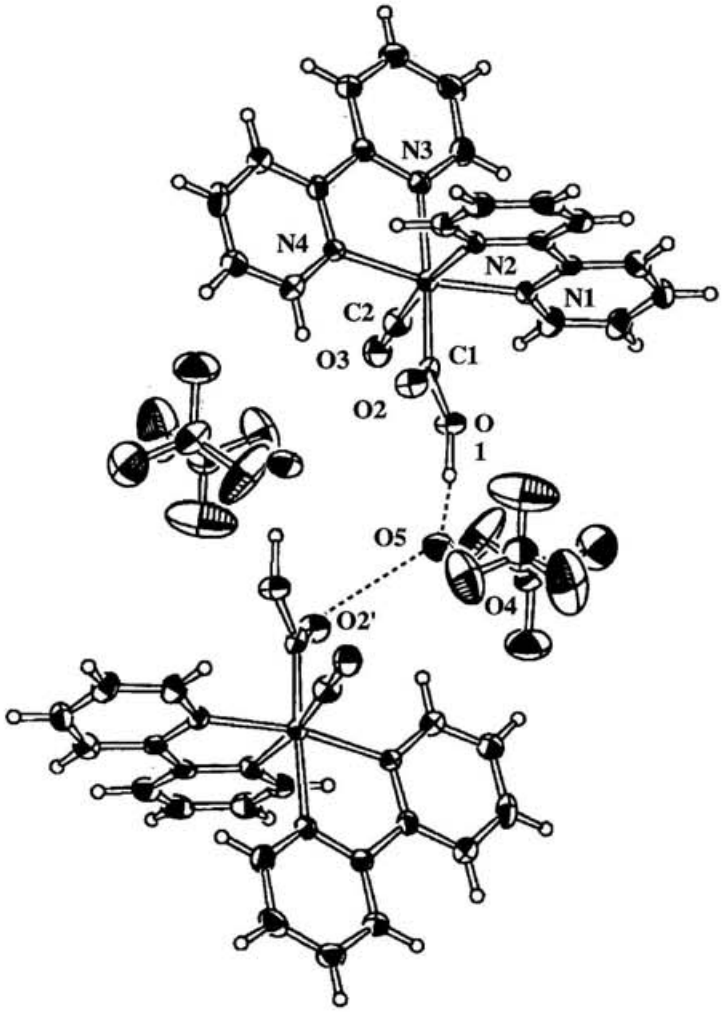

Figure 2-2 Hydrogen bonds in the crystal structure of **1**.

Table S1a. Crystal parameters and expermental data for X-ray diffraction measured on $[Ru(bpy)_2(CO)(C(O)OH)](CF_3SO_3)\cdot H_2O$

Empirical Formula	$C_{23}H_{19}O_7N_4F_3SRu$
Formula Weight	653.55
Crystal Color, Habit	brown, prismatic
Crystal Dimensions	0.20 X 0.20 X 0.10 mm
Crystal System	triclinic
Lattice Parameters	a = 11.988(3) Å b = 13.424(2) Å c = 8.700(1) Å α = 96.90(1) β = 110.43(1) γ = 72.02(2) V = 1247.9(5) Å^3
Space Group	P $\bar{1}$ (#2)
Z value	2
Dcalc	1.739 g/cm^3
F000	656.00
μ(MoKα)	7.87 cm^{-1}
Diffractometer	Rigaku AFC5R
Radiation	MoKα (λ = 0.71069 Å) graphite monochromated
Temperature	23.0°C
Scan Type	ω-2θ
Scan Rate	8.0°/min (in ω) -- up to 2 scans
Scan Width	(1.21 + 0.50 tan θ)°
2θmax	60.0°
No. of Reflections Measured	Total: 7599 Unique: 7275 (Rint = 0.061)
Corrections	Lorentz-polarization Absorption (DIFABS [a]) (trans. factors: 0.9399 - 1.0484) Decay (0.21% increase)
Structure Solution	Direct Methods (SAPI91 [b])
Refinement	Full-matrix least-squares
Least Squares Weights	1/σ^2(Fo)
Anomalous Dispersion	All non-hydrogen atoms
No. Observations (I > 3.00 σ(I))	3861
No. Variables	352
Residuals: R; Rw	0.058 ; 0.042
Goodness of Fit Indicator	2.35
Max Shift/Error in Final Cycle	0.01
Maximum peak in Final Diff. Map	0.76 e-/Å^3
Minimum peak in Final Diff. Map	-0.83 e-/Å^3

a DIFABS: Walker, N. & Stuart, Acta Cryst. A39, 158-166 (1983).An empirical absorption correction program.

b Fan Hai-Fu (1991). Structure Analysis Programs with Intelligent Control, Rigaku Corporation,Tokyo, Japan.

Table S2a. Atomic coordinates and B_{iso}/B_{eq}

atom	x	y	z	Beq
Ru	0.17451(6)	0.24001(5)	-0.19635(7)	2.52(1)
S	-0.3316(3)	0.2794(2)	-0.2639(3)	6.09(7)
F(1)	-0.4035(7)	0.3768(5)	-0.0324(9)	14.8(3)
F(2)	-0.4468(6)	0.4672(5)	-0.2317(10)	14.9(3)
F(3)	-0.2673(5)	0.4265(5)	-0.0728(8)	10.9(2)
O(1)	0.1488(4)	0.0403(4)	-0.1368(5)	4.5(1)
O(2)	0.1511(4)	0.1483(3)	0.0720(5)	4.1(1)
O(3)	-0.0049(4)	0.3907(4)	-0.0575(6)	4.6(1)
O(4)	-0.2894(6)	0.3092(6)	-0.3787(7)	10.8(2)
O(7)	-0.4483(7)	0.2559(5)	-0.3343(8)	10.2(2)
O(6)	-0.2451(7)	0.2056(5)	-0.1452(7)	12.8(2)
O(5)	0.1053(4)	-0.0089(4)	0.2094(6)	5.3(1)
N(1)	0.3304(5)	0.2448(4)	-0.0028(6)	2.7(1)
N(2)	0.3157(5)	0.1238(4)	-0.2612(6)	2.7(1)
N(3)	0.1893(5)	0.3496(4)	-0.3436(6)	2.9(1)
N(4)	0.0430(5)	0.2296(4)	-0.4215(6)	2.8(1)
C(1)	0.1553(6)	0.1288(5)	-0.0815(8)	3.1(2)
C(2)	0.0666(6)	0.3331(5)	-0.1134(8)	3.4(2)
C(3)	0.4386(6)	0.1879(5)	-0.0157(7)	2.8(2)
C(4)	0.5515(6)	0.1918(6)	0.1003(8)	3.9(2)
C(5)	0.5522(7)	0.2549(6)	0.2366(9)	4.6(2)
C(6)	0.4409(7)	0.3128(6)	0.2552(8)	4.4(2)
C(7)	0.3313(7)	0.3056(5)	0.1313(8)	4.0(2)
C(8)	0.4324(6)	0.1154(5)	-0.1536(8)	3.0(2)
C(9)	0.5332(6)	0.0389(5)	-0.1742(8)	3.8(2)
C(10)	0.5168(7)	-0.0321(6)	-0.3021(9)	4.6(2)
C(11)	0.3992(7)	-0.0235(5)	-0.4110(8)	4.0(2)
C(12)	0.3021(6)	0.0567(5)	-0.3842(8)	3.5(2)
C(13)	0.1157(6)	0.3535(5)	-0.5021(7)	2.8(1)
C(14)	0.1095(6)	0.4240(5)	-0.6116(8)	3.8(2)
C(15)	0.1825(7)	0.4916(6)	-0.5587(9)	4.4(2)
C(16)	0.2587(7)	0.4875(6)	-0.3983(9)	4.5(2)
C(17)	0.2591(6)	0.4151(5)	-0.2953(8)	3.9(2)
C(18)	0.0388(6)	0.2817(5)	-0.5457(7)	2.9(2)

Table S2a. Atomic coordinates and B_{iso}/B_{eq}

atom	x	y	z	B_{eq}
C(19)	-0.0355(6)	0.2698(5)	-0.7064(8)	3.8(2)
C(20)	-0.1068(6)	0.2002(6)	-0.7375(8)	4.6(2)
C(21)	-0.1055(6)	0.1496(6)	-0.6107(9)	4.0(2)
C(22)	-0.0305(6)	0.1673(6)	-0.4553(8)	3.9(2)
C(23)	-0.3625(9)	0.3898(7)	-0.143(1)	6.4(3)
H(1)	0.1371	0.0837	0.1355	4.9131
H(2)	0.6275	0.1511	0.0853	4.5968
H(3)	0.6285	0.2586	0.3170	5.5123
H(4)	0.4384	0.3564	0.3491	5.2297
H(5)	0.2541	0.3456	0.1429	4.7770
H(6)	0.6143	0.0349	-0.1001	4.3781
H(7)	0.5859	-0.0863	-0.3151	5.4088
H(8)	0.3850	-0.0708	-0.5013	4.6811
H(9)	0.2207	0.0634	-0.4595	4.1274
H(10)	0.0555	0.4258	-0.7219	4.5277
H(11)	0.1800	0.5400	-0.6319	5.1258
H(12)	0.3100	0.5329	-0.3581	5.2004
H(13)	0.3122	0.4124	-0.1844	4.5130
H(14)	-0.0377	0.3082	-0.7928	4.4881
H(15)	-0.1558	0.1884	-0.8466	5.6516
H(16)	-0.1549	0.1032	-0.6286	4.6668
H(17)	-0.0313	0.1330	-0.3666	4.7000

$$B_{eq} = \frac{8}{3}\pi^2 (U_{11}(aa^*)^2 + U_{22}(bb^*)^2 + U_{33}(cc^*)^2 + 2U_{12}aa^* bb^* \cos\gamma + 2U_{13}aa^* cc^* \cos\beta + 2U_{23}bb^* cc^* \cos\alpha$$

Table S3a. Anisotropic displacement parameters

atom	U_{11}	U_{22}	U_{33}	U_{12}	U_{13}	U_{23}
Ru	0.0314(3)	0.0340(3)	0.0308(2)	-0.0106(2)	0.0088(2)	0.0008(2)
S	0.097(2)	0.070(2)	0.052(1)	-0.011(2)	0.019(1)	0.002(1)
F(1)	0.315(8)	0.136(6)	0.225(7)	-0.100(6)	0.208(6)	-0.055(5)
F(2)	0.109(6)	0.087(5)	0.313(10)	-0.001(4)	-0.004(6)	0.060(6)
F(3)	0.096(5)	0.143(5)	0.177(6)	-0.060(4)	0.042(4)	-0.058(4)
O(1)	0.076(4)	0.046(3)	0.058(3)	-0.021(3)	0.028(3)	-0.006(3)
O(2)	0.070(3)	0.053(3)	0.045(3)	-0.024(3)	0.028(3)	-0.001(2)
O(3)	0.054(3)	0.056(4)	0.062(3)	-0.013(3)	0.016(3)	0.001(3)
O(4)	0.161(6)	0.217(8)	0.080(4)	-0.091(6)	0.069(4)	-0.015(5)
O(7)	0.149(6)	0.125(6)	0.124(6)	-0.090(5)	0.011(5)	-0.004(5)
O(6)	0.216(8)	0.078(5)	0.079(5)	0.065(5)	-0.005(5)	0.016(4)
O(5)	0.074(4)	0.056(3)	0.085(4)	-0.018(3)	0.040(3)	0.013(3)
N(1)	0.035(3)	0.038(3)	0.030(3)	-0.011(3)	0.010(2)	0.000(2)
N(2)	0.037(3)	0.034(3)	0.037(3)	-0.013(3)	0.019(3)	-0.007(2)
N(3)	0.037(3)	0.040(3)	0.038(3)	-0.018(3)	0.010(3)	0.000(3)
N(4)	0.036(3)	0.045(4)	0.028(3)	-0.016(3)	0.009(2)	0.002(2)
C(1)	0.038(4)	0.037(4)	0.034(4)	-0.005(4)	0.005(3)	0.000(3)
C(2)	0.047(5)	0.033(4)	0.043(4)	0.005(4)	0.025(3)	-0.010(3)
C(3)	0.045(4)	0.038(4)	0.032(3)	-0.019(3)	0.013(3)	0.004(3)
C(4)	0.044(5)	0.055(5)	0.052(4)	-0.018(4)	0.016(4)	0.002(4)
C(5)	0.042(5)	0.076(6)	0.058(5)	-0.028(4)	0.001(4)	0.015(4)
C(6)	0.065(5)	0.055(5)	0.040(4)	-0.023(4)	0.006(4)	-0.006(4)
C(7)	0.055(5)	0.049(5)	0.043(4)	-0.015(4)	0.010(4)	-0.005(4)
C(8)	0.039(4)	0.035(4)	0.047(4)	-0.009(3)	0.021(3)	0.011(3)
C(9)	0.049(5)	0.042(5)	0.059(5)	-0.008(4)	0.026(4)	0.006(4)
C(10)	0.055(5)	0.050(5)	0.076(5)	0.004(4)	0.042(4)	0.018(4)
C(11)	0.065(5)	0.045(5)	0.048(4)	-0.016(4)	0.029(4)	-0.006(4)
C(12)	0.053(5)	0.041(4)	0.045(4)	-0.018(4)	0.022(4)	-0.004(3)
C(13)	0.030(4)	0.035(4)	0.040(4)	-0.003(3)	0.014(3)	0.004(3)
C(14)	0.046(4)	0.056(5)	0.049(4)	-0.020(4)	0.012(3)	0.013(4)
C(15)	0.054(5)	0.057(5)	0.060(5)	-0.011(4)	0.022(4)	0.019(4)
C(16)	0.052(5)	0.051(5)	0.078(5)	-0.023(4)	0.023(4)	0.006(4)
C(17)	0.044(5)	0.047(5)	0.053(4)	-0.014(4)	0.006(4)	0.009(4)
C(18)	0.031(4)	0.040(4)	0.035(4)	-0.008(3)	0.010(3)	-0.003(3)

Table S3a. Anisotropic displacement parameters (continued)

atom	U_{11}	U_{22}	U_{33}	U_{12}	U_{13}	U_{23}
C(19)	0.045(5)	0.058(5)	0.040(4)	-0.015(4)	0.012(3)	0.004(4)
C(20)	0.039(5)	0.074(6)	0.048(5)	-0.016(4)	-0.001(4)	-0.011(4)
C(21)	0.049(5)	0.053(5)	0.055(5)	-0.018(4)	0.017(4)	0.005(4)
C(22)	0.050(5)	0.061(5)	0.037(4)	-0.018(4)	0.008(3)	0.007(4)
C(23)	0.088(8)	0.066(7)	0.093(7)	-0.029(6)	0.021(6)	0.014(6)

The general temperature factor expression:

$$\exp\{-2\pi^2 (a^* 2U_{11}h^2 + b^* U_{22}k^2 + c^* U_{33}l^2 + 2a^* b^* U_{12}hk + 2a^* c^* U_{13}hl + 2b^* c^* U_{23}kl)\}$$

Table S4a. Bond lengths(Å)

atom	atom	distance	atom	atom	distance
Ru	N(1)	2.046(5)	Ru	N(2)	2.108(5)
Ru	N(3)	2.147(5)	Ru	N(4)	2.063(5)
Ru	C(1)	2.003(7)	Ru	C(2)	1.787(7)
S	O(4)	1.410(6)	S	O(7)	1.435(6)
S	O(6)	1.409(6)	S	C(23)	1.732(10)
F(1)	C(23)	1.27(1)	F(2)	C(23)	1.303(9)
F(3)	C(23)	1.306(9)	O(1)	C(1)	1.242(7)
O(2)	C(1)	1.345(7)	O(3)	C(2)	1.167(7)
N(1)	C(3)	1.322(7)	N(1)	C(7)	1.339(7)
N(2)	C(8)	1.364(7)	N(2)	C(12)	1.312(7)
N(3)	C(13)	1.350(7)	N(3)	C(17)	1.330(7)
N(4)	C(18)	1.334(7)	N(4)	C(22)	1.333(8)
C(3)	C(4)	1.390(8)	C(3)	C(8)	1.446(8)
C(4)	C(5)	1.372(9)	C(5)	C(6)	1.375(10)
C(6)	C(7)	1.401(8)	C(8)	C(9)	1.375(8)
C(9)	C(10)	1.375(9)	C(10)	C(11)	1.376(9)
C(11)	C(12)	1.387(9)	C(13)	C(14)	1.390(8)
C(13)	C(18)	1.464(8)	C(14)	C(15)	1.382(9)
C(15)	C(16)	1.372(9)	C(16)	C(17)	1.398(9)
C(18)	C(19)	1.392(8)	C(19)	C(20)	1.395(9)
C(20)	C(21)	1.357(9)	C(21)	C(22)	1.378(8)
O(2)	H(1)	1.16	C(4)	H(2)	0.95
C(5)	H(3)	0.95	C(6)	H(4)	0.95
C(7)	H(5)	0.95	C(9)	H(6)	0.95
C(10)	H(7)	0.95	C(11)	H(8)	0.95
C(12)	H(9)	0.95	C(14)	H(10)	0.95
C(15)	H(11)	0.95	C(16)	H(12)	0.95
C(17)	H(13)	0.95	C(19)	H(14)	0.95
C(20)	H(15)	0.95	C(21)	H(16)	0.95
C(22)	H(17)	0.95			

Table S5a. Bond angles(°)

atom	atom	atom	angle	atom	atom	atom	angle
N(1)	Ru	N(2)	77.4(2)	N(1)	Ru	N(3)	95.7(2)
N(1)	Ru	N(4)	167.4(2)	N(1)	Ru	C(1)	89.1(2)
N(1)	Ru	C(2)	96.2(3)	N(2)	Ru	N(3)	89.2(2)
N(2)	Ru	N(4)	92.5(2)	N(2)	Ru	C(1)	87.9(2)
N(2)	Ru	C(2)	172.2(3)	N(3)	Ru	N(4)	76.4(2)
N(3)	Ru	C(1)	173.8(2)	N(3)	Ru	C(2)	95.9(3)
N(4)	Ru	C(1)	98.2(2)	N(4)	Ru	C(2)	94.4(3)
C(1)	Ru	C(2)	87.6(3)	O(4)	S	O(7)	114.3(4)
O(4)	S	O(6)	117.5(5)	O(4)	S	C(23)	105.4(5)
O(7)	S	O(6)	111.8(5)	O(7)	S	C(23)	104.3(5)
O(6)	S	C(23)	101.4(4)	Ru	N(1)	C(3)	117.2(4)
Ru	N(1)	C(7)	124.9(5)	C(3)	N(1)	C(7)	117.8(5)
Ru	N(2)	C(8)	114.1(4)	Ru	N(2)	C(12)	127.4(4)
C(8)	N(2)	C(12)	118.4(6)	Ru	N(3)	C(13)	115.2(4)
Ru	N(3)	C(17)	127.5(4)	C(13)	N(3)	C(17)	117.3(5)
Ru	N(4)	C(18)	117.6(4)	Ru	N(4)	C(22)	124.6(4)
C(18)	N(4)	C(22)	117.5(5)	Ru	C(1)	O(1)	126.4(5)
Ru	C(1)	O(2)	118.7(5)	O(1)	C(1)	O(2)	114.9(6)
Ru	C(2)	O(3)	177.4(7)	N(1)	C(3)	C(4)	122.7(6)
N(1)	C(3)	C(8)	115.6(6)	C(4)	C(3)	C(8)	121.5(6)
C(3)	C(4)	C(5)	119.3(7)	C(4)	C(5)	C(6)	119.1(7)
C(5)	C(6)	C(7)	117.9(7)	N(1)	C(7)	C(6)	123.1(7)
N(2)	C(8)	C(3)	114.9(6)	N(2)	C(8)	C(9)	120.7(6)
C(3)	C(8)	C(9)	124.2(6)	C(8)	C(9)	C(10)	120.1(7)
C(9)	C(10)	C(11)	119.2(7)	C(10)	C(11)	C(12)	117.6(6)
N(2)	C(12)	C(11)	124.0(6)	N(3)	C(13)	C(14)	122.3(6)
N(3)	C(13)	C(18)	114.4(5)	C(14)	C(13)	C(18)	123.2(6)
C(13)	C(14)	C(15)	119.4(6)	C(14)	C(15)	C(16)	118.7(6)
C(15)	C(16)	C(17)	118.5(6)	N(3)	C(17)	C(16)	123.7(6)
N(4)	C(18)	C(13)	115.8(5)	N(4)	C(18)	C(19)	122.2(6)
C(13)	C(18)	C(19)	122.0(6)	C(18)	C(19)	C(20)	118.4(6)
C(19)	C(20)	C(21)	119.4(6)	C(20)	C(21)	C(22)	118.1(7)
N(4)	C(22)	C(21)	124.2(6)	S	C(23)	F(1)	113.7(7)

Table S5a. Bond angles(°) (continued)

S	C(23)	F(2)	110.7(7)	S	C(23)	F(3)	113.5(8)
F(1)	C(23)	F(2)	106.1(10)	F(1)	C(23)	F(3)	108.3(9)
F(2)	C(23)	F(3)	103.9(8)				

Table S5a. Bond angles(°) (continued)

atom	atom	atom	angle	atom	atom	atom	angle
C(1)	O(2)	H(1)	117.7	C(3)	C(4)	H(2)	120.4
C(5)	C(4)	H(2)	120.4	C(4)	C(5)	H(3)	120.4
C(6)	C(5)	H(3)	120.4	C(5)	C(6)	H(4)	121.0
C(7)	C(6)	H(4)	121.1	N(1)	C(7)	H(5)	118.5
C(6)	C(7)	H(5)	118.5	C(8)	C(9)	H(6)	120.0
C(10)	C(9)	H(6)	119.9	C(9)	C(10)	H(7)	120.4
C(11)	C(10)	H(7)	120.4	C(10)	C(11)	H(8)	121.2
C(12)	C(11)	H(8)	121.2	N(2)	C(12)	H(9)	118.0
C(11)	C(12)	H(9)	118.0	C(13)	C(14)	H(10)	120.3
C(15)	C(14)	H(10)	120.3	C(14)	C(15)	H(11)	120.6
C(16)	C(15)	H(11)	120.6	C(15)	C(16)	H(12)	120.7
C(17)	C(16)	H(12)	120.8	N(3)	C(17)	H(13)	118.2
C(16)	C(17)	H(13)	118.1	C(18)	C(19)	H(14)	120.8
C(20)	C(19)	H(14)	120.8	C(19)	C(20)	H(15)	120.3
C(21)	C(20)	H(15)	120.3	C(20)	C(21)	H(16)	120.9
C(22)	C(21)	H(16)	120.9	N(4)	C(22)	H(17)	117.9
C(21)	C(22)	H(17)	117.9				

2. Cyclic voltammogram of **1**

The cyclic voltammogram of **1** under N_2 shows two reversible redox couples at -1.38 V and -1.56 V in E_c vs. Ag/AgCl and an irreversible anodic peak at 1.12 V. After CO_2 was bubbled into the solution for 30 seconds, a catalytic cathodic current was observed at potentials more negative than -1.65V (Figure 2-3).

3. Controlled potential electrolysis of $[Ru(bpy)_2(CO)(\eta^1\text{-}C(O)OH)]^+$

The decomposition pathway of $[Ru(bpy)_2(CO)(\eta^1\text{-}C(O)OH)]^+$ under an electrochemical condition would lead to elucidation of the catalytic cycle for the CO_2 reduction. The controlled potential electrolysis of an acetonitrile solution of $[Ru(bpy)_2(CO)(\eta^1\text{-}C(O)OH)]^+$ in the presence of Me_4NBF_4 at -1.4 V~ -1.5 V (vs. Ag/AgCl) under CO_2 atmosphere resulted in CO evolution with a current efficiency of 10% without accompanying by HC(O)OH and oxalate generations and blue powder precipitated. Air oxidation of the solution caused dissolution of the blue solid and then the solution gradually changed to yellow in color. The blue precipitate, therefore, may be polymeric $[Ru(bpy)(CO)_2]_n$, which was proposed as the active species for CO evolution in the electrochemical reduction of CO_2 in the presence of $[Ru(bpy)(CO)_2Cl_2]$. [22] On the other hand, the same electrolysis of $[Ru(bpy)_2(CO)(\eta^1\text{-}C(O)OH)]^+$ in the absence of CO_2 produced $[Ru(bpy)_2(CO)(H)]^+$ in a 58 % yield based on the bpy protons in the ^{1}H-NMR, and neither CO nor HC(O)OH was detected in the electrolysis.

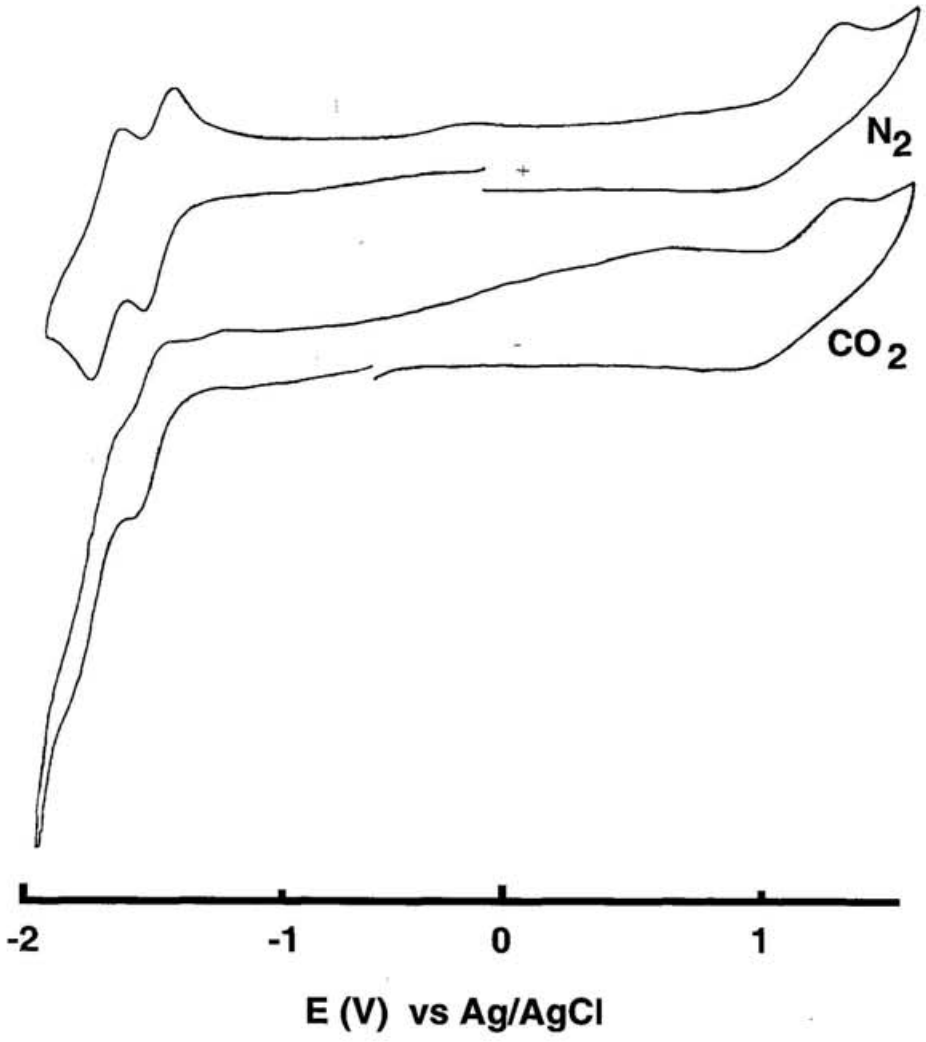

Figure 2-3 Cyclic voltammogram of **1** in 0.1M n-Bu4NBF4/acetonitrile.

Discussion

1. Crystallization of $[Ru(bpy)_2(CO)(\eta^1\text{-}C(O)OH)]^+$

This work provides the molecular structure of a metallacarboxylic acid which is formed via protonation of a metal-η^1-CO_2 adduct. The difficulty in crystallization of metallacarboxylic acids is associated with their amphoteric properties, which are likely to form stable hydrogen bonds between two metallacarboxylic acids. Such a dimer structure would also assist the disproportionation reaction in solution. A monomeric structure of $[Ru(bpy)_2(CO)(\eta^1\text{-}C(O)OH)]^+$ in the solid state is ascribed to the existence of a hydrate water molecule connecting two C(O)OH moieties.

The platinum complex, *trans*-$[Pt(C_6H_5)(PEt_3)_2(\eta^1\text{-}C(O)OH)]$ does not dissociate proton even in the presence of tertiary amines. This is quite contrast to $[Ru(bpy)_2(CO)(\eta^1\text{-}C(O)OH)]^+$, which reversibly dissociate the proton at pK_a 9.5 in H_2O (25°C). Such a distinct difference in the acidity of both complexes would result from the electron density on the carboxylic group depending on an electron donating ability of ligands.

2. Structure of metallacarboxylic acids

The coordination sphere of reaction intermediates is very interested in the viewpoint of the bond formation of substrates to the reaction center. The Ru-N bond distances of **1** are largely influenced by the π-acceptor and σ-donor characters of the CO and C(O)OH moieties. The Ru-N1 and Ru-N4 bond distances of 2.046 and 2.062 Å (trans to bpy) are significantly shorter than the Ru-N2 and Ru-N3 distances of 2.109 and 2.146 Å (trans to CO and C(O)OH) (Figure 2-2). On the basis of the fact that the average of the Ru-N bond length of 2.054 Å (trans to bpy) of **1** is same as that of $[Ru(bpy)_2Cl_2]$ (2.054 Å), [23] the distinct lengthening of the Ru-N bond trans to the CO and C(O)OH moieties of **1** suggests a low π-acceptor ability of bpy compared with those of CO and C(O)OH ligands. The difference between the Ru-N2 and Ru-N3 bond distances of 2.109 and 2.146 Å of **1** (trans to CO and C(O)OH), respectively, on the other hand, would be ascribed to a strong σ-donor ability of the C(O)OH moiety compared with the neutral CO ligand.

3. Structural comparison among CO_2, C(O)OH and CO complexes

The structures of $[Ru(bpy)_2(CO)(\eta^1\text{-}CO_2)]$, $[Ru(bpy)_2(CO)_2]^{2+}$, and $[Ru(bpy)_2(CO)(C(O)OCH_3)]^+$ as the structural model of hydroxycarbonyl compound, have been reported. The comparison of the molecular structures of $[Ru(bpy)_2(CO)(\eta^1\text{-}C(O)OH)]^+$, $[Ru(bpy)_2(CO)_2]^{2+}$, and $[Ru(bpy)_2(CO)(\eta^1\text{-}CO_2)]$ is particularly interested in the viewpoint of the smooth interconversion among those complexes. The most notable feature in the comparison of the molecular structure of $[Ru(bpy)_2(CO)(\eta^1\text{-}C(O)OH)]^+$ with that of the deprotonated species, $[Ru(bpy)_2(CO)(\eta^1\text{-}CO_2)]$ (2), is that not only the Ru-C(O)OH but also the Ru-N bond distances (trans to C(O)OH) of **1** (2.003 and 2.146 Å, respectively) are much shorter than the Ru-CO_2 and Ru-N ones (trans to CO_2) of **2** (2.064 and 2.204 Å, respectively) (Figure 2-4). The shortening of the Ru-C(O)OH bond of **1** compared with the Ru-CO_2 one of **2** is explained by an increase in a π- acceptor ability of the C(O)OH moiety. This tendency of the bonds shortening is observed in the comparison with $[Ru(bpy)_2(CO)_2]^{2+}$ (Ru-CO; 1.786 Å, Ru-N(trans CO); 2.109 Å). The decrease in the electron density on Ru of **1**, therefore, may be compensated by σ- donor ability of bpy. Thus, a protonation to Ru-CO_2 causes an intramolecular electron transfer from the bpy to the C(O)OH moiety through Ru. This view revealed that the diffusion controlled interconversion between **1** and **2** in H_2O is largely assisted by synergetic σ- donor and π-acceptor characters of bpy.

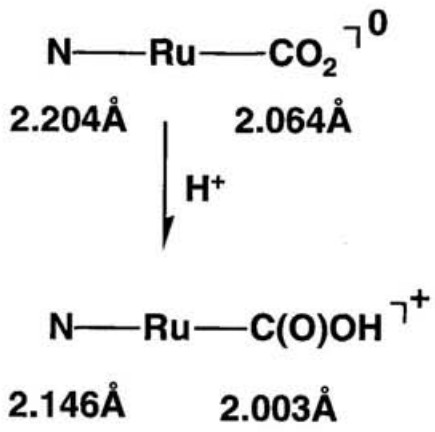

Figure 2-4. Contraction of the Ru-C(O)OH and Ru-bpy (trans to C(O)OH) bonds in **1** by a protonation of **2**.

4. Electrochemical property of **1**

The electrochemical property of **1** is very similar to that of the analogs with an anionic ligand, $[Ru(bpy)_2(CO)(X)]^+$ (X = H, Cl, CH_2OH), in Table 2-1. The LUMO in the series of complexes would be π^*-orbitals on the bpy ligands. A ligand centered reduction does not cause a serious change in the electronic configuration of d-orbitals of metals. On the other hand, a metal centered reduction is likely to dissociate a Ru-X bond due to an accumulation of too much electrons on metals.

Table 2-1 Potentials ($E_{1/2}$ vs. Ag/AgCl) of $[Ru(bpy)_2(CO)X]^+$ (X = Cl, C(O)OH, $C(O)OCH_3$, H, CH_2OH, CHO) in acetonitrile containing 0.1M n-Bu_4NBF_4

X	C(O)OH	$C(O)OCH_3$	Cl	H	CH_2OH	CHO
E_1 1/2 (V)	1.35	1.35	1.26	1.40	1.41	1.38
E_2 1/2 (V)	1.54	1.56	1.45	1.61	1.60	1.57

The cyclic voltammogram of **1** showed a catalytic carrent at potentials more negative than the onset cathodic wave of the $[Ru(bpy)_2(CO)(\eta^1\text{-}C(O)OH)]^{0/-}$ couple (-1.55 V) under CO_2 atmosphere. The controlled potential electrolysis of **1** at -1.50 V in CO_2-saturated CH_3CN produced CO as the main product. On the other hand, the same electrolysis in the absence of CO_2 resulted in evolution of CO_2 moiety with generation of $[Ru(bpy)_2(CO)(H)]^+$. Taking into account that $[Ru(bpy)_2(CO)_2]^0$ is the precursor to CO evolution, $[Ru(bpy)_2(CO)_2]^0$ and $[Ru(bpy)_2(CO)(H)]^+$ would be produced in the two electron reduction of $[Ru(bpy)_2(CO)(\eta^1\text{-}C(O)OH)]^+$ in the presence and absence of CO_2, respectively. The assistance of CO_2 in the conversion from $[Ru(bpy)_2(CO)(\eta^1\text{-}C(O)OH)]^-$ to $[Ru(bpy)_2(CO)_2]^0$ suggests that the dissociation of OH^- from the former in CH_3CN is much slower than the generation of $HOCO_2^-$ by the reaction with CO_2. Thus, CO_2 plays the role of the "oxygen sink" in the transformation from hydroxycarbonyl to carbonyl group in CH_3CN. On the other hand, in the absence of CO_2 and proton, the η^1-C(O)OH group in $[Ru(bpy)_2(CO)(\eta^1\text{-}C(O)OH)]^-$ undergoes the β-elimination reaction, which effectively reduces the electron density on Ru, and the resulting $[Ru(bpy)_2(CO)(H)]^-$ functions as precursors to HC(O)OH and H_2 generation (Scheme 2-1).

Scheme 2-1 Schematic illustration of the reactivity of $[Ru(bpy)_2(CO)(C(O)OH)]^+$ in electrolysis

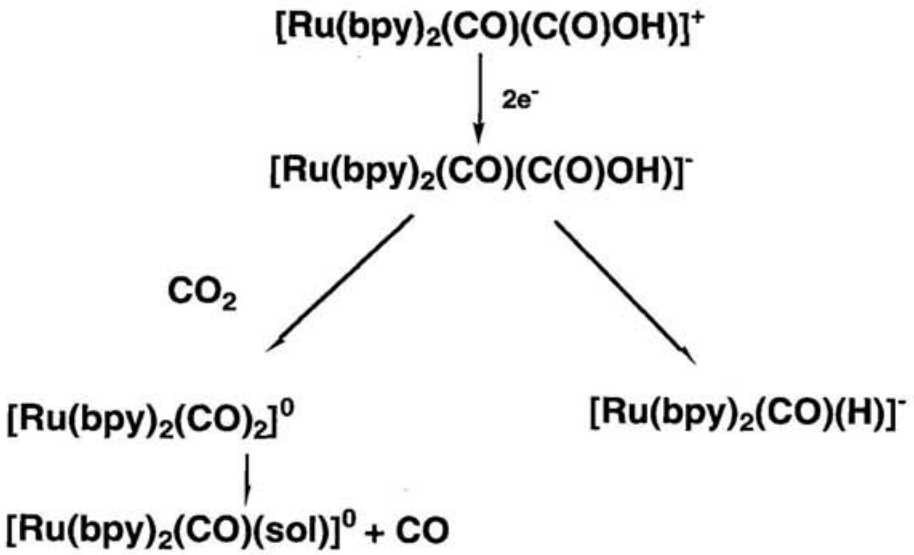

Conclusion

Hydroxycarbonyl metal complexes function as the key roles in both CO_2 reduction and Water Gas Shift Reaction. The amphoteric reactivity and the vast range of pK_a values for hydroxycarbonyl complexes (from 2.5 to over 14) compared with those for organic carboxylic acids are scarcely understood due to the lack of the crystal structure of a metal-η^1-C(O)OH complex. Although the molecular structure of $[Pt(C_6H_5)(PEt_3)_2(^1\eta\text{-}C(O)OH)]$ has been reported, the complex has no proton donor ability even in the presence of tertiary amines. On the other hand, a diffusion controlled interconversion between $[Ru(bpy)_2(CO)(\eta^1\text{-}C(O)OH)]^+$ (**1**) (pK_a 9.5) and $[Ru(bpy)_2(CO)(\eta^1\text{-}CO_2)]$ (**2**) is the key process in electro- and photochemical CO_2 reductions in H_2O. The fact that the crystal structure of **1** (pK_a 9.5) and the comparison of the structure with that of **2** shows that the protonation of **2** shortens the Ru-C(O)OH bond distance compared with the Ru-CO_2 one, and synergetic σ-donor and π-acceptor abilities of both CO and bpy ligands also assist the enhancement of $d\pi$-$p\pi^*$ interaction upon the protonation of **2**.

Chapter 3

The Direct Evidence of Metallocarbene-like Structure of [Ru(bpy)$_2$(CO)(η^1-CO$_2$)] as the Intermediate in Carbon Dioxide Reduction in Organic Solvents

Introduction

The activation of CO_2 on metal complexes is initiated by the coordination of CO_2 to metals. There are three potential binding modes for the coordination of CO_2 to monomeric metal centers such as η^2(C,O)-, η^1(C)- and η^1(O)-modes. Metal complexes with an η^2(C,O)- and an η^1(C)-CO_2 group have been prepared and structurally characterized, [5, 20, 24] but evidence for the formation of metal complexes with an η^1(O)-CO_2 ligand is not provided so far. Metal complexes with η^2(C,O)-CO_2 are generally more stable than η^1(C)-CO_2 complexes. On the other hand, the η^1(C)-CO_2 coordination mode is much more suitable than the η^2(C,O)- one for the reductive conversion of CO_2 to CO on metals. Electro- and photochemical CO_2 reductions catalyzed by [Ru(bpy)$_2$(CO)(η^1-CO$_2$)] produces CO and/or HC(O)OH through a hydroxycarbonyl complex (Scheme 3-1). The relative formation ratio of CO/HC(O)OH in the CO_2 reductions largely depends on the pH in aqueous media and solvents. In acidic aqueous solutions, CO is the main product, while $HC(O)O^-$ is predominantly produced in alkaline solutions. In contrast to this, Meyer et al. have

Scheme 3-1 A proposed mechanism of CO_2 conversion on the Ru complex

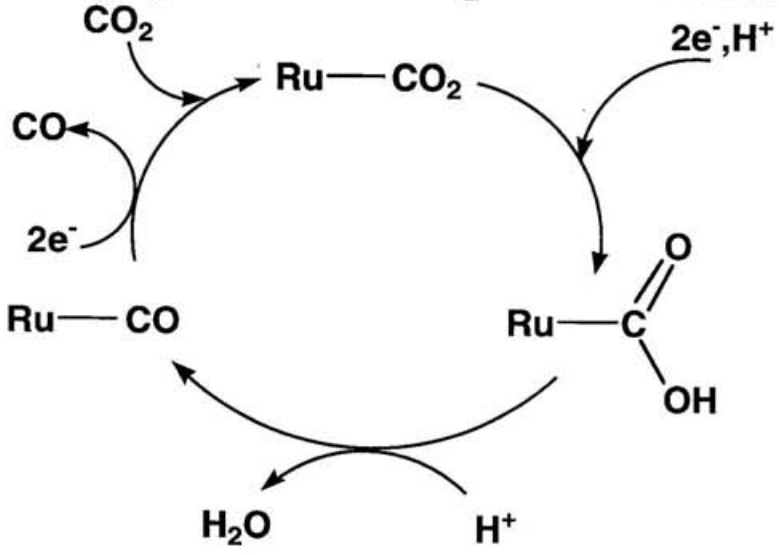

reported that $HC(O)O^-$ formation through $[Ru(bpy)_2(CO)(H)]^+$ in the electrochemical reduction of CO_2 catalyzed by $[Ru(bpy)_2(CO)(Cl)]^+$ in the presence of very small amount of water in acetonitrile. [16c] The variation in the reaction path in the CO_2 reduction may be also explained by the reactivity of CO_2 metal complexes as an intermediate depending on the reaction media. Taking into the account that $[Ru(bpy)_2(CO)(CO_2)]$ is the most reasonable reaction intermediate in the CO_2 reduction catalyzed by $[Ru(bpy)_2(CO)X]^{n+}$ (n = 1, 2; X = H, Cl, CO etc.), the elucidation of the reactivity of the η^1(C)-CO_2 complex in various media would give the fundamental knowledge about the reaction mechanism. The X-ray structure analysis of $[Ru(bpy)_2(CO)(\eta^1(C)\text{-}CO_2)]\cdot 3H_2O$ reveals three dimensional hydrogen bonding networks formed among oxygens of the η^1-CO_2 moiety and H_2O molecules. Fujita et al. have shown the existence of intramolecular hydrogen bondings between the oxygen of CO_2 and the hydrogen of NH in L of $[Co(L)(CO_2)]$ (L= tetraazamacrocycle) in solution. [15] In contrast to this, $[Ru(bpy)_2(CO)(\eta^1\text{-}CO_2)]\cdot 3H_2O$ easily decomposes in organic media unless the complex forms stable hydrogen bondings with the media. Thus, an accumulation of electrons on the η^1(C)-CO_2 group due to a π-back donation from Ru is effectively depressed by the intermolecular hydrogen bonds. The color of a $[Ru(bpy)_2(CO)(CO_2)]$ solution is also seriously influenced by the existence of hydrogen bonds between the η^1(C)-CO_2 group and the solvent molecules; in non-protic solvents such as acetonitrile and DMSO the complex is blue, while it turns to red in protic solvents such as alcohol and H_2O. On the basis of the fact that $[Ru(bpy)_2(CO)(CO_2)]$ decomposes to $[Ru(bpy)_2(CO_3)]$ in CH_3CN and DMSO under air, the path may reveal the reactivity of an electron rich η^1-CO_2 group in non-protic media. Furthermore, the lability of $[Ru(bpy)_2(CO)(CO_2)]$ in non-protic media resulting from the destruction of the hydrogen bonds is overcome by an addition of Li^+ to the solution. In this Chapter, the stabilization of $[Ru(bpy)_2(CO)(CO_2)]$ assisted by Li^+ in aprotic media and the decomposition pathway in organic solvents are discussed.

Experiments

1. Preparation of ^{13}C labeled $[Ru(bpy)_2(CO)_2](PF_6)_2$

$[Ru(bpy)_2(^{13}CO)(^{12}CO)](PF_6)_2$ was prepared from $[Ru(bpy)_2(H_2O)(^{13}CO)](PF_6)_2$.

a. Preparation of $[Ru(bpy)_2(H_2O)(^{13}CO)](PF_6)_2$

A red solution of 2 g of $[Ru(bpy)_2(H_2O)_2](PF_6)_2$ in 20 ml of methoxyethanol in a sealed 50 ml-round-bottom schlenk was stirred at atmospheric pressure of ^{13}CO for 24 hours. The resulted pale yellow solution was reduced to half under vacuo. An addition of aqueous PF_6^- solution gave a yellow precipitate of $[Ru(bpy)_2(H_2O)(^{13}CO)](PF_6)_2$ (IR;. 1931 cm^{-1} ($\nu^{13}CO$))

b. Preparation of $[Ru(bpy)_2(^{13}CO)(^{12}CO)](PF_6)_2$

A suspension of $[Ru(bpy)_2(H_2O)(^{13}CO)](PF_6)_2$ in H_2O was vigorously stirred in an autoclave at 140°C at 20 kg/cm^3 pressure of ^{12}CO for 12 hours. Addition of an aqueous PF_6^- to the resulted colorless solution gave a white precipitate of $[Ru(bpy)_2(^{13}CO)(^{12}CO)](PF_6)_2$. (IR; 2077, 2008 cm^{-1} ($\nu^{13}CO$), ^{13}C-NMR; 190.4 ppm (CO in CD_3CN)).

2. Preparation of $[Ru(bpy)_2(^{13}CO_3)]$

Crystals of ^{13}C labeled $[Ru(bpy)_2(CO)(CO_2)]$ was suspended to dry acetonitrile under the air at 75°C for 15 minutes. This suspension turned to a blue solution, then blue ^{13}C labeled $[Ru(bpy)_2(CO_3)]$ was gradually precipitated (^{13}C-NMR; 168 ppm (CO_3 in d_6-DMSO)).

3. Preparation of $[Ru(bpy)_2(CO)(CO_2)]$ (**2**)

$[Ru(bpy)_2(CO)(CO_2)]$ (**2**) was tried to prepare in two kinds of solvents; acetonitrile and dimethyl sulfoxide.

a. In acetonitrile

A suspension of $[Ru(bpy)_2(CO)(C(O)OH)](PF_6)$ (**1**) (60 mg) in dry acetonitrile (2 ml) was treated with equimolar amount of Bu_4NOH/CH_3OH at room temperature. The

resulted red solution was stood for 1 day in refrigerator, red prismatic crystal appeared (IR; 1911 cm^{-1} ($\nu^{12}CO$), 1869 cm^{-1} ($\nu^{13}CO$)).

b. In DMSO

To a solution of **1** in d^6-DMSO in an NMR-tube, the same amount of Bu_4NOH/CH_3OH was added. The yellow solution turned to blue. ^1H- and ^{13}C-NMR spectra were measured in situ.

4. Treatment of **2** with acetonitrile

a. Under N_2

2 (0.1 mg) is added to d^3-acetonitrile in an NMR tube at ambient temperature under N_2. A pale yellow solution was obtained by heating at 70°C with sonication and gave a characteristic signal of $[Ru(bpy)_2(CO)(H)]^+$ (**4**) in the ^1H-NMR spectrum (δ -11.8 ppm ; 0.8H).

b. Under atmosphere

^{13}C labeled **2** (0.1 mg) was added to d^3-acetonitrile in an NMR tube at ambient temperature under air. After the blue solution was heated at 70°C with sonication, a blue precipitate gradually appeared as the solution was getting cool. The blue precipitate thus obtained gave characteristic signals of $[Ru(bpy)_2(CO_3)]$ in the ^{13}C-NMR spectrum (δ 168 ppm) and IR spectrum (νC=O; 1587 cm^{-1}).

c. Under $^{18}O_2$

2 was added to nitrogen bubbled acetonitrile (5 ml) in a 10 ml-glass tube at room temperature. $^{18}O_2$ (5 ml) was bubbled to the tube, then the solution was stirred at 70°C for 1 hour. The orange crystals of the complex were dissolved into the blue solution, and then a blue precipitate was appeared. A FAB mass measurement was carried out for the precipitate.

5. Treatment of **2** with acetonitrile containing Li^+

2 (1 mg) was treated with a portion of 0.5 ml of acetonitrile containing $LiCF_3SO_3$ (3.2 mg). In contrast to the low solubility of **2** to pure acetonitrile, **2** was really soluble to the Li^+ containing acetonitrile. The yellow solution was allowed to stand at room temperature for a few hours. IR spectrum, ^1H- and ^{13}C-NMR spectra were recorded in situ.

Results

1. Synthesis of $[Ru(bpy)_2(CO)(CO_2)]$ (**2**) in organic solvents

Compared with the preparation of $[Ru(bpy)_2(CO)(\eta^1\text{-}CO_2)]\cdot 3H_2O$ in the reaction of $[Ru(bpy)_2(CO)_2]^{2+}$ with 2 equiv. of OH^- in CH_3OH/H_2O (1/1 v/v), the reaction of $[Ru(bpy)_2(CO)(C(O)OH)]^+$ with Bu_4NOH in CH_3CN gave a better yield (~70 %) for the red crystal of **2**. The crystal of **2** also contained three molecules of H_2O, and is merely soluble to acetonitrile.

2. Reaction of **2** with H_2O in acetonitrile under N_2

The red crystals of **2** were not soluble in acetonitrile at room temperature. Sonication of **2** suspended in CD_3CN around 80 °C under N_2 gave a brown solution with evolution of CO_2. The ^1H-NMR spectrum in the CD_3CN solution showed a characteristic Ru-H signal of $[Ru(bpy)_2(CO)(H)]^+$ at -12 ppm in an 80 % yield based on bpy signals.

3. Reactivity of **2** with O_2 in acetonitrile

The similar solubilization of **2** in CD_3CN in air gave a blue solution. A blue precipitate, which gradually appeared on cooling the solution, did not show a $\nu(C{\equiv}O)$ band in the IR spectra. The blue complex was characterized as $[Ru(bpy)_2(CO_3)]$ on the basis of both ^1H-NMR and FAB-mass spectra.

4. Stabilization of **2** by treatment with Li^+ in acetonitrile

In contrast to insolubility of $[Ru(bpy)_2(CO)(CO_2)]\cdot 3H_2O$ (**2**) in CH_3CN, an addition of $LiCF_3SO_3$ to a CD_3CN suspension of **2** readily gave a clear yellow solution without heating. The NMR spectrum of the yellow solution displayed a typical pattern for $[Ru(bpy)_2(CO)X]^+$ (X = anionic ligand) in acetonitrile. The pattern was essentially unchanged in the range of mole ratio of $Li^+/[Ru(bpy)_2(CO)(CO_2)]$ from 20 to 5, but the color of the solution changed from yellow to brown in the mole ratio from 1 to 2. An addition of H^+ to the yellow solution of **2** in the presence of 5 mole excess of Li^+ gave a colorless solution of $[Ru(bpy)_2(CO)_2]^{2+}$. The change in color by an addition of H^+ was followed by the UV-vis spectra, which showed isosbestic points at 260 and 305 nm. Thus, the yellow complex formed in the reaction of **2** with Li^+ in CH_3CN contains a Ru-CO_2 bond.

The IR spectra of the yellow solution displays $\nu_{asym}(CO_2)$ and $\nu sym(CO_2)$ band at 1467 cm^{-1} and 1246 cm^{-1}, respectively, which underwent isomer shift by ^{18}O labeling. The comparison of the Raman spectra of **2** in CH_3OH and in CH_3CN containing $LiCF_3SO_3$ revealed that the ν(Ru-C) band of $[Ru(bpy)_2(CO)(CO_2)]$ appeared at 510 cm^{-1}, and that of the yellow complex emerged at 520 cm^{-1} (The assignment of the stretching mode is described in the Chapter 5.)

Discussion

1. Stabilization of the CO_2 complex by contribution of Ru=C carbenoid structure

Three H_2O molecules are linked to **2** in the solid state and three dimensional hydrogen bond networks are formed in the crystal lattice. On the basis of the facts that **2** is stable in H_2O and alcohols while easily decomposes in aprotic media, the hydrogen bondings between η^1-CO_2 of **2** and hydrated H_2O or protic media in the solid and solutions, respectively, effectively stabilize the CO_2 complex. The reactivity and physical properties of $[Ru(bpy)_2(CO)(CO_2)]$ in aprotic media, therefore, are largely interested from the viewpoint of the elucidation of the role of hydrogen bond networks in the stabilization of the η^1-CO_2 complex. Although $[Ru(bpy)_2(CO)(\eta^1\text{-}CO_2)]\cdot 3H_2O$ is almost insoluble in

CH_3CN and DMSO at room temperature, the complex was solubilized into these solvents at 80°C possibly due to thermal destruction of hydrogen bonds. However, solubilization of **2** in CH_3CN and DMSO at 80°C caused decomposition of the complex, which made it difficult to elucidate the reactivity of **2** in aprotic media. Accordingly, Li^+ assisted solubilization of **2** in acetonitrile would serve for the understanding the stability of the η^1-CO_2 group in aprotic media. The solubilization of **2** in CH_3CN may be ascribed to a strong oxygen affinity of Li^+, which presumably coordinate to the oxygens of the η^1-CO_2 group with destruction of the three dimensional networks of hydrogen bonds. The relative affinity of H_2O and Li^+ to the η^1-CO_2 would be detected by the shift of the ν(Ru-C) and $\nu(CO_2)$ bands in CH_3OH/H_2O and CH_3CN containing Li^+. The IR spectrum of $[Ru(bpy)_2(CO)(CO_2)]$ in CH_3CN containing Li^+ showed $\nu_{asym}(CO_2)$ and $\nu_{sym}(CO_2)$ in the region of 1700 to 1200 cm^{-1}, ^{18}O labeling of **2** caused an isomer shift by 1467 cm^{-1} of a band at 1422 cm^{-1} and by 1217 cm^{-1} of a band at 1246 cm^{-1}. These low bands as νC=O indicates its single bond character in the CO_2 moiety rather than the normal C=O double bond one. The Raman spectra of **2** in both media showed the ν(Ru-C) band at 519 and 511 cm^{-1}, respectively (the assignment is detailed in the Chapter 5). The observations of the low bands of the $\nu(CO_2)$ and the blue shift of the ν(Ru-C) band in CH_3CN containing Li^+ may be reasonably explained in terms of Li^+ assisted carbene-like structure (I).

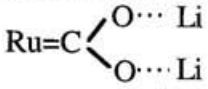

I

The lack of the knowledge concerning the M-CO_2 bond character is ascribed to a very limited number of the X-ray analysis of monomeric η^1-CO_2 structures. On the other hand, dimeric metal complexes with μ_2- and μ_3-CO_2 ligands are well characterized compared with of η^1-CO_2 metal complexes. [25] A series of Re-μ-CO_2-M complexes, [ReCp*(CO)(NO)(CO_2)][metal], has been characterized by Mashuta et al. [25a] The binding modes of the Re-CO_2 group to another metal are classified into two types. One is a μ_2-(η^1-C, η^1-O)-CO_2 complex (II) having a C-O single bond (~ 1.35 Å) and a C=O double one

(~ 1.25 Å). Another is a μ_3-(η^1-C, η^2-O,O')-CO_2 complex (III) with almost the same carbon-oxygen bond lengths. The M-C bond lengths of 2.100 Å and 2.089 Å in II and III,

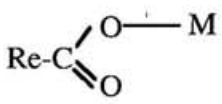

II

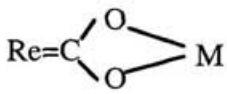

III

respectively, also indicate the contribution of the M=C bond character in III rather than in II. Each ^{13}C signal of the CO_2 ligand of II and III is observed at 207 and 219 ppm, respectively. In accordance with this, the ^{13}C NMR spectrum of $[RuCp^*(CO)_3(\mu_3\text{-}CO_2)][ZrCp_2Cl]$ also showed the μ_3-CO_2 signal at 212 ppm in C_6D_6. The chemical shifts of ^{13}C NMR of $[Ru(bpy)_2(CO)X]^+$ (X = CO_2, C(O)OH) are listed in Table 3-1. As described in a previous section, the chemical shift of CO_2 is largely influenced by the media, and the signal at 215 ppm in CH_3CN containing Li^+ (Figure 3-1) is quite close to that of the μ_3-CO_2 ligand of $[RuCp^*(CO)_3(\mu_3\text{-}CO_2)][ZrCp_2Cl]$. Thus, ^{13}C-NMR spectrum of **2** in the presence of Li^+ also supports the carbene-like structure.

Attempts to prepare $[Ru(bpy)_2(CO)(=C(OR)_2)]$ (R = H, alkyl) by the reaction of **2** with electrophiles such as H^+, CH_3I, and alkyl halides in place of Li^+ have been unsuccessful, but only $[Ru(bpy)_2(CO)(C(O)OH)]^+$ and $[Ru(bpy)_2(CO)(C(O)OR)]^+$ were obtained. The carbenoid structure assisted by Li^+ ($[Ru(bpy)_2(CO)(=C(OLi)_2)]^{2+}$) (II) is attributable to the C^+-O^- polarization of the CO_2 group caused by coordination to Li^+, which also induces the Ru=C double bond character due to the π electron donation from Ru to C. Thus, the less electron density of the CO_2 moiety is the crucial factor in the stabilization of the carbenoid CO_2 complex. On the basis of the difference in the electron densities between the $C(O)OR^-$ ligand of $[Ru(bpy)_2(CO)(C(O)OR)]^+$ (R = H, CH_3) and the $C(OLi)_2$ one of $[Ru(bpy)_2(CO)(=C(OLi)_2)]^{2+}$, the former is apparently not suitable for the acceptance of π electrons from Ru. The reaction of **2** with R^+, therefore, preferably afford ester complexes, $[Ru\text{-}C(O)OR]^+$, rather than carbene ones.

Table 3-1 Chemical shifts in ^{13}C NMR of CO_2 and C(O)OH complexes in organic medias

solvent	CD_3CN		CD_3CN with 5mol Li^+		CD_3OD		d^6-DMSO		CD_2Cl_2	
assignment	CO_2	CO	CO_2	CO	CO_2	CO	CO_2	CO	CO_2	CO
$[Ru(bpy)_2(CO)(C(O)OH)]^+$	204.9	201.29	-	-	205.1	201.5	204.3	201.5	-	-
$[Ru(bpy)_2(CO)(CO_2)]$	-	-	214.9	203.4	210.2	203.9	-	-	-	-
$[ReCp^*(CO)(NO)(CO_2)]SnL_3$	-	-	-	-	-	-	-		201.1	206.9
$[ReCp^*(CO)(NO)(CO_2)]ReL'$	-	-	-	-	-	-	-	-	219.2	206.4

L = Ph, L' = $(CO)_3(PPh_3)$; ref 25a

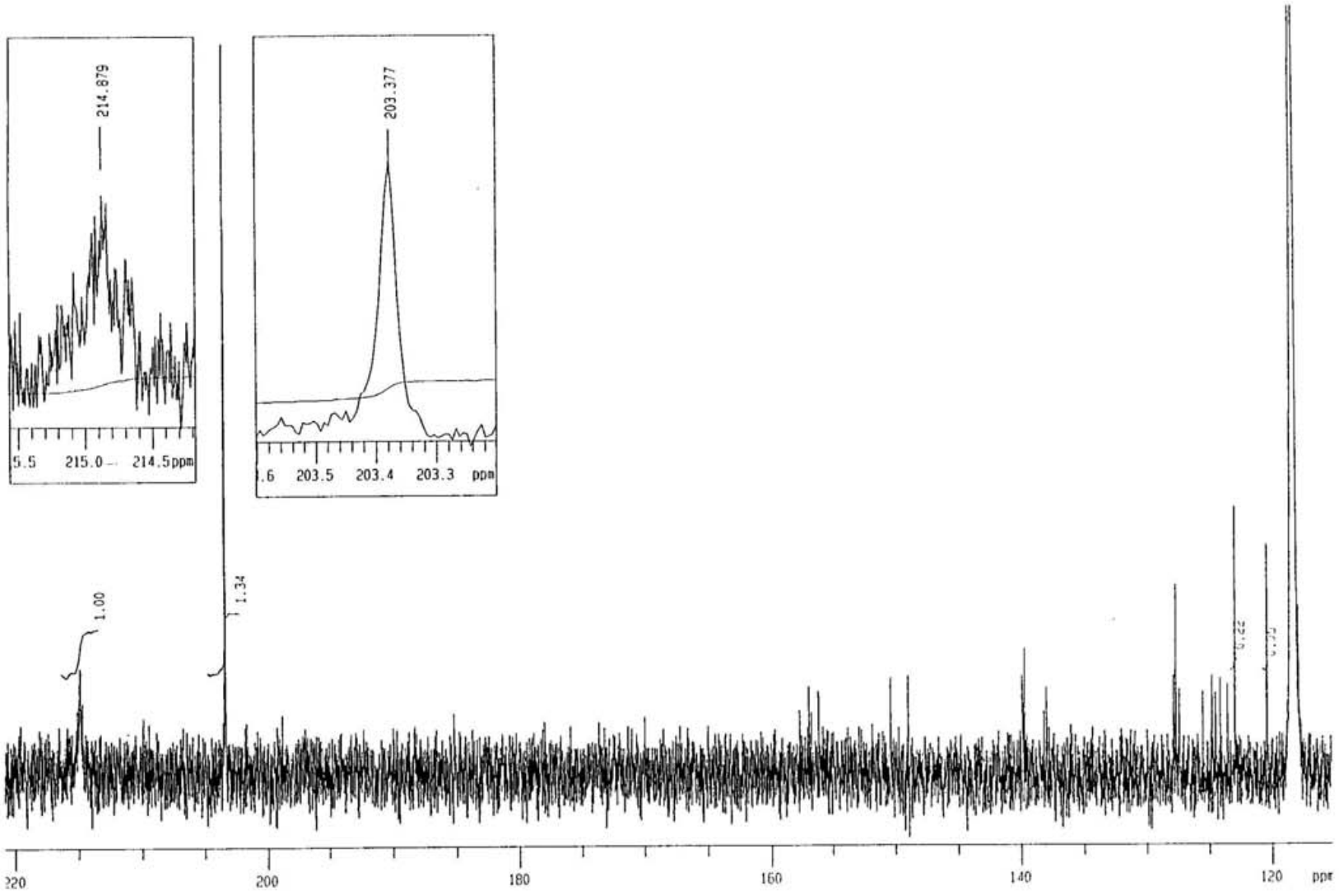

Figure 3-2 ^{13}C NMR spectrum of $[Ru(bpy)_2(CO)(CO_2)]$ in the Li^+-containing acetonitrile.

Cooper et al. reported a reductive disproportionation of CO_2 on $[W(CO)_5]$, in which $[W(=CO_2)(CO)_5]$ was proposed for the intermediate. [26] The reactivity of the CO_2 metal complexes with an M=C bond is, therefore, of interest in the CO_2 reduction. An addition of H^+ to the CH_3CN solution containing **2** and Li^+ resulted in the quantitative formation of $[Ru(bpy)_2(CO)_2]^{2+}$. The reaction was monitored by the electronic absorption spectra and isosbestic points were observed at 260 and 305 nm during the reaction, suggesting that no stable reaction intermediate involved in the conversion from the carbenoid complex to $[Ru(bpy)_2(CO)_2]^{2+}$. On the other hand, the conversion from **2** to $[Ru(bpy)_2(CO)_2]^{2+}$ in aqueous solutions takes place through $[Ru(bpy)_2(CO)(C(O)OH)]^+$. Such a difference may be explained a strong basicity of the oxygen atoms of the $C(OLi)_2$ moiety compared with the CO_2 one in **2**. An electrophilic attack of H^+ to the former may cause a simultaneous dissociation of OH^- and two Li^+ or LiOH and Li^+ from $[Ru(bpy)_2(CO)(=C(OLi)_2)]^{2+}$.

2. Cleavage of the Ru-C bond of $[Ru(bpy)_2(CO)(CO_2)]$ (**2**) in non protic media.

Red crystals of $[Ru(bpy)_2(CO)(\eta^1\text{-}CO_2)]\cdot 3H_2O$ is almost insoluble in non protic media due to the three dimensional hydrogen bonding networks, which effectively reduce an accumulation of too much electrons in the η^1-CO_2 moiety. The Li^+ assisted enhancement of the polarization of the η^1-CO_2 moiety is also a suitable methodology for the stabilization of the CO_2 complex in aprotic solvents. In addition to the stabilization of η^1-CO_2 metal complexes by hydrogen bondings and Li^+ in protic and aprotic media, the M-CO_2 bond cleavage is also very important to understand the reactivity of η^1-CO_2 metal complexes. As mentioned above, $[Ru(bpy)_2(CO)(CO_2)]\cdot 3H_2O$ is not soluble in CH_3CN and DMSO. Application of heat of the complex suspended in these solvents destroys the hydrogen bonding networks and produces $[Ru(bpy)_2(CO)(H)]^+$ under N_2. This reaction is explained by dissociation of CO_2 from $[Ru(bpy)_2(CO)(CO_2)]$ and the subsequent an electrophilic attack of H^+ to the resulting Ru(0) as similar to that in the Water-Gas-Shift-Reaction. A presumed $[Ru(bpy)_2(CO)]^0$ formed in the cleavage of the Ru-CO_2 bond in $[Ru(bpy)_2(CO)(CO_2)]$ would be also oxidized by oxygen. The decomposition on heating a

suspension of $[Ru(bpy)_2(CO)(CO_2)]\cdot 3H_2O$ in CH_3CN under the air gave $[Ru(bpy)_2(CO_3)]$ with evolving CO_2. The difference in the thermolysis of $[Ru(bpy)_2(CO)(CO_2)]\cdot 3H_2O$ under N_2 and air also supports the existence of the $[Ru(bpy)_2(CO)]^0$ intermediate, which would undergo an electrophilic attack of O_2 to form an O_2 adduct as a precursor to $[Ru(bpy)_2(CO_3)]$. Because a CO ligand $[Ir(PR_3)_2(CH_3)(CO)(O_2)]$ is oxidized intramolecurally by the O_2 group and $[Ir(PR_3)_2(CH_3)(CO)(CO_3)]$ is produced. [27] Roundhill et al. also reported the same mechanism for CO oxidation on $[Rh^0(O_2)]$. [28] Taking into account that the low valent metals with O_2 easily oxidize a CO ligand to CO_3 in the coordination sphere, $[Ru(bpy)_2(CO_3)]$ is considered to be formed by the intramolecular reaction of the CO and O_2 ligands in $[Ru(bpy)_2(CO)(O_2)]$. Although ^{18}O labeled oxygen was applied to the oxidation, there has not been clear evidence for the formation of ^{18}O labeled CO_3 moiety because of the presumable exchange of oxygen between the CO_3 moiety and contaminated water during the heating.

$[Ru(bpy)_2(CO)(H)]^+$ resulted from the cleavage of the Ru-CO_2 bond in non protic media is the proposed intermediate for HC(O)OH formation in electro- and photochemical CO_2 reductions. Destabilization of CO_2 complex is subject to dissociation of CO_2 which preferably leads to the formation of HC(O)OH in the CO_2 reduction. The schematic illustration of the reactivity of the CO_2 complex is summarized in Scheme 3-2.

Scheme 3-2 Schematic illustration of the reactivity of 2 in organic solvent

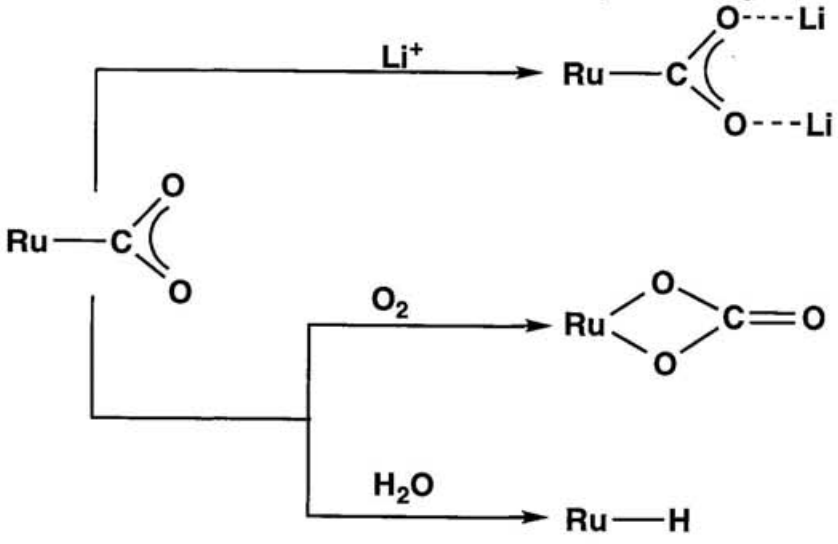

Conclusion

The chemical stability and reactivity of $[Ru(bpy)_2(CO)(CO_2)]$, which is an intermediate in the CO_2 reduction, were largely influenced by media. The change in the ratio of HC(O)OH/CO production in the CO_2 reduction through $[Ru(bpy)_2(CO)(CO_2)]$ is also dependent on the solvent and proton sources. An addition of Li^+ as a strong Lewis acid to the CO_2 complex effectively enhances the polarization of the C-O bonds in the CO_2 group and stabilizes the carbenoid structure. The lithiated CO_2 moiety is directly converted to CO by an addition of H^+ because of its large C^+-O^- polarization. On the other hand, the thermolysis of $[Ru(bpy)_2(CO)(\eta^1\text{-}CO_2)]$ causes a homolytic Ru-CO_2 bond cleavage to produce $[Ru(bpy)_2(CO)]^0$ and CO_2 in non protic media. An electrophilic attack of H_2O to $[Ru(bpy)_2(CO)]^0$ readily gave $[Ru(bpy)_2(CO)(H)]^+$, which produces HC(O)OH under CO_2 by an electrochemical activation.

Chapter 4

Ruthenium Formyl Complexes as the Branch Point in Two- and Multi-Electron Reductions of CO_2 and C-C bond Formation with C^- migration to CO_2 from Ru

Introduction

There are a number of studies on electro- and photochemical CO_2 reductions affording CO and/or HC(O)OH by metal complexes. [4, 5, 7] Recently, highly reduced products such as HCHO, CH_3OH, HO(O)CCHO, and $HO(O)CCH_2OH$ together with HC(O)OH and a small amount of CO have been obtained in electrochemical CO_2 reduction catalyzed by $[Ru(bpy)(trpy)(CO)]^{2+}$ (bpy=2,2'-bipyridine; trpy=2,2',6',2"-terpyridine) in $EtOH/H_2O$ at -20°C. [18] In this process, $[Ru(bpy)(trpy)(CHO)]^+$ and $[Ru(bpy)(trpy)(CH_2OH)]^+$ which resulted from two-electron or four-electron reduction of $[Ru(bpy)(trpy)(CO)]^{2+}$ function as key intermediates for the multi-electron reduction of CO_2. This Chapter describes a new pathway for HC(O)OH formation through an formyl intermediate, and the C-C bond formation by CO_2 insertion to a $Ru-CH_2OH$ bond.

Hydroxycarbonyl complexes (M-C(O)OH) have been proposed as precursors for HC(O)OH generation in protic media. [17] Despite the immediate conversion from $[Ru(bpy)(trpy)(CO_2)]$ to $[Ru(bpy)(trpy)(CO)]^{2+}$ through $[Ru(bpy)(trpy)(C(O)OH)]^+$ in protic media, the ratio of HC(O)OH to CO generation (1: 0.015 at 100 C passed) in the CO_2 reduction catalyzed by $[Ru(bpy)(trpy)(CO)]^{2+}$ has raised a question about the precursor to HC(O)OH. Taking into account a hydride donor ability of M-C(O)H as well as M-H complexes, [29-31] M-CHO formed by two-electron reduction of M-CO in protic media also may be a precursor to HC(O)OH generation. Although $[Ru(bpy)_2(CO)(CHO)]^+$ is not involved in the CO_2 reduction because of a spontaneous Ru-CO bond cleavage in the two-electron reduction of $[Ru(bpy)_2(CO)_2]^{2+}$, $[Ru(bpy)_2(CO)(CHO)]^+$ is a convenient model to elucidate the reactivity of $[Ru(bpy)(trpy)(CHO)]^+$, which is known as the key intermediate in the multi-electron reduction of CO_2.

The mechanism of carbon-carbon bond formation in CO_2 reductions is also interested in utilization of CO_2. There has been a report for the multielectron reduction of CO_2 affording $HO(O)CCH_2OH$ and HO(O)CCHO, and hydroxymethyl (Ru-CH_2OH) and formyl (Ru-C(O)H) complexes are proposed as the reaction intermediates. This Chapter describes the synthesis and reactivity of $[Ru(bpy)_2(CO)(CHO)]^+$ as a mechanistic model of $[Ru(bpy)(trpy)(CHO)]^+$, and the C-C bond formation by the reaction of CO_2 with $[Ru(bpy)_2(CO)(CH_2OH)]^+$.

Experiments

Materials

Guaranteed solvents purchased from Nacalai Tesque were used without further purification for synthesis. Acetonitrile for electrochemical procedures was distilled over CaH_2. Preparation of Cl^- and PF_6^- salts of *cis*-$[Ru(bpy)_2(CO)_2]^{2+}$ was described elsewhere.

1. Preparation of $[Ru(bpy)_2(CO)(CHO)](PF_6)$ (**5**)

Addition of a 1.5 molar excess of $NaBH_4$ to a colorless $MeOH/H_2O$ (2:1 v/v) solution of $[Ru(bpy)_2(CO)_2](PF_6)_2$ at -5°C resulted in gradual precipitation of yellow $[Ru(bpy)_2(CO)(CHO)](PF_6)$ (**5**). The product was collected by filtration and washed with cold water. Yield 75 %. Anal. Found: C, 42.64; H, 2.85; N, 9.04. Calcd for $C_{22}H_{17}N_4O_2RuPF_6$: C, 42.93; H, 2.76; N, 9.11. IR spectrum (KBr): ν(C=O) 1608 cm^{-1} and ν(C≡O) 1950 cm^{-1}. ^1H- and ^{13}C-NMR spectra: δ 13.9 ppm and δ 265 ppm (CHO) (Figure 4-1).

2. Preparation of $[Ru(bpy)(trpy)(CHO)]^+$

$[Ru(bpy)(trpy)(CO)](PF_6)_2$ [18] was obtained from $[Ru(bpy)(trpy)(Cl)]^+$ under 20 kgm^{-2} CO at 140°C. After a stoichiometric addition of $LiBEt_3H$ to a yellow CD_3CN

solution of $[Ru(bpy)(trpy)(CO)](PF_6)_2$ at -40°C, the ^{1}H-NMR spectra of the resulting violet solution revealed almost quantitative formation of $[Ru(bpy)(trpy)(CHO)]^+$ based on the comparison of the signal intensities between the formyl proton at δ 13.8 ppm and the aromatic protons. Further identification was not conducted because of its unstability (Figure 4-2).

3. Preparation of $[Ru(bpy)_2(CO)(CH_2OH)](PF_6)$

An addition of 1 ml of aqueous solution of $NaBH_4$ to a colorless solution of $[Ru(bpy)_2(CO)_2](PF_6)_2$ in acetonitrile at room temperature gave an orange solution of $[Ru(bpy)_2(CO)(CH_2OH)]^+$ immediately. After the filtration, the filtrate was evaporated to dryness under reduced pressure. The resulting yellow solid was dissolved into a small amount of acetonitrile, and an addition of aqueous NH_4PF_6 to the solution resulted in a precipitation of an orange powder of $[Ru(bpy)_2(CO)(CH_2OH)](PF_6)$ (Figure 4-3).

4. Electrolysis of $[Ru(bpy)_2(CO)(CH_2OH)]^+$

(a) In aqueous condition

$[Ru(bpy)_2(CO)(CH_2OH)]^+$ (10 mM) was achieved to the electrolysis in 0.2 % aqueous acetonitrile solution containing 0.05M of n-Bu_4NBF_4 at -1.5 V vs. Ag/AgCl.

(b) Under CO_2

An acetonitrile solution containing 10 mM of $[Ru(bpy)_2(CO)(CH_2OH)]^+$ and 0.05M of n-Bu_4NBF_4 passing CO_2 gas for 5 minutes was electrolyzed at -1.5 V vs. Ag/AgCl.

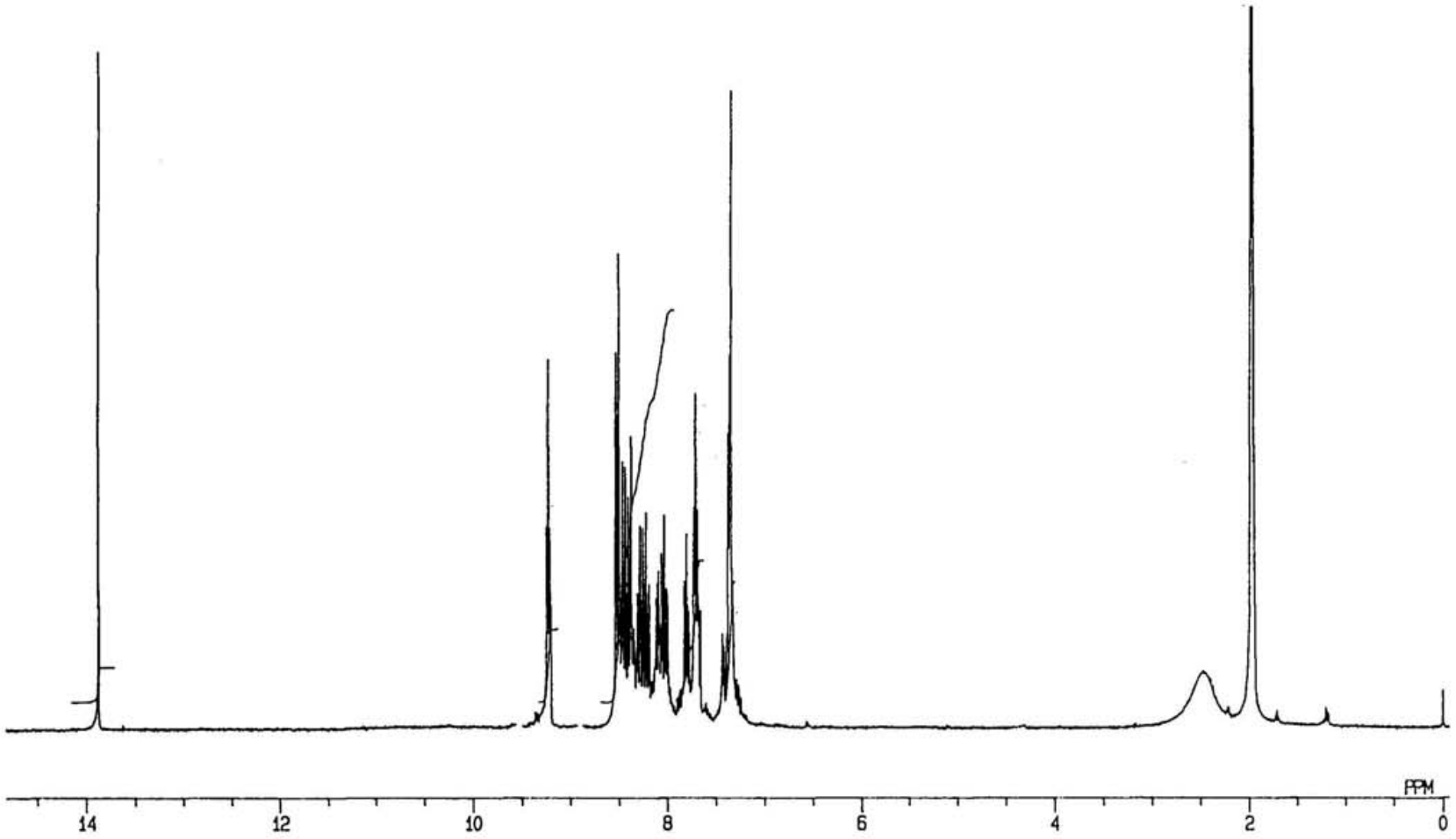

Figure 4-1-1 ^{1}H NMR spectrum of $[Ru(bpy)_2(CO)(CHO)](PF_6)$ (in CD_3CN at -40°C).

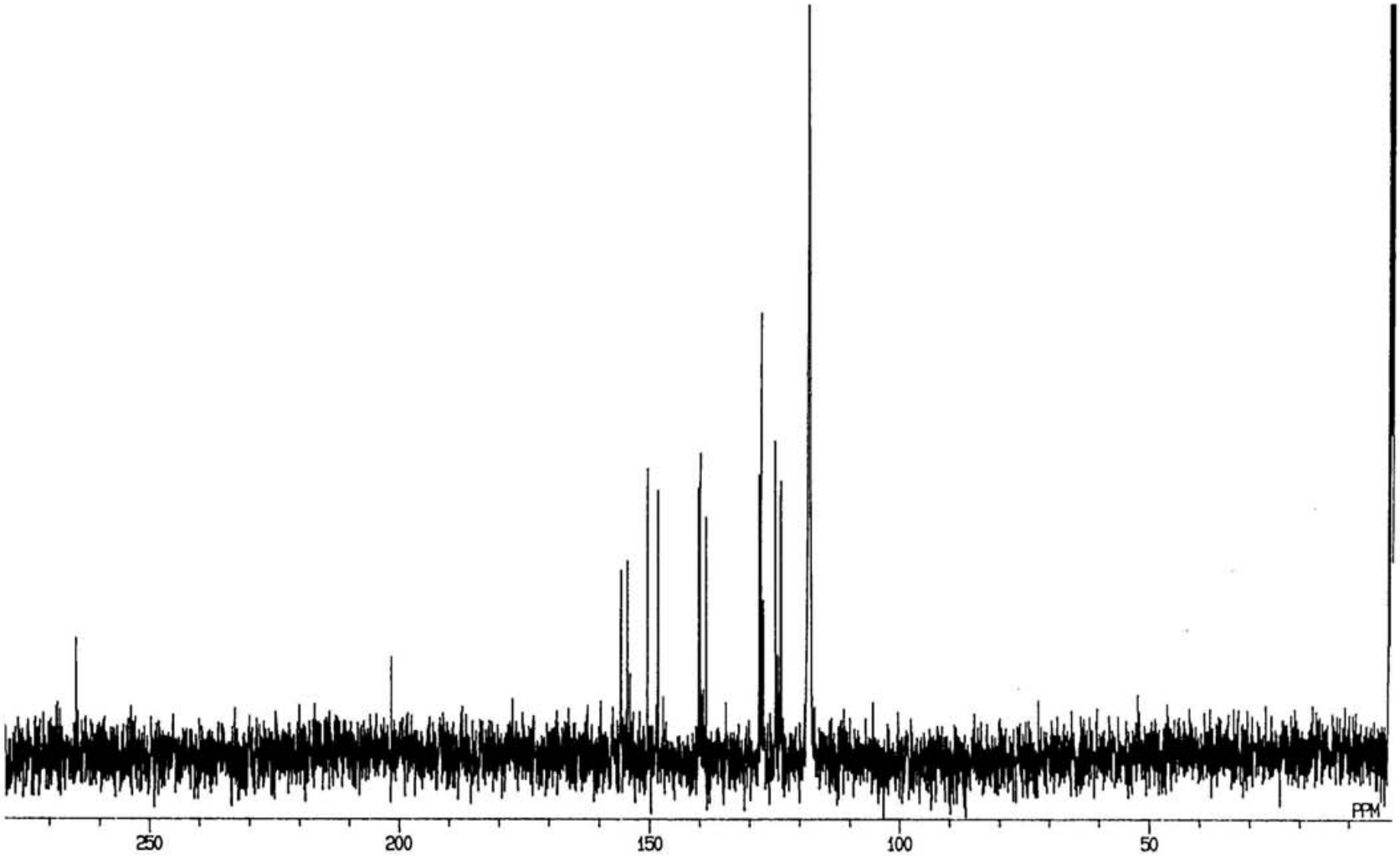

Figure 4-1-2 ^{13}C NMR spectrum of $[Ru(bpy)_2(CO)(CHO)](PF_6)$ (in CD_3CN at -40°C).

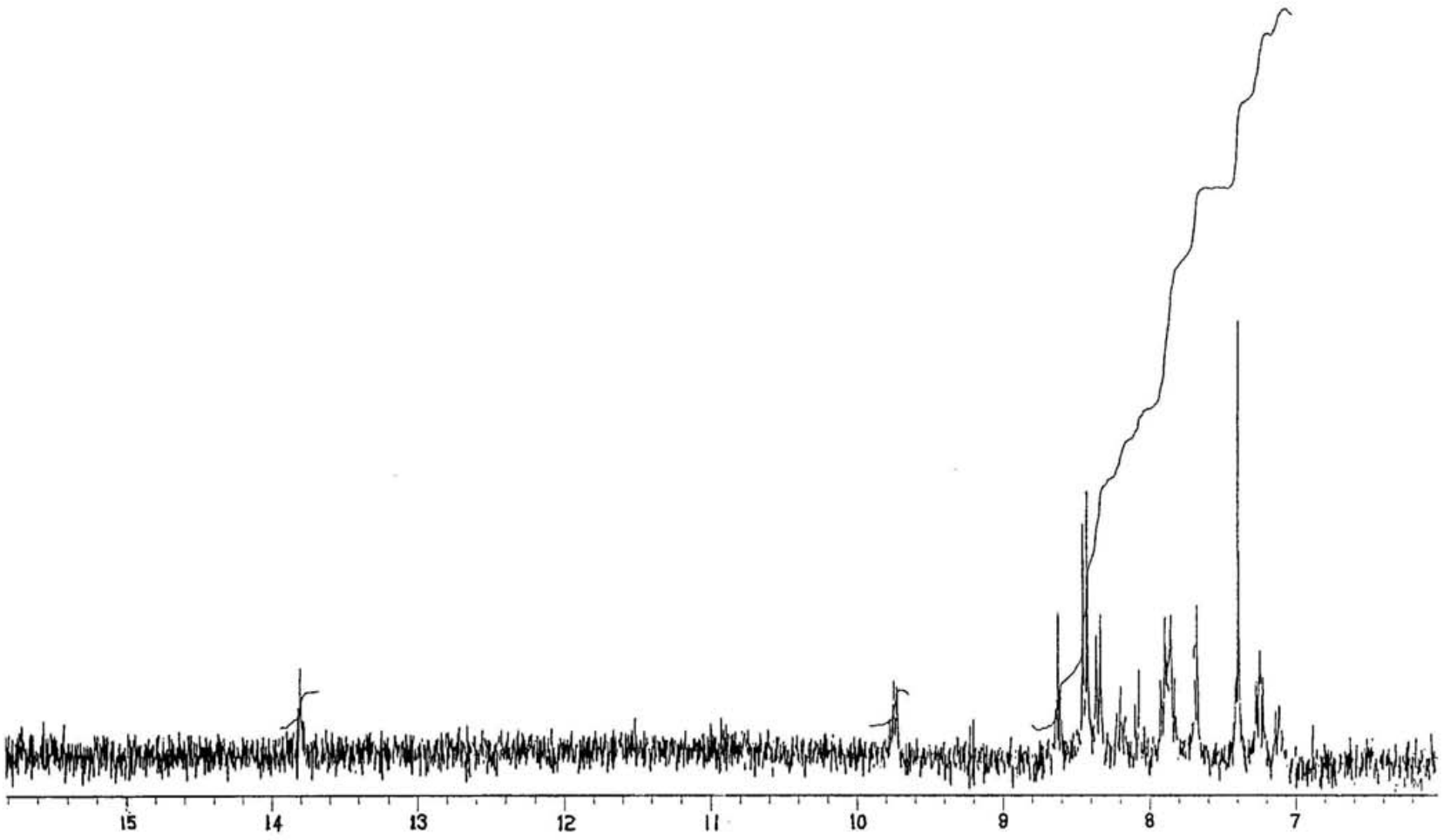

Figure 4-2 ^{1}H NMR spectrum of [Ru(bpy)(trpy)(CHO)](PF_6) (in CD_3CN at -40°C).

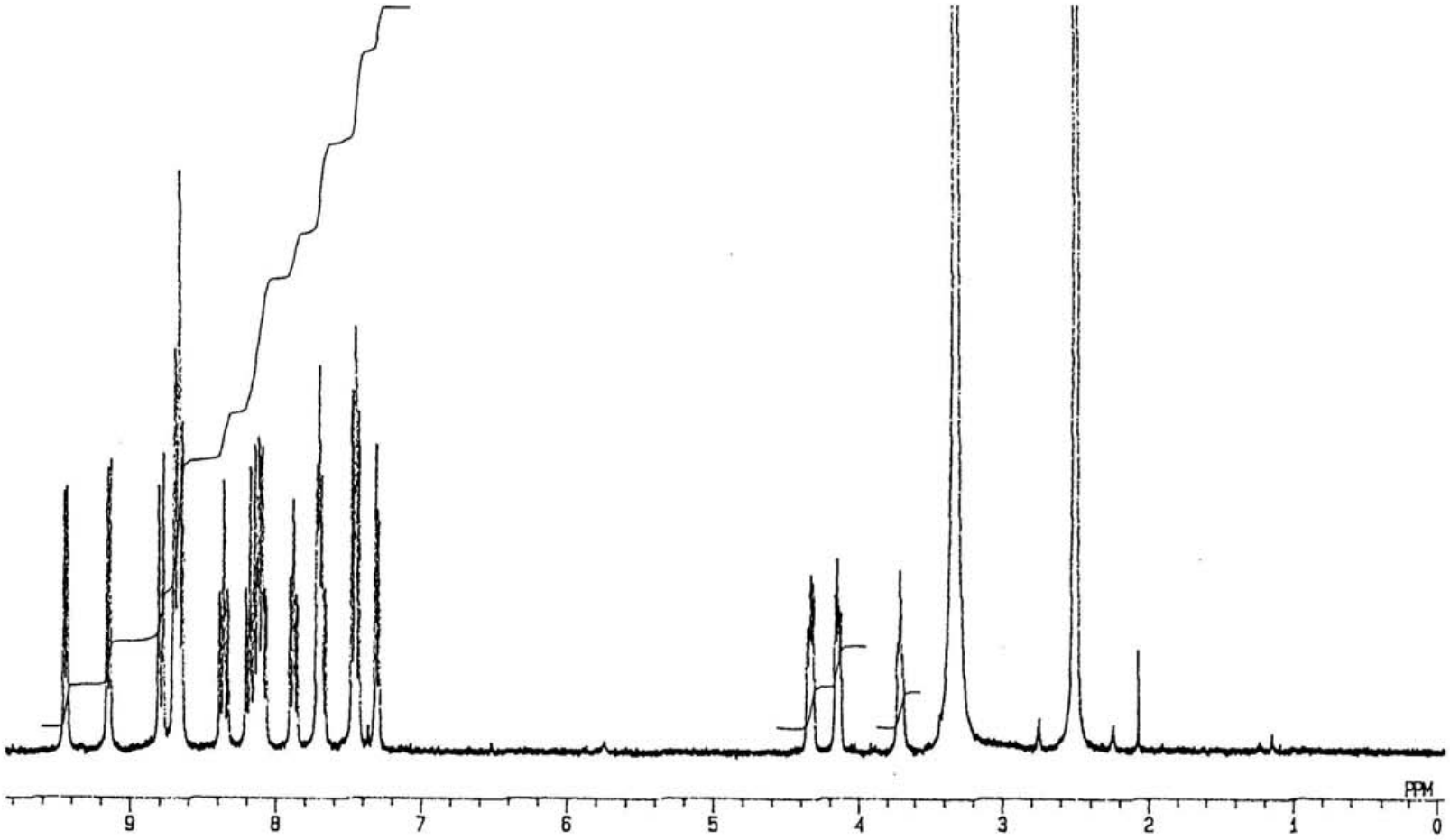

Figure 4-3-1 ^{1}H NMR spectrum of $[Ru(bpy)_2(CO)(CH_2OH)](PF_6)$ (in d^6-DMSO).

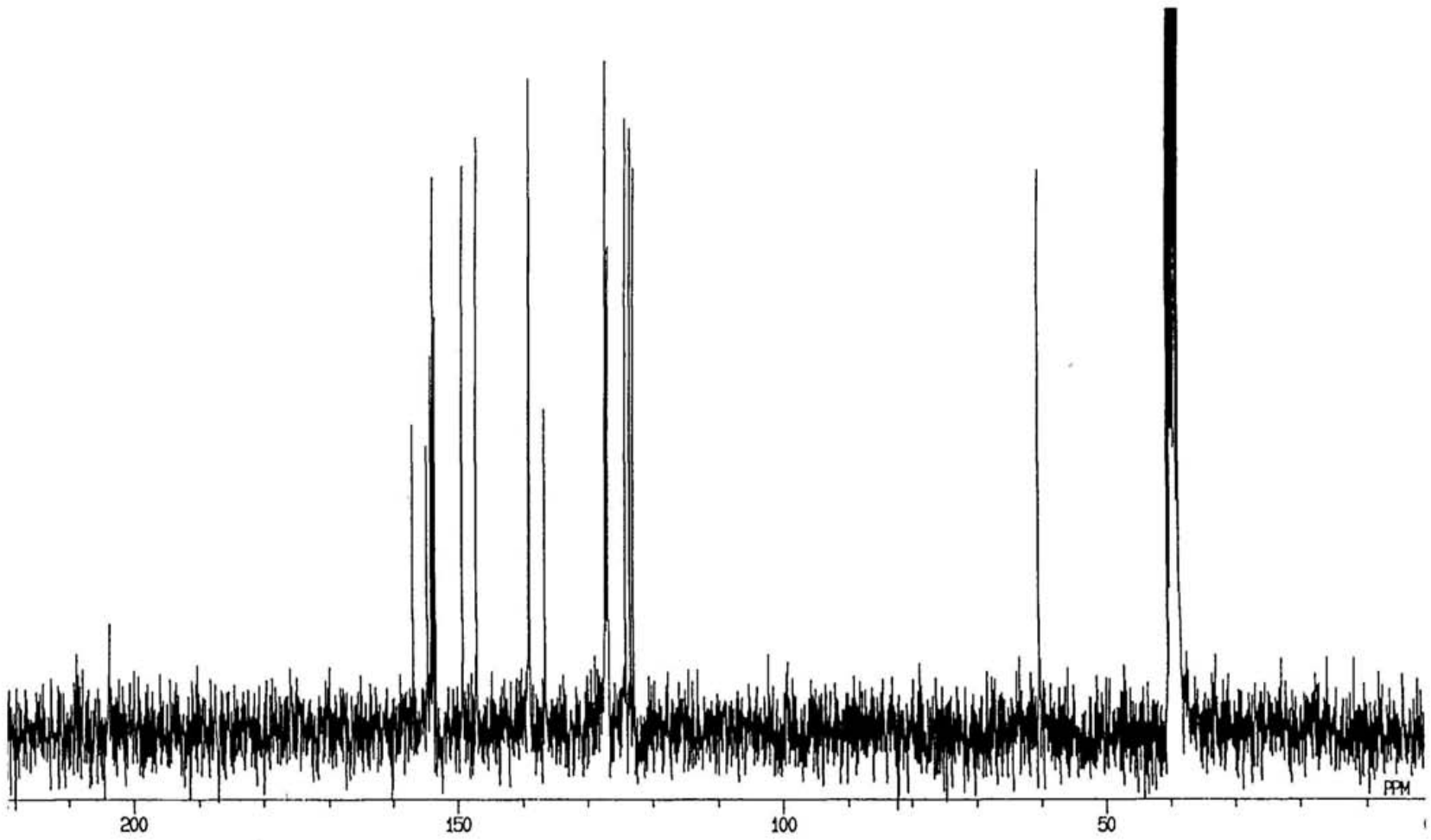

Figure 4-3-2 ^{13}C NMR spectrum of $[Ru(bpy)_2(CO)(CH_2OH)](PF_6)$ (in d^6-DMSO).

Results

1. Synthesis of the formyl complexes

The reaction of $[Ru(bpy)_2(CO)_2]^{2+}$ with BH_4^- in CH_3OH/H_2O (2:1 v/v) produced $[Ru(bpy)_2(CO)(CHO)]^+$ (**5**) as a yellow precipitate, while the similar reaction conducted in CH_3CN/H_2O under otherwise the same reaction conditions selectively produced $[Ru(bpy)_2(CO)(CH_2OH)](PF_6)$ (**6**) (80 % yield) without a precipitate of **5**. Thus, $[Ru(bpy)_2(CO)(CHO)]^+$ is easily reduced to $[Ru(bpy)_2(CO)(CH_2OH)]^+$ in solutions.

Similarly, $[Ru(bpy)(trpy)(CHO)](PF_6)$ (**7**), that is the key intermediate in the multi-electron reduction of CO_2 by $[Ru(bpy)(trpy)(CO)]^{2+}$, was also obtained by a stoichiometric addition of $LiBEt_3H$ to a CH_3CN solution of $[Ru(bpy)(trpy)(CO)](PF_6)_2$ at -40°C. The ^1H-NMR spectrum of the resulting violet solution revealed almost quantitative formation of **7** based on the comparison of the signal intensities between the formyl proton at δ 13.8 ppm and the aromatic protons.

2. Reactivity of $[Ru(bpy)_2(CO)(CHO)]^+$ in CH_3OH

In contrast to thermal stability of **2** in CH_3OH and CH_3CN, **5** slowly decomposed above -20°C in those solvents. Thermal decomposition of **5** in CH_3OH at 0 °C gave $[Ru(bpy)_2(CO)(C(O)OCH_3)](PF_6)$ (80 % yield) (eq 1). Concomitant H_2 evolution (10 %

$$[Ru(bpy)_2(CO)(CHO)]^+ + CH_3OH \longrightarrow [Ru(bpy)_2(CO)(C(O)OCH_3)]^+ + H_2 \quad (1)$$

in 30 min) indicates that $[Ru(bpy)_2(CO)(C(O)OCH_3)]^+$ is formed by the reaction of $[Ru(bpy)_2(CO)_2]^{2+}$ with CH_3O^-. On the other hand, a mixture of $[Ru(bpy)_2(CO)(CH_3CN)](PF_6)_2$, $[Ru(bpy)_2(CO)_2](PF_6)_2$, and **2** were obtained upon

warming a CH_3CN solution of **5** to ambient temperature. The formation of the latter two, though the yield of **2** was 5 %, implies a hydride migration between two formyl complexes presumably in the presence of contaminated water.

3. Reactivity of $[Ru(bpy)_2(CO)(CHO)]^+$ with CO_2

Similar thermolysis of **5** in CO_2-saturated CH_3CN at 0 °C gave $HC(O)O^-$ (60 % yield) with generation of $[Ru(bpy)_2(CO)_2]^{2+}$ and a small amount of $[Ru(bpy)_2(CO)(CH_3CN)]^{2+}$ (eq 2).

$$[Ru(bpy)_2(CO)(CHO)]^+ + CO_2 \longrightarrow [Ru(bpy)_2(CO)_2]^{2+} + HCOO^- \quad (2)$$

4. Reactivity of $[Ru(bpy)(trpy)(CHO)]^+$

An introduction of CO_2 into the violet solution by bubbling resulted in regeneration of a yellow $[Ru(bpy)(trpy)(CO)]^{2+}$ solution at -40°C and $HC(O)O^-$ was generated in 60 % yield.

5. Electrolysis of $[Ru(bpy)_2(CO)(CH_2OH)](PF_6)$

The cyclic voltammogram (CV) of $[Ru(bpy)_2(CO)(CH_2OH)](PF_6)$ in CH_3CN containing 0.1M n-Bu_4NBF_4 showed two reversible redox couples ($E_{1/2}$) at -1.41 and -1.50 V under N_2 atmosphere (Figure 4-4). On the other hand, the CV under CO_2 displayed a catalytic current at potentials more negative than the onset potential of the second cathodic wave, which indicates that two electron reduced form of the hydroxymethyl complex readily reacts with CO_2. In fact, the controlled potential electrolysis of $[Ru(bpy)_2(CO)(CH_2OH)](PF_6)$ in CH_3CN at -1.60 V in the presence of H_2O produced CH_3OH in a 85 % yield, and the similar electrolysis in CO_2-saturated dry CH_3CN afforded $^-O(O)CCH_2OH$ (66% yield based on Ru). Thus, a hydroxymethyl complex is subject to an

electrophilic attack of CO_2 and a proton to afford $HO(O)CCH_2OH$ and CH_3OH, respectively, as a six-electron reduction products of CO_2.

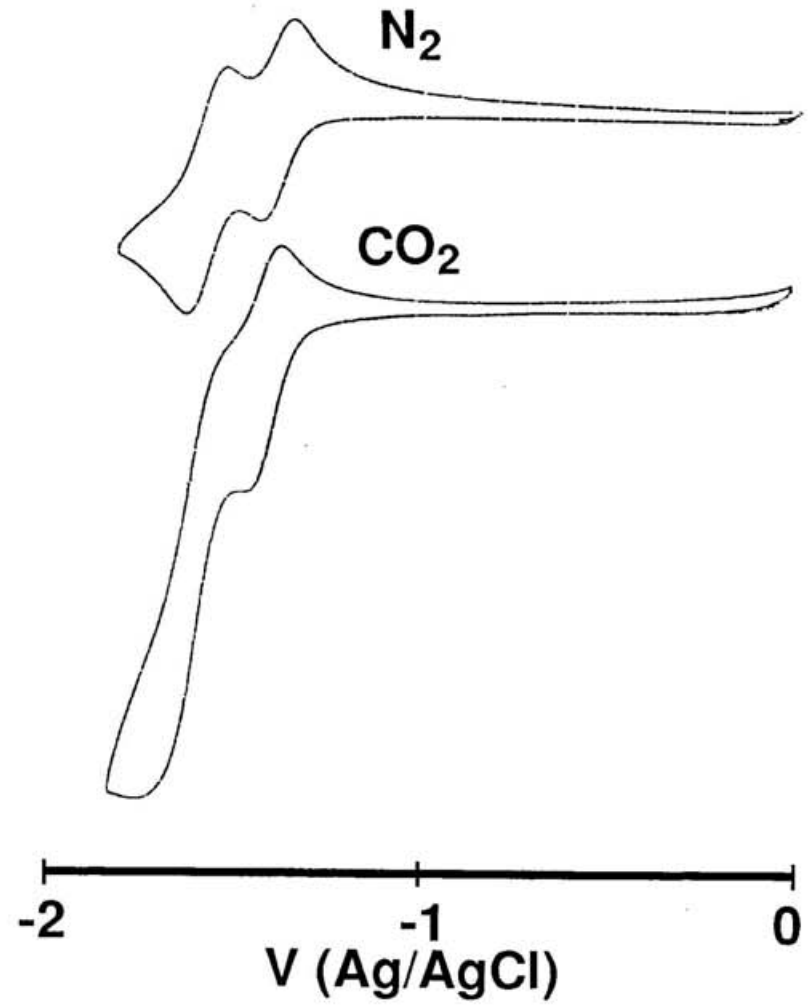

Figure 4-4 Cyclic voltammogram of $[Ru(bpy)_2(CO)(CH_2OH)]^+$ (1 mM) in 0.1M n-Bu_4NBF_4/acetonitrile.

Discussion

1. Mechanism of HC(O)OH formation in the multi-electron reduction system

Photo- and electrochemical CO_2 reductions catalyzed by $[Ru(bpy)_2(CO)H]^+$ has been shown to proceed via $[Ru(bpy)_2(CO)(OC(O)H)]^0$, which is formed by CO_2 insertion into the Ru-H bond of one electron reduced form of $[Ru(bpy)_2(CO)(H)]^+$, and the subsequent dissociation of $HC(O)O^-$ upon further one electron reduction of $[Ru(bpy)_2(CO)(OC(O)H)]^0$. [16c] On the other hand, the author found that $HC(O)O^-$ is readily produced in the reaction of CO_2 with **5** and **7** even at low temperature (eqs 2 and 3). It should be noticed that $[Ru(bpy)_2(CO)H]^+$, in contrast to **5**, does not react with CO_2 at

$$[Ru(bpy)(trpy)(CHO)]^+ + CO_2 \longrightarrow [Ru(bpy)(trpy)(CO)]^{2+} + HCOO^- \quad (3)$$

room temperature without electrochemical activatinon of the complex. Only formato (M-OC(O)H) and hydroxycarbonyl (M-C(O)OH) species have been proposed as precursors for $HC(O)O^-$ formation in electro- and photochemical CO_2 reductions so far. The above results, however, strongly indicate that formyl complexes are also possible intermediates for $HC(O)O^-$ formation.

Formyl and hydroxymethyl intermediates have been proposed in the multielectron reduction of CO_2 on Ru. Conversion from CO_2 to CO on metals can be explained by an acid-base equilibrium of metal-CO_2 adducts, and CO evolution is ascribed to a metal-CO bond cleavage upon the irreversible reduction. Formyl complexes are produced competitively by a two-electron reduction and a protonation under similar conditions. Further a reduction and a protonation of formyl complexes produce hydroxymethyl species which are precursors to CH_3OH. In addition to the further reduction to hydroxymethyl spieces, the formyl complexes can react with CO_2 producing $HC(O)O^-$ with regeneration of metal carbonyl complexes which are precursors for CO evolution. The presence of formyl intermediates as the branch point for two- and multi-electron reductions of CO_2 may,

therefore, explain the reason why most of the reduction products have been limited to CO and/or HC(O)OH in electro- and photochemical CO_2 reductions catalyzed by metal complexes.

2. The mechanism for formation of C2 compounds in the multi-electron reduction of CO_2

CO_2 reduction accompanied by C-C bond formation producing oxalate, ethane, propanol and so on has been achieved by using heterogeneous catalysts. [9] For oxalate formation in heterogeneous system, $CO_2^{\cdot-}$ coupling is proposed as a main process for the C-C bond formation. As for the activation of CO_2 on solid, ligation of CO_2 via O and C atoms to the surface of the solid is proposed, although direct evidence for the binding modes is not provided so far. It has been shown that HO(O)CCHO and $HO(O)CCH_2OH$ were produced through an η^1-CO_2 intermediate in the CO_2 reduction catalyzed by $[Ru(bpy)(trpy)(CO)]^{2+}$. According to the lack of oxalate in the products in the multi-electron reduction, those C2 materials must be formed through a different way from the oxalate formation mechanism. Formyl and hydroxymethyl complexes are proposed for intermediates in the multi-electron reduction of CO_2 catalyzed by $[Ru(bpy)(trpy)(CO)]^{+}$. The reaction path to the hydroxymethyl intermediate has not been well explored. In addition to two-electron reduction of the formyl complex in protic media, the hydroxymethyl complex is also expected to be produced by the disproportionation of the formyl by considering the hydride donor ability of the formyl complex. In fact, the thermal decomposition of the formyl complex afforded a small amount of the hydroxymethyl complex (eq. 4). The fact that $[Ru(bpy)_2(CO)(CH_2OH)]^{+}$ is formed through $[Ru(bpy)_2(CO)(C(O)H)]^{+}$ indicates that

$$2[Ru(bpy)_2(CO)(CHO)]^{+} + H^{+} \longrightarrow [Ru(bpy)_2(CO)_2]^{2+} + [Ru(bpy)_2(CO)(CH_2OH)]^{+} \quad (4)$$

the former is a suitable mechanistic model of the reductive C-C bond formation, though $[Ru(trpy)(bpy)(CH_2OH)]^+$ has not been synthesized. A large catalytic current in the cyclic voltammogram of $[Ru(bpy)_2(CO)(CH_2OH)]^+$ was observed at potentials more negative than the second cathodic wave in the presence of CO_2 or H^+, suggesting that $[Ru(bpy)_2(CO)(CH_2OH)]^-$ readily reacts with CO_2 through an associative or an dissociative path. The associative path (CO_2 insertion to the Ru-CH_2OH bond) would produce $[Ru(bpy)_2(CO)(OC(O)CH_2OH)]^-$. Then, the Ru-O bond cleavage will produce $^-O(O)CCH_2OH$ and $[Ru(bpy)_2(CO)]^0$, the latter of which again undergoes an electrophilic attack of CO_2 to form $[Ru(bpy)_2(CO)(\eta^1\text{-}CO_2)]^0$. An alternative path is the fragmentation of the Ru-CH_2OH bond to $[Ru^{2+}]^0$ and $^-CH_2OH$, and both react with CO_2 to give the same products. Lack of a catalytic current in the CV of $[Ru(bpy)_2(CO)(CH_2OH)]^+$ under N_2 might show that the former path would be included in a more reasonable mechanism for this C-C bond formation reaction.

Conclusion

Multi-electron reduction of CO_2 in protic media is of interest in not only industrial use of CO_2 but also the mechanistic study for biosynthesis. The ruthenium complex, $[Ru(bpy)(trpy)(CO)]^{2+}$, is a unique homogeneous catalyst which proves to be active in multielectron reduction of CO_2. The author found that $[Ru(bpy)(trpy)(CHO)]^+$ smoothly reacted with CO_2 to form $HC(O)O^-$. The hydride donor ability of formyl complexes is considered to be the main factor which strongly hampers the formation of CH_2O and CH_3OH in the reduction of CO_2 by metal complexes. On the other hand, once $[Ru(bpy)(trpy)(CH_2OH)]^+$ is formed by the two-electron reduction of $[Ru(bpy)(trpy)(CHO)]^+$ in protic media, CH_3OH and $HO(O)CCH_2OH$ would be produced by a protonation and a carboxylation of $[Ru(bpy)(trpy)(CH_2OH)]^+$ under electrolysis conditions. Thus a proposed mechanism for the catalytic reduction could be summarized in Scheme 4-1.

Scheme 4-1 A proposed mechanism of multielectron reduction on $[Ru(bpy)(trpy)(CO)]^{2+}$.

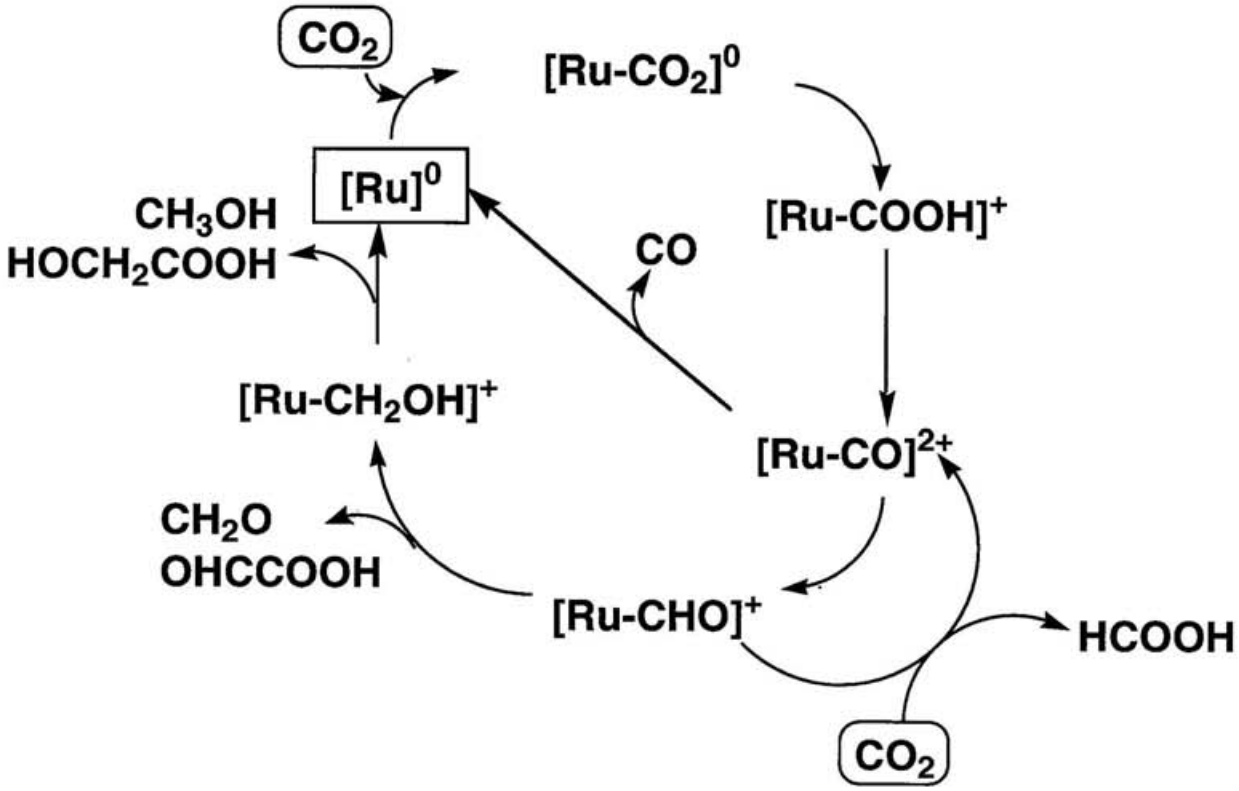
CO2
[Ru-CO2]0
[Ru]0
CH3OH
HOCH2COOH
[Ru-COOH]+
CO
[Ru-CH2OH]+
[Ru-CO]2+
CH2O
OHCCOOH
[Ru-CHO]+
HCOOH
CO2

Chapter 5

Comparison of Ru-C Bond Characters Involved in Successive Reduction of Ru-CO_2 to Ru-C(O)OH, Ru-CO, Ru-CHO and Ru-CH_2OH

Introduction

Multi-electron reduction of CO_2 is more favorable than two-electron reduction in a thermodynamic sense, because the E° values (25°C, pH = 0) for HC(O)OH, CO, HCHO, CH_3OH, and CH_4 formation are -0.199, -0.103, -0.071, +0.030 and +0.169 V vs. NHE, respectively. Not only HC(O)OH and CO but also HCHO, CH_3OH, HO(O)CCHO, and $HO(O)CCH_2OH$ have been obtained in electrochemical CO_2 reduction by $[Ru(bpy)(trpy)(CO)]^{2+}$ in $EtOH/H_2O$ at -20°C , in which Ru-CO_2, Ru-C(O)OH, Ru-CO, Ru-CHO, and Ru-CH_2OH species have been suggested to participate in the catalytic cycle. Such multi-step conversion of CO_2 on Ru is inevitably accomplished by variation in the carbon orbital of the Ru-C bonds (sp^2, sp, and sp^3), which would also give crucial influence on the formation energy of HC(O)OH, CO, HCHO, CH_3OH, and CH_4 in multi-electron reduction of CO_2 by metal complexes. Vibrational spectroscopy may provide useful information about the Ru-C bond characters in the conversion from Ru-CO_2 to Ru-CH_2OH.

Vibrational studies on organometallic compounds including metal-CO_2 adducts have been well documented and elucidated the presence of various couplings of metal-carbon stretching modes with many vibrational modes of other ligands. The author, therefore, has undertaken Raman spectra of a series of *cis*-$[Ru(bpy)_2(CO)X]^{n+}$ (X = CO_2, C(O)OH, $C(O)OCH_3$, CO, CHO, and CH_2OH; n = 0, 1, 2) and their ^{18}O or deuterium substituted analogs to assign ν(Ru-X) bands. Comparison of the Raman spectra among those homologous complexes would permit reasonable assignments of the ν(Ru-X) bands without serious variations in the extent of couplings with other vibrational modes.

Experiments

Materials

Commercially available $H_2{}^{18}O$ and $NaBD_4$ were used without further purification. Preparation of Cl^- and PF_6^- salts of *cis*-$[Ru(bpy)_2(CO)_2]^{2+}$ was described elsewhere. The remaining *cis*-$[Ru(bpy)_2(CO)(COOH)](PF_6)$, *cis*-$[Ru(bpy)_2(CO)(CO_2)]$, and *cis*-$[Ru(bpy)_2(CO)(CH_2OH)](PF_6)$ were prepared by reactions of *cis*-$[Ru(bpy)_2(CO)_2](PF_6)_2$ with Bu_4NOH and $NaBH_4$ as reported previously. Deuterium substituted *cis*-$[Ru(bpy)_2(CO)(CD_2OH)]^+$ was prepared by the reaction of *cis*-$[Ru(bpy)_2(CO)_2]^{2+}$ with $NaBD_4$ in CH_3CN/H_2O.

1. Raman spectroscopy

Raman spectra were measured on a Perkin-Elmer FT-Raman 2000, which comprises a Nd:YAG laser (laser power, 500mW at Rayleigh scattering 1064 nm, resolution in 4 cm^{-1}) and an InGaAs detector. All measurements were carried out in KBr disks or solutions (ca. 50 $mmol/dm^3$) in a 10 mm diameter glass tube at room temperature.

2. X-ray analysis of $[Ru(bpy)_2(CO)(CH_2OH)](PF_6)$

Although we have reported the structure of the hydroxymethyl complex, [6a] detailed investigation on the IR and Raman spectra of *cis*-$[Ru(bpy)_2(CO)(CH_2OH)]^+$ suggested the existence of two isomers in the solid state. We carefully examined the final difference Fourier map again and found that the oxygen atom of hydroxymethyl group was disordered in two sites giving two isomers. The least square calculation including the disordered oxygen atom and the structure was successfully refined. All the calculation was carried out on a Silicon Graphics IRIS indigo computer system using TEXSAN. The *R* and *Rw* values converged to 0.048 and 0.053 with the disordered oxygen atom while they were 0.059 and 0.070 without the disordered atom. The bond lengths and angles are almost the same values as those in the previously determined structure except the hydroxymethyl group.

The crystallographic data, final atomic parameter, bond lengths and angles have been summarized in Table S1b-S5b.

Results

Raman spectra have been widely employed to assess metal-carbon bond characters of organometallic complexes, and metal-carbon stretching modes usually emerge in the range of 1000 to 200 cm^{-1}. To assign ν(Ru-CO) and ν(Ru-X) bands of *cis*-$[Ru(bpy)_2(CO)X]^{n+}$ (X = CO_2, C(O)OH, $C(O)OCH_3$, CO, CHO, and CH_2OH; n = 0, 1, 2) in the Raman spectra, oxygen or hydrogen atoms in the substituent X were replaced by their isotopes because of the difficulty in synthesis of *cis*-$[[Ru(bpy)_2(^{13}CO)_2]^{2+}$ as the starting compound for the preparation of the series of the complexes. Substitutions of oxygen atoms of *cis*-$[Ru(bpy)_2(C^{16}O)_2]^{2+}$ and *cis*-$[Ru(bpy)_2(CO)(C^{16}O_2)]$ by ^{18}O were conducted by taking advantage of a smooth equilibrium reaction of eq 1 in $H_2{}^{18}O$. The assignments of the Ru-

$$\underset{\text{colorless}}{[Ru(bpy)_2(CO)_2]^{2+}} \underset{H^+}{\overset{OH^-}{\rightleftharpoons}} \underset{\text{yellow}}{[Ru(bpy)_2(CO)(C(O)OH)]^{+}} \underset{H^+}{\overset{OH^-}{\rightleftharpoons}} \underset{\text{orange}}{[Ru(bpy)_2(CO)(CO_2)]} \qquad (1)$$

C stretching bands in the Raman spectra of *cis*-$[Ru(bpy)_2(CO)_2]^{2+}$ and *cis*-$[Ru(bpy)_2(CO)(CO_2)]$ were, therefore, based on the isomer shifts caused by the replacement of ^{16}O by ^{18}O. The conversion from *cis*-$[Ru(bpy)_2(C^{16}O)_2]Cl_2$ to *cis*-$[Ru(bpy)_2(C^{18}O)_2]Cl_2$ was easily monitored by disappearance of the two ν($C^{16}O$) bands at 2098.7 and 2052.3 (m) cm^{-1} of the former and appearance of the two ν($C^{18}O$) bands at 2049.7 and 2002.7 (m) cm^{-1} of the latter in the Raman spectra in $H_2{}^{18}O/CH_3OH$ (4:1 v/v) (Figure 5-1). Besides those ν(CO) bands, only one band at 443.6 (m) cm^{-1} observed in $H_2{}^{16}O/CH_3OH$ shows the isotope shift to 430.0 (m) cm^{-1} in $H_2{}^{18}O/CH_3OH$. Not only band positions but also the patterns of all other peaks detected in $H_2{}^{16}O$ and $H_2{}^{18}O$ are consistent with each other within ±1.0 cm^{-1}. The 443.6 cm^{-1} band, therefore, is

reasonably assigned to ν_{sym}(Ru-CO) of *cis*-$[Ru(bpy)_2(CO)_2]^{2+}$. The ν_{asym}(Ru-CO) band in the Raman spectrum of *cis*-$[Ru(bpy)_2(CO)_2]Cl_2$ may be weakened by its local C_{2v} symmetry of *cis*-$[Ru(bpy)_2(CO)_2]^{2+}$.

Similarly, the ν(CO) band at 1947.9 (m) cm^{-1} of *cis*-$[Ru(bpy)_2(C^{16}O)(C^{16}O_2)]$ in $CH_3OH/H_2{}^{16}O$ (4:1 v/v) moves to 1908.9 (m) cm^{-1} in $CH_3OH/H_2{}^{18}O$ (4:1 v/v) (Figure 5-2). Furthermore, shift of a band at 1242.3 cm^{-1} in $CH_3OH/H_2{}^{16}O$ to 1224.8 cm^{-1} in $CH_3OH/H_2{}^{18}O$ is associated with the $\nu_{sym}(CO_2)$ band. On the basis of an assignment of the $\nu_{asym}(CO_2)$ band at 1442.5 cm^{-1} in the IR spectrum, the band may be obscured in the change in the optical intensity around 1450 cm^{-1} in the Raman spectra. Besides the isotope shifts of ν(CO) and $\nu(CO_2)$ bands, other two bands undergo isotope shift in the region of 1000 to 200 cm^{-1}; the bands at 520.2 (m) and 474.7 (w) cm^{-1} in $CH_3OH/H_2{}^{16}O$ shift to 509.1 (m) and 472.7 (s) cm^{-1} in $CH_3OH/H_2{}^{16}O$ (Figure 5-2). In accordance with this, an IR spectrum of a η^1-CO_2 titanium complex showed isotopic shifts of the bands of 1187 and 722 cm^{-1} by ^{18}O substitution and a strong coupling of the Ti -C stretching mode with the O-C-O bending mode is suggested by normal coordination calculations. The replacement of oxygen atoms between *cis*-$[Ru(bpy)_2(C^{16}O)(C^{16}O_2)]$ and *cis*-$[Ru(bpy)_2(C^{18}O)(C^{18}O_2)]$ would give more serious effects on the $\nu(Ru\text{-}CO_2)$ mode than the ν(Ru-CO) one. From the extent of the isotope shifts of two bands ($\Delta\nu$ = 11.1 and 2.0 cm^{-1}), the main contributions on the 520.1 and 474.7 cm^{-1} bands of *cis*-$[Ru(bpy)_2(C^{16}O)(C^{16}O_2)]$, therefore, result from $\nu(Ru\text{-}CO_2)$ and ν(Ru-CO) modes, respectively.

In the equilibrium reaction of eq 1, *cis*-$[Ru(bpy)_2(CO)(C(O)OH)]^+$ always exists as an equilibrium mixture with *cis*-$[Ru(bpy)_2(CO)_2]^{2+}$ and *cis*-$[Ru(bpy)_2(CO)(CO_2)]$ or either of them, which hampered the measurement of the Raman spectra of *cis*-$[Ru(bpy)_2(CO)(C(O)OH)]^+$ in aqueous conditions. Accordingly, the assignment of ν(Ru-C(O)OH) and ν(Ru-CO) bands of *cis*-$[Ru(bpy)_2(CO)(C(O)OH)](PF_6)$ was conducted by the comparison of the Raman spectra of *cis*-$[Ru(bpy)_2(CO)(C(O)OCH_3)](PF_6)$ in KBr disks. The ν(CO) bands of *cis*-$[Ru(bpy)_2(CO)(C(O)OH)](PF_6)$ and *cis*-

$[Ru(bpy)_2(CO)(C(O)OCH_3)](PF_6)$ are observed at 1973.7 (m) and 1951.3 (m) cm^{-1}, respectively. On the other hand, both Raman spectra are quite similar to each other in the region of 1000 to 200 cm^{-1} within ± 1.0 cm^{-1} except for two bands at 511.3 (m) and 473.1 (s) cm^{-1} of *cis*-$[Ru(bpy)_2(CO)(C(O)OH)](PF_6)$, and 518.1 (m) and 471.7 cm^{-1} (s) of *cis*-$[Ru(bpy)_2(CO)(C(O)OCH_3)](PF_6)$. The relative shifts of both bands between the two complexes ($\Delta\nu$ = 6.8 and 1.4 cm^{-1}) indicate that the 511.3 and 473.1 cm^{-1} bands of *cis*-$[Ru(bpy)_2(CO)(C(O)OH)](PF_6)$ mainly reflect the ν(Ru-C(O)OH) and ν(Ru-CO) modes, respectively, because the ν(Ru-C(O)OH) mode would undergo more pronounced perturbation than the ν(Ru-CO) one by esterification of the C(O)OH moiety.

A yellow powder of *cis*-$[Ru(bpy)_2(CO)(CHO)](PF_6)$ was quite stable in the solid state, but the formyl complex begins to decompose at -15°C in CH_3CN solution. So the Raman spectrum of *cis*-$[Ru(bpy)_2(CO)(CHO)](PF_6)$ was measured in KBr disk. The substitution of the CHO moiety of *cis*-$[Ru(bpy)_2(CO)(CHO)](PF_6)$ by the CDO one causes small shift of the ν(CO) band from 1950.0 to 1946.9 cm^{-1}. Besides the shift of ν(CO) band, the comparison of the spectra of *cis*-$[Ru(bpy)_2(CO)(CHO)](PF_6)$ and *cis*-$[Ru(bpy)_2(CO)(CDO)](PF_6)$ demonstrates the isotope shifts of only two bands from 518.9 (m) and 472.3 (w) cm^{-1} of the former to 515.6 (m) and 471.3 cm^{-1} (w) of the latter (Figure 5-3). Such shift also permits to assign the 518.9 (m) and 472.3 cm^{-1} (w) bands of *cis*-$[Ru(bpy)_2(CO)(CHO)]^+$ to the ν(Ru-CHO) and ν(Ru-CO) modes, respectively.

The ν(CO) band of *cis*-$[Ru(bpy)_2(CO)(CH_2OH)](PF_6)$ is dependent on the medium. In the solid state, a small splitting of ν(CO) band is observed at 1925 and 1934 cm^{-1}, while two ν(CO) bands clearly appear at 1944.5 and 1986.9 cm^{-1} in CH_2Cl_2. Similarly, *cis*-$[Ru(bpy)_2(CO)(CD_2OH)](PF_6)$ shows the same splitting of ν(CO) both in solid and solutions. Furthermore, four bands at 558.9 (m), 523.5 (m), 477.7 (w) and 471.6 (sh) cm^{-1} of *cis*-$[Ru(bpy)_2(CO)(CH_2OH)](PF_6)$ undergo isotope shift to 534.6 (m) and 511.1 (m), 475.7 (w) and ~ 470 (sh) cm^{-1}, respectively, in the Raman spectrum of *cis*-$[Ru(bpy)_2(CO)(CD_2OH)](PF_6)$ (Figure 5-4). The isotope shifts of the four bands between *cis*-$[Ru(bpy)_2(CO)(CH_2OH)]^+$ and *cis*-$[Ru(bpy)_2(CO)(CD_2OH)]^+$ in the solid states were

also detected in CH_3CN at almost identical wavenumbers. This is in contrast to the pattern of the Raman spectra of the *cis*-$[Ru(bpy)_2(CO)X]^{n+}$ (X = CO_2, C(O)OH, $C(O)OCH_3$, CHO) showing a medium ν(Ru-X) band and a weak ν(Ru-CO) band around 530 and 470 cm^{-1}, respectively. The appearance of two medium and two weak bands in the Raman spectra of *cis*-$[Ru(bpy)_2(CO)(CH_2OH)]^+$ in this region is not explained by the disorder between CO and CH_2OH of *cis*-$[Ru(bpy)_2(CO)(CH_2OH)](PF_6)$ suggested in a previous X-ray crystal analysis. The discrepancy, therefore, presumed us the reexamination of the crystal structure of *cis*-$[Ru(bpy)_2(CO)(CH_2OH)](PF_6)$ to confirm configurational isomers. Reinvestigation of the X-ray analysis of the crystal structure of $[Ru(bpy)_2(CO)(CH_2OH)](PF_6)$ clearly showed the presence of two isomers with respect to the orientation of the $RuCH_2$-OH bond directed toward below and above the equatorial plane. The former is the same structure as the previously reported one with the Ru-C(22)-O(2) bond angle of 105° (Figure 5-5a). The latter is the Ru-C(23)-O(3) angle of 108° and a weak interaction between O(3) and the carbonyl carbon estimated from a relatively short distance (3.1 Å) would give two ν(Ru-X) and ν(Ru-CO) bands in the Raman spectra. Thus, the four bands (558.9 (m), 523.5 (m), 477.7 (w) and 471.6 (w) cm^{-1}) of *cis*-$[Ru(bpy)_2(CO)(CH_2OH)](PF_6)$ are concluded to result from those two isomers. From the relative intensity of those four bands, a pair of the 558.9 (m) and 477.7 (w) cm^{-1} bands, and that of 523.5 (m) and 471.6 (w) cm^{-1} ones are reasonably assigned to ν(Ru-CH_2OH) and ν(Ru-CO) modes, respectively, of the two isomers. The finding of two isomers of *cis*-$[Ru(bpy)_2(CO)(CH_2OH)]^+$ also results from the reasonable assignment of the ν(Ru-CH_2OH) bands and ν(Ru-CO) bands.

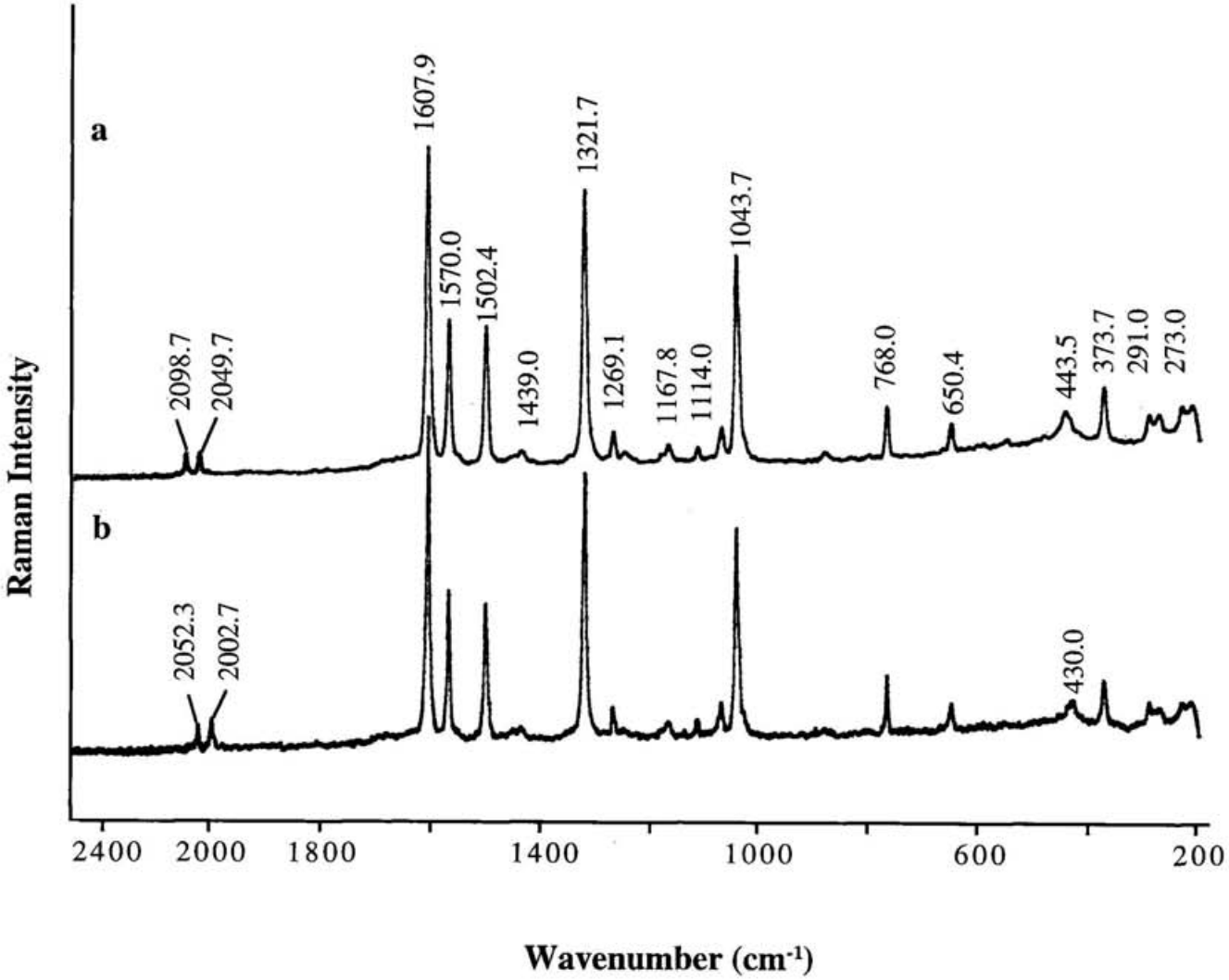

Figure 5-1 Raman spectra of *cis*-[Ru(bpy)$_2$(C^{16}O)$_2$](Cl)$_2$ (a) in H$_2$^{16}O and *cis*-[Ru(bpy)$_2$(C^{18}O)$_2$](Cl)$_2$ (b) in H$_2$^{18}O/CH$_3$OH = 4/1 (v/v).

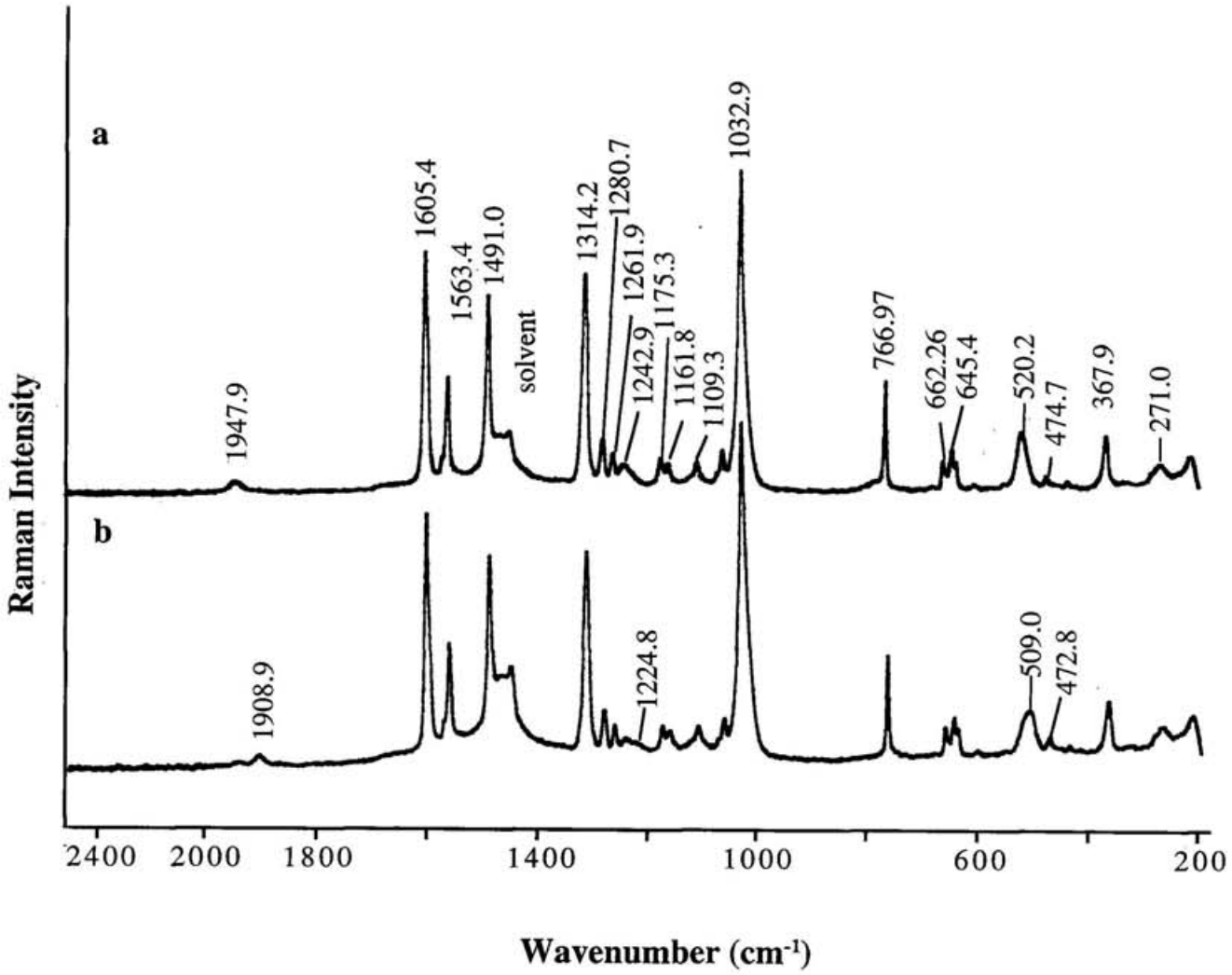

Figure 5-2 Raman spectra of *cis*-[Ru(bpy)$_2$($C^{16}O$)($C^{16}O_2$)] (a) in $H_2{}^{16}O$/CH_3OH and *cis*-[Ru(bpy)$_2$($C^{18}O$)($C^{18}O_2$)]Cl_2 (b) in $H_2{}^{18}O$/CH_3OH = 4/1 (v/v).

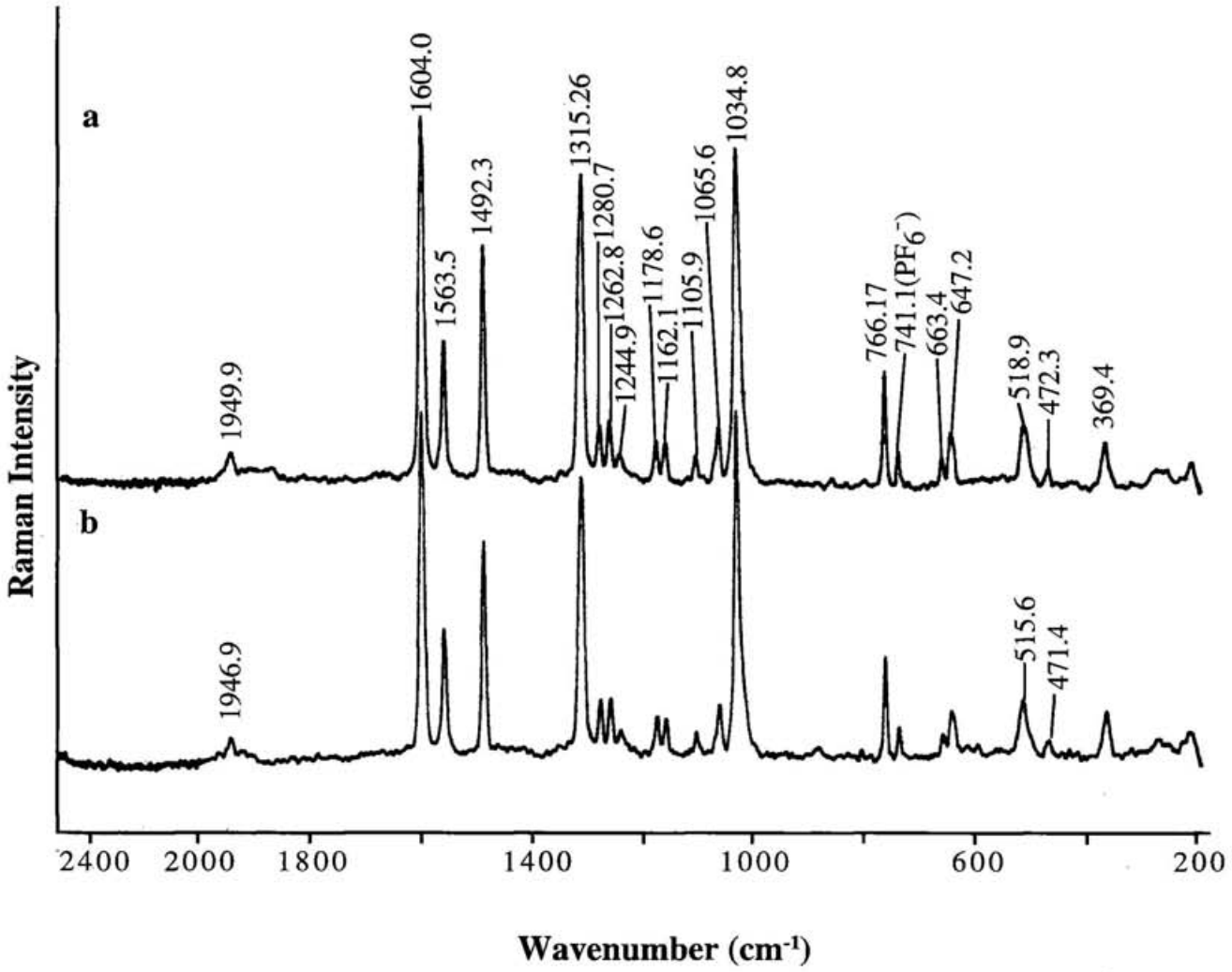

Figure 5-3 Raman spectra of *cis*-[Ru(bpy)$_2$(CO)(CHO)](PF$_6$) (a) and *cis*-[Ru(bpy)$_2$(CO)(CDO)](PF$_6$) (b) in KBr disks.

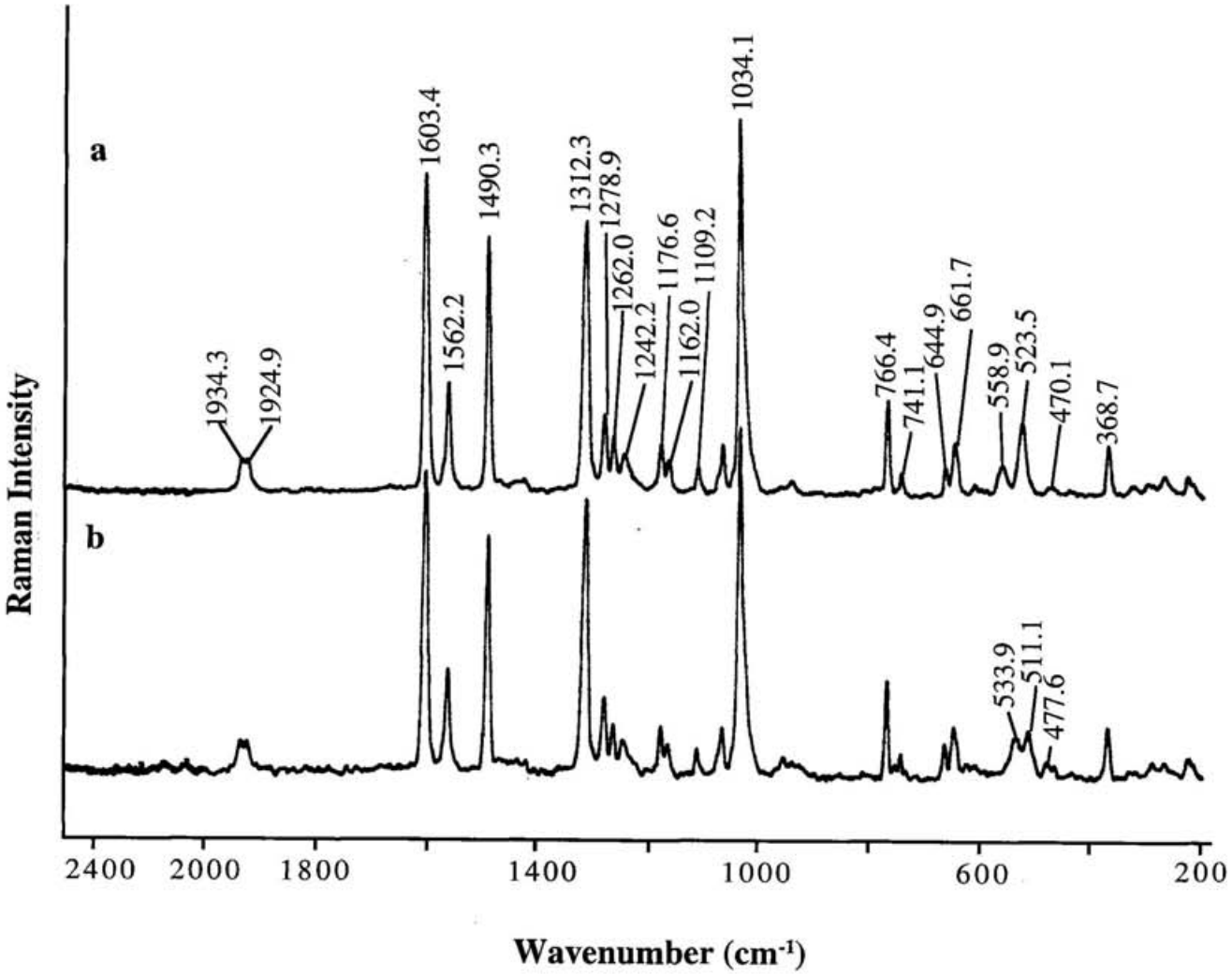

Figure 5-4 Raman spectra of *cis*-[Ru(bpy)$_2$(CO)(CH$_2$OH)](PF$_6$) (a) and *cis*-[Ru(bpy)$_2$(CO)(CD$_2$OH)](PF$_6$) (b) in KBr disks.

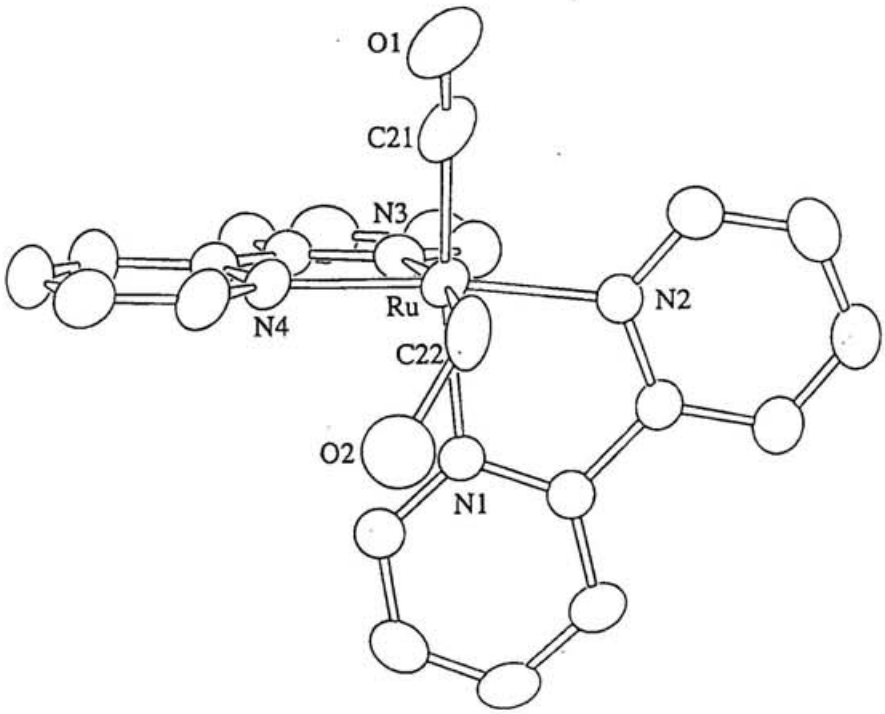

Figure 5-5a Molecular structure of one of the two conformers of *cis*-[Ru(bpy)$_2$(CO)(CH$_2$OH)](PF$_6$).

The thermal ellipsoids are drawn at the 30%

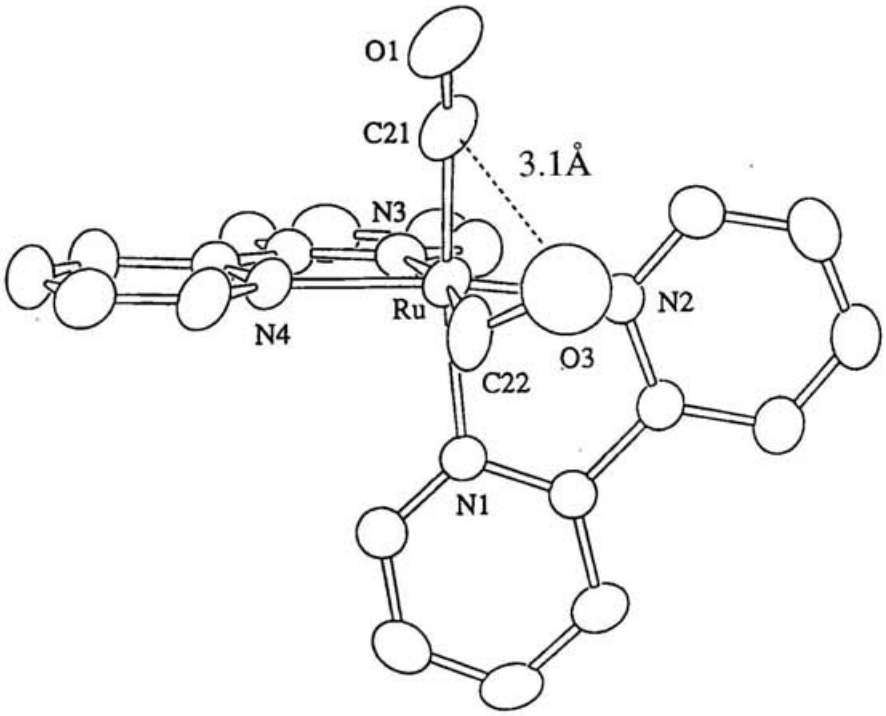

Figure 5-5b Molecular structure of one of the two conformers of *cis*-[Ru(bpy)$_2$(CO)(CH$_2$OH)](PF$_6$).

The thermal ellipsoids are drawn at the 30%

Table S1b. Crystal parameters and Experimental Data

for X-ray Diffraction Measured on $[Ru(CH_2OH)(CO)(bpy)_2](PF_6)$

Empirical Formula	$RuPF_6O_2N_4C_{22}H_{19}$
Formula Weight	617.45
Crystal Color, Habit	red, prism
Crystal Dimensions	0.35 x 0.33 x 0.21 mm
Crystal System	monoclinic
Lattice Parameters	a = 30.931(4) Å
	b = 7.4867(6) Å
	c = 24.873(3) Å
	β = 124.677(9)°
	V = 4736(1) $Å^3$
Space Group	C2/c (#15)
Z value	8
D_{calc}	1.73 g/cm^3
F(000)	2464
μ(MoKα)	8.05 cm^{-1}
Diffractometer	CAD4
Radiation	MoKα (λ = 0.71069 Å)
	graphite monochromated
Temperature	23.0C
Scan Type	2θ-ω
Scan Width	0.80 + 0.35 tanθ
$2\theta_{max}$(degree)	49.9
No. of Reflections Measured	Total: 8994
	Unique: 4514

Corrections	Lorentz-polarization
	Absorption(DIFABS[a])
	(trans. factors: 0.9012 - 1.1493)
Structure Solution	Direct Methods (SAPI91[b])
Refinement	Full-matrix least-squares
Least Squares Weights	$1/\sigma^2(F_o)$
Anomalous Dispersion	All non-hydrogen atoms
No. Observations ($F_o>3\sigma(F_o)$)	3160
No. Variables	324
Residuals: R; R_w	0.052 ; 0.054
Goodness of Fit Indicator	4.06
Max Shift/Error in Final Cycle	0.01
Maximum peak in Final Diff. Map	0.75 $e^-/Å^3$
Minimum peak in Final Diff. Map	-0.56 $e^-/Å^3$

[a] DIFABS: Walker, N. & Stuart, Acta Cryst., **1983**, *A39* , 158-166.

[b] SAPI91: Fan Hai-Fu (1991). Structure Analysis Programs with Intelligent Control, Rigaku Corporation, Tokyo, Japan.

Table S2b. Atomic coordinates and Biso/Beq

atom	x	y	z	B_{eq}
Ru	0.37229(2)	-0.00372(7)	-0.30665(2)	4.60(1)
P	0.11062(8)	0.7247(3)	-0.46292(10)	5.70(5)
F1	0.1251(3)	0.9241(7)	-0.4507(3)	12.9(2)
F2	0.0595(2)	0.7671(9)	-0.4684(3)	11.8(2)
F3	0.0952(3)	0.5279(7)	-0.4766(4)	14.5(3)
F4	0.1617(2)	0.6827(7)	-0.4596(3)	10.9(2)
F5	0.1364(2)	0.6973(9)	-0.3898(2)	12.8(2)
F6	0.0829(2)	0.7520(9)	-0.5374(2)	13.3(2)
O1	0.4391(4)	-0.247(1)	-0.3231(4)	18.0(4)
O2	0.2680(5)	-0.173(2)	-0.3487(6)	10.2(3)
O3	0.2999(7)	-0.176(3)	-0.4311(9)	15.2(5)
N1	0.3168(2)	0.1659(6)	-0.3077(2)	4.1(1)
N2	0.3498(2)	0.1615(7)	-0.3849(2)	4.6(1)
N3	0.4319(2)	0.1642(7)	-0.2295(2)	4.4(1)
N4	0.3929(2)	-0.1397(6)	-0.2219(2)	4.7(1)
C1	0.2924(2)	0.2809(7)	-0.3586(3)	4.0(1)
C2	0.2515(3)	0.3879(9)	-0.3707(3)	5.8(2)
C3	0.2360(3)	0.377(1)	-0.3286(4)	7.3(2)
C4	0.2620(3)	0.264(1)	-0.2763(4)	7.9(3)
C5	0.3016(3)	0.160(1)	-0.2682(3)	6.1(2)
C6	0.3126(2)	0.2848(7)	-0.3995(3)	4.1(1)
C7	0.2957(2)	0.4067(8)	-0.4504(3)	5.2(2)
C8	0.3165(3)	0.4012(10)	-0.4863(3)	6.2(2)
C9	0.3537(3)	0.274(1)	-0.4711(3)	7.2(2)

Table S2b. Atomic coordinates and B_{iso}/B_{eq} (continued)

atom	x	y	z	B_{eq}
C10	0.3696(3)	0.156(1)	-0.4206(3)	6.6(2)
C11	0.4526(2)	0.1047(8)	-0.1689(3)	4.3(1)
C12	0.4901(3)	0.206(1)	-0.1152(3)	5.9(2)
C13	0.5056(3)	0.368(1)	-0.1244(4)	6.7(2)
C14	0.4840(3)	0.4292(10)	-0.1857(5)	6.7(2)
C15	0.4478(3)	0.325(1)	-0.2381(3)	6.0(2)
C16	0.4318(2)	-0.0665(8)	-0.1652(3)	4.5(1)
C17	0.4494(3)	-0.150(1)	-0.1060(3)	6.2(2)
C18	0.4264(4)	-0.307(1)	-0.1070(4)	7.3(2)
C19	0.3868(3)	-0.3778(10)	-0.1639(4)	6.8(2)
C20	0.3715(3)	-0.2940(9)	-0.2205(3)	6.1(2)
C21	0.4174(4)	-0.144(1)	-0.3151(4)	10.0(3)
C22	0.3057(3)	-0.1763(8)	-0.3746(3)	6.3(2)
H1	0.2344	0.4668	-0.4071	8.0000
H2	0.2076	0.4480	-0.3359	8.0000
H3	0.2528	0.2582	-0.2460	8.0000
H4	0.3188	0.0790	-0.2323	8.0000
H5	0.2698	0.4932	-0.4600	8.0000
H6	0.3055	0.4834	-0.5210	8.0000
H7	0.3686	0.2675	-0.4955	8.0000
H8	0.3953	0.0679	-0.4109	8.0000
H9	0.5050	0.1619	-0.0722	8.0000
H10	0.5313	0.4371	-0.0878	8.0000
H11	0.4937	0.5428	-0.1927	8.0000

Table S2b. Atomic coordinates and B_{iso}/B_{eq} (continued)

atom	x	y	z	B_{eq}
H12	0.4335	0.3664	-0.2812	8.0000
H13	0.4768	-0.0981	-0.0658	8.0000
H14	0.4386	-0.3677	-0.0672	8.0000
H15	0.3698	-0.4842	-0.1645	8.0000
H16	0.3445	-0.3466	-0.2607	8.0000

$$B_{eq}=\frac{3}{8}\pi^2(U_{11}(aa^*)^2+U_{22}(bb^*)^2+U_{33}(cc^*)^2+2U_{12}aa^*bb^*\cos\gamma+2U_{13}aa^*cc^*\cos\beta+2U_{23}bb^*cc^*\cos\alpha)$$

Table S3b. Anisotropic displacement parameters

atom	U_{11}	U_{22}	U_{33}	U_{12}	U_{13}	U_{23}
Ru	0.0611(3)	0.0512(3)	0.0538(3)	0.0118(3)	0.0275(2)	0.0038(3)
P	0.074(1)	0.068(1)	0.077(1)	0.0121(9)	0.044(1)	0.0072(10)
F1	0.269(8)	0.084(3)	0.266(8)	-0.015(4)	0.228(7)	-0.018(4)
F2	0.110(4)	0.215(6)	0.152(5)	0.009(4)	0.091(4)	-0.023(5)
F3	0.297(8)	0.099(4)	0.261(7)	-0.062(5)	0.222(7)	-0.061(5)
F4	0.094(3)	0.134(4)	0.196(5)	0.024(3)	0.089(4)	0.000(4)
F5	0.179(5)	0.188(6)	0.075(3)	0.008(5)	0.045(4)	0.015(4)
F6	0.185(5)	0.231(7)	0.094(4)	0.081(5)	0.082(4)	0.045(4)
O1	0.30(1)	0.27(1)	0.130(6)	0.230(9)	0.134(7)	0.079(6)
N1	0.046(3)	0.054(3)	0.056(3)	0.002(2)	0.029(2)	0.005(2)
N2	0.060(3)	0.067(3)	0.045(3)	0.008(3)	0.028(3)	0.003(2)
N3	0.045(3)	0.062(3)	0.066(3)	-0.003(2)	0.034(3)	0.003(3)
N4	0.062(3)	0.053(3)	0.060(3)	0.010(3)	0.032(3)	0.013(3)
C1	0.052(3)	0.048(3)	0.050(3)	-0.003(3)	0.028(3)	-0.004(3)
C2	0.070(4)	0.073(5)	0.071(4)	0.021(4)	0.036(4)	0.004(4)
C3	0.083(5)	0.101(6)	0.103(6)	0.042(5)	0.060(5)	0.017(5)
C4	0.101(6)	0.132(8)	0.101(6)	0.030(6)	0.077(5)	0.023(6)
C5	0.067(4)	0.094(5)	0.078(5)	0.015(4)	0.046(4)	0.024(4)
C6	0.055(3)	0.046(3)	0.046(3)	-0.001(3)	0.024(3)	-0.004(3)
C7	0.067(4)	0.062(4)	0.057(4)	-0.004(3)	0.029(3)	0.001(3)
C8	0.090(5)	0.073(5)	0.066(5)	-0.003(4)	0.041(4)	0.010(4)
C9	0.084(5)	0.130(7)	0.062(4)	-0.001(5)	0.044(4)	0.011(5)
C10	0.076(5)	0.109(6)	0.067(5)	0.020(4)	0.043(4)	0.008(4)
C11	0.045(3)	0.066(4)	0.050(4)	0.002(3)	0.026(3)	0.000(3)

Table S3b. Anisotropic displacement parameters (continued)

atom	U_{11}	U_{22}	U_{33}	U_{12}	U_{13}	U_{23}
C12	0.069(4)	0.087(5)	0.066(4)	-0.002(4)	0.036(4)	-0.007(4)
C13	0.063(5)	0.097(6)	0.082(6)	-0.013(4)	0.034(4)	-0.026(5)
C14	0.067(5)	0.076(5)	0.111(6)	-0.023(4)	0.050(5)	-0.008(5)
C15	0.064(4)	0.083(5)	0.082(5)	-0.004(4)	0.041(4)	0.014(4)
C16	0.052(4)	0.063(4)	0.060(4)	0.009(3)	0.034(3)	0.010(3)
C17	0.085(5)	0.086(5)	0.059(4)	0.004(4)	0.037(4)	0.012(4)
C18	0.114(7)	0.084(6)	0.091(6)	0.026(5)	0.066(5)	0.041(5)
C19	0.085(5)	0.063(5)	0.113(7)	0.003(4)	0.057(5)	0.019(5)
C20	0.076(5)	0.058(4)	0.078(5)	0.002(4)	0.032(4)	0.014(4)
C21	0.173(9)	0.130(8)	0.074(5)	0.102(7)	0.068(6)	0.031(5)
C22	0.126(6)	0.044(4)	0.050(4)	-0.006(4)	0.039(4)	-0.001(3)

The general temperature factor expression:

$$\exp(-2\pi^2(a^{*2}U_{11}h^2+b^{*2}U_{22}k^2+c^{*2}U_{33}l^2+2a^*b^*\,U_{12}hk+\,2a^*c^*U_{13}hl+2b^*c^*U_{23}kl))$$

Table S4b. Bond lengths (Å)

atom	atom	distance	atom	atom	distance
RU	N1	2.124(4)	RU	N2	2.063(5)
RU	N3	2.153(5)	RU	N4	2.086(5)
RU	C21	1.851(9)	RU	C22	2.193(7)
P	F1	1.539(6)	P	F2	1.542(5)
P	F3	1.526(5)	P	F4	1.568(5)
P	F5	1.528(5)	P	F6	1.549(5)
O1	C21	1.111(9)	O2	C22	1.62(1)
O3	C22	1.31(2)	N1	C1	1.351(7)
N1	C5	1.309(8)	N2	C6	1.352(7)
N2	C10	1.337(8)	N3	C11	1.333(7)
N3	C15	1.363(8)	N4	C16	1.344(7)
N4	C20	1.343(8)	C1	C2	1.379(8)
C1	C6	1.466(8)	C2	C3	1.380(9)
C2	H1	0.95	C3	C4	1.37(1)
C3	H2	0.95	C4	C5	1.367(10)
C4	H3	0.95	C5	H4	0.95
C6	C7	1.398(8)	C7	C8	1.367(9)
C7	H5	0.95	C8	C9	1.369(10)
C8	H6	0.95	C9	C10	1.380(10)
C9	H7	0.95	C10	H8	0.95
C11	C12	1.391(8)	C11	C16	1.460(8)
C12	C13	1.37(1)	C12	H9	0.95
C13	C14	1.35(1)	C13	H10	0.95
C14	C15	1.379(10)	C14	H11	0.95

Table S4b. Bond lengths(Å) (continued)

atom	atom	distance	atom	atom	distance
C15	H12	0.95	C16	C17	1.392(8)
C17	C18	1.37(1)	C17	H13	0.95
C18	C19	1.34(1)	C18	H14	0.95
C19	C20	1.356(10)	C19	H15	0.95
C20	H16	0.95			

Table S5b. Bond angles(°)

atom	atom	atom	angle	atom	atom	atom	angle
N1	RU	N2	78.1(2)	N1	RU	N3	86.4(2)
N1	RU	N4	94.9(2)	N1	RU	C21	173.8(3)
N1	RU	C22	86.8(2)	N2	RU	N3	98.6(2)
N2	RU	N4	171.8(2)	N2	RU	C21	96.1(3)
N2	RU	C22	87.8(2)	N3	RU	N4	76.7(2)
N3	RU	C21	96.6(3)	N3	RU	C22	169.5(2)
N4	RU	C21	91.1(3)	N4	RU	C22	96.0(2)
C21	RU	C22	90.9(4)	F1	P	F2	89.2(3)
F1	P	F3	178.7(4)	F1	P	F4	90.7(3)
F1	P	F5	89.9(4)	F1	P	F6	90.5(4)
F2	P	F3	90.2(4)	F2	P	F4	178.2(3)
F2	P	F5	87.0(4)	F2	P	F6	91.4(3)
F3	P	F4	89.8(3)	F3	P	F5	91.2(4)
F3	P	F6	88.3(4)	F4	P	F5	94.8(3)
F4	P	F6	86.8(3)	F5	P	F6	178.3(4)
RU	N1	C1	114.1(4)	RU	N1	C5	127.0(4)
C1	N1	C5	118.7(5)	RU	N2	C6	116.3(4)
RU	N2	C10	124.8(5)	C6	N2	C10	118.9(5)
RU	N3	C11	115.4(4)	RU	N3	C15	125.3(4)
C11	N3	C15	119.2(5)	RU	N4	C16	115.9(4)
RU	N4	C20	125.1(5)	C16	N4	C20	118.9(5)
N1	C1	C2	121.9(6)	N1	C1	C6	115.7(5)
C2	C1	C6	122.5(6)	C1	C2	C3	118.2(6)
C1	C2	H1	120.9	C3	C2	H1	120.9

Table S5b. Bond angles(°) (continued)

atom	atom	atom	angle	atom	atom	atom	angle
C2	C3	C4	119.1(6)	C2	C3	H2	120.4
C4	C3	H2	120.4	C3	C4	C5	119.3(7)
C3	C4	H3	120.3	C5	C4	H3	120.3
N1	C5	C4	122.8(6)	N1	C5	H4	118.6
C4	C5	H4	118.6	N2	C6	C1	115.6(5)
N2	C6	C7	120.8(6)	C1	C6	C7	123.6(5)
C6	C7	C8	120.0(6)	C6	C7	H5	120.0
C8	C7	H5	120.0	C7	C8	C9	118.2(7)
C7	C8	H6	120.9	C9	C8	H6	120.9
C8	C9	C10	120.5(7)	C8	C9	H7	119.8
C10	C9	H7	119.8	N2	C10	C9	121.6(7)
N2	C10	H8	119.2	C9	C10	H8	119.2
N3	C11	C12	120.4(6)	N3	C11	C16	114.8(5)
C12	C11	C16	124.9(6)	C11	C12	C13	120.0(7)
C11	C12	H9	120.0	C13	C12	H9	120.0
C12	C13	C14	119.5(7)	C12	C13	H10	120.2
C14	C13	H10	120.3	C13	C14	C15	119.3(7)
C13	C14	H11	120.3	C15	C14	H11	120.3
N3	C15	C14	121.5(7)	N3	C15	H12	119.2
C14	C15	H12	119.2	N4	C16	C11	117.1(5)
N4	C16	C17	120.3(6)	C11	C16	C17	122.5(6)
C16	C17	C18	118.6(7)	C16	C17	H13	120.7
C18	C17	H13	120.7	C17	C18	C19	120.6(7)
C17	C18	H14	119.7	C19	C18	H14	119.7

Table S5b. Bond angles(°) (continued)

atom	atom	atom	angle	atom	atom	atom	angle
C18	C19	C20	118.8(7)	C18	C19	H15	120.6
C20	C19	H15	120.6	N4	C20	C19	122.7(7)
N4	C20	H16	118.7	C19	C20	H16	118.7
RU	C21	O1	170(1)	RU	C22	O2	105.0(6)
RU	C22	O3	108.8(10)	O2	C22	O3	137(1)

Discussion

From the large isotope shift in the Raman spectra between *cis*-$[Ru(bpy)_2(C^{16}O)_2]^{2+}$ and *cis*-$[Ru(bpy)_2(C^{18}O)_2]^{2+}$, $\nu_{sym}(Ru\text{-}C^{16}O)$ is straightforwardly assigned at 443 cm^{-1}. A series of *cis*-$[Ru(bpy)_2(CO)X]^{n+}$ (X = CO_2, C(O)OH, $C(O)OCH_3$, CHO, and CH_2OH; n= 0, 1, 2) shows characteristic one medium intensity band in the range of 558.9 to 511.3 cm^{-1} and a weak band around 470 cm^{-1}. The medium intensity band undergoes obvious isotope shifts compared to the weak one, and all the remaining bands in those complexes are almost invariant with the substituent X in the region from 1000 to 200 cm^{-1}. The bands around 530 (m) and 470 (w) cm^{-1}, therefore, are reasonably associated with the Ru-X and Ru-CO stretching modes, respectively, and the coupling of ν(Ru-CO) and ν(Ru-X) modes would be very small due to a nearly perpendicular X-Ru-CO bond angle (Table 5-1). In addition, the deviation of the Raman spectrum of *cis*-$[Ru(bpy)_2(CO)(CH_2OH)]^{+}$ from other complexes has led to the confirmation of the two isomers. These facts suggest small or negligible contributions of other moieties to the ν(Ru-X) and ν(Ru-C) bands in the series of *cis*-$[Ru(bpy)_2(CO)X]^{n+}$. The ν (Ru-X) and ν(Ru-CO) bands tentatively assigned are also collected in Table 5-1.

The ν(CO) and ν(Ru-X) bands in *cis*-$[Ru(bpy)_2(CO)X]^{n+}$ are in the range of 2098.9 (X=CO) to 1934.3 ($X=CH_2OH$), and of 558.9 ($X= CH_2OH$) to 443.5 cm^{-1} (X= CO), respectively, and the shift of ν(Ru-CO) is quite small compared with that of ν(Ru-X). Although no clear correlation is observed between ν(Ru-X) and the mass of X (from CO to $C(O)OCH_3$) or the charge of the complexes (n = 0, 1, 2), ν(CO) bands move to lower wavenumbers as ν(Ru-X) bands shift to higher ones (Figure 5-6). The order of the shift of the ν(CO) bands to lower wavenumbers (X = CO < C(O)OH < CHO < CO_2 < CH_2OH) is correlated with the electron donating ability of the substituent X. The correlation between ν(Ru-X) and ν(CO) in Figure 5-6, therefore, is explained by an enhancement of σ- and π-bonding characters of the Ru-X and Ru-CO bond, respectively, with increasing electron donating ability of X.

Table 5-1 Relevant raman bands and bond parameters of $[Ru(bpy)_2(CO)X]^{n+}$ (X=CO_2, C(O)OH,$C(O)OCH_3$ CO, CHO, CH_2OH; n=0, 1, 2)

X (color)	ν(Ru-X) cm^{-1} labeled		ν(Ru-CO) cm^{-1} labeled		ν(CO) cm^{-1} labeled		d(Ru-CO) Å	d(Ru-X) Å	<X-Ru-CO deg
CO_2[1] (red)	520.2	509.1	474.7	472.7	1947.9	1908.9	1.81	2.06	88.5
C(O)OH (yellow)	511.3	-	473.1	-	1973.7	-	1.79	2.00	90.9
$C(O)OCH_3$ (yellow)	518.1	-	471.7	-	1951.2	-	1.80	2.04	88.5
CO[1] (colorless)	443.6	430.0	-	-	2098.7 2052.3	2049.7 2002.7	1.87 1.91	1.87 1.91	88.8
CHO[2] (yellow)	518.9	515.6	472.3	471.3	1950.0	1946.9	-	-	-
CH_2OH[2] (orange)	558.9 523.5	534.6 511.1	477.7 471.6	475.7 ~470	1934.3 1923.1	1934.9 1923.7	1.85	2.19	90.9

[1]labeled by ^{18}O. [2]labeled by D.

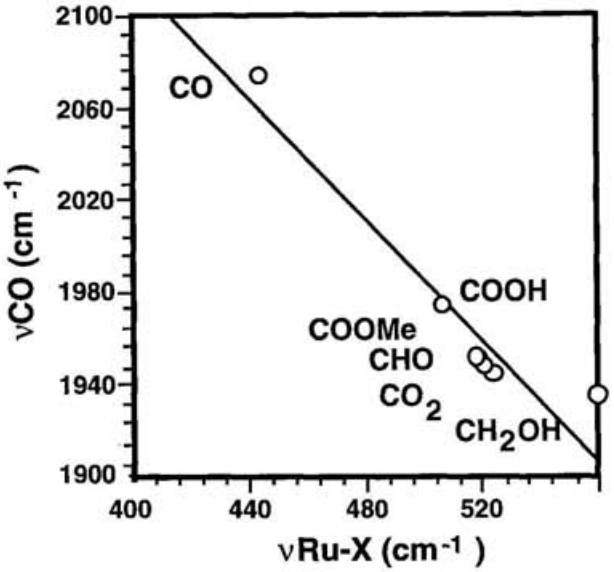

Figure 5-6 A plot of ν(C≡O) bands and ν(Ru-X) bands of *cis*-$[Ru(bpy)_2(CO)X]^{n+}$. (n=0,1,2: X=CO, C(O)OH, $C(O)OCH_3$, CO_2,CHO, CH_2OH).

The crystal structures of most of these complexes including the two isomers of *cis*-$[Ru(bpy)_2(CO)(CH_2OH)]^+$ have been determined with X-ray analysis. The Ru-CO and Ru-X bond distances are also summarized in Table 5-1. There is no clear correlation between the Ru-CO bond distance and the ν(Ru-X). On the other hand, a plot of the Ru-X bond distance (d(Ru-X)) against the ν(Ru-X) band gives a linear correlation (Figure 5-7). The gradual shortening of the Ru-X bond distances from Ru-CH_2OH to Ru-CO_2 to Ru-$C(O)OCH_3$ to Ru-CO is reasonably ascribed to the contraction of the radical radius of the carbon atom with the change of the hybridization from the sp^3, sp^2, to sp. The order of the shortening of Ru-X distances also reflects an increase in the dπ-pπ interactions between Ru

and carbon. The order of their π-electron acceptor ability is, therefore, inverse to that of the σ-electron donor ability of the substituents estimated from the shift of ν(CO) bands of *cis*-$[Ru(bpy)_2(CO)X]^{n+}$ ($CH_2OH > CO_2 > CHO > C(O)OH > CO$). The unusual relationship of ν(Ru-X) bands shifting to higher wavenumbers as the Ru-X distances are lengthened (Figure 5-7) may be explained by an assumption that the multiple bond characters between carbon and oxygen (C≡O, C=O, and C-O) in the substituent X (CO, C(O)OH, $C(O)OCH_3$, CO_2, CHO, CH_2OH) give more influence on the observed ν(Ru-X) band than the Ru-C bond characters in these *cis*-$[Ru(bpy)_2(CO)X]^{n+}$ complexes.

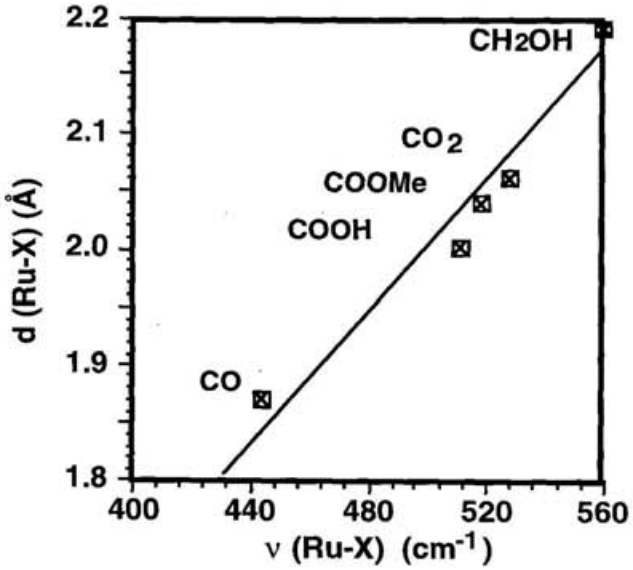

Figure 5-7 Relationship between Ru-X bond lengths (d(Ru-X)) and ν(Ru-X) bands of *cis*-$[Ru(bpy)_2(CO)X]^{n+}$.
(n=0,1,2: X=CO, C(O)OH, $C(O)OCH_3$, CO_2,CHO, CH_2OH)

Conclusion

The Ru-C bond is the fundamental interaction for the activation of CO_2. Especially, in mutielectron reduction of CO_2, the evitable change of the bond character of the Ru-C is of interest in the consequent multielectron transfer through Ru-C bond. In this view, the estimation of the Ru-X bond in the series of the complexes, $[Ru(bpy)_2(CO)(X)]^{n+}$ (X = CO_2, C(O)OH, CHO, CH_2OH; n = 0, 1, 2), was carried out using by Raman spectroscopy. Those Ru-X stretching bands around 500 cm^{-1} were assigned by D or ^{18}O labeling. The order of the shift of the ν(Ru-X) bands to higher wavenumbers (X = CO < C(O)OH < CHO < CO_2 < CH_2OH) was observed. Furthermore, the order of the shift of the ν(CO) bands to lower wavenumbers (X = CO < C(O)OH < CHO < CO_2 < CH_2OH) showed the electron donating ability of the substituent X. The drastic change of the property of Ru-X is supported by the electronic property of bpy and CO ligands.

Chapter 6

General Conclusion

Electrochemical reduction of CO_2 is one of the most feasible methodology for the utilization of CO_2, when the required electricity is provided by solar and nuclear energy in the near future. The electrochemical reduction of CO_2 using well-designed metal complexes as homogeneous catalysts greatly serves for the elucidation of the reaction mechanism including the role of ligands and metals in the reactions. Furthermore, the isolation and characterization of the reaction intermediates led us for the profound understanding of the mechanism. The purpose of this study was to elucidate the reactivity of the reaction intermediate depending on both ligands and solvents. Furthermore, the importance in a highly reactive formyl intermediate in multi-electron reduction of CO_2 was also discussed.

Intensive efforts have been paid to the electrochemical reduction of CO_2 affording CO, HC(O)OH or oxalate and electrocarboxylation of olefins and aromatic compounds. Recently, multielectron reduction of CO_2 accompanied by C-C bond formation has been achieved by carboxylation of a metal-CHO and $-CH_2OH$ species resulting from multi-electron reduction of η^1-CO_2 metal complexes. On the other hand, a carboxylation reaction by using an η^1-CO_2 metal complex to unsaturated organic molecules would also give a fascinating research area for the development of CO_2 chemistry.

Carbon dioxide has been using industrially as a carbon source although the number of reactions is not so many. The coordination chemistry of CO_2 metal complexes is particularly important for the designing of molecular catalyst directed toward industrial carboxylation and reduction of CO_2. The "Tailor-made" metal complex would enable a high selective synthesis of organic chemicals either by the reduction of CO_2 or carboxylation. Thus, the activation of CO_2 on metal complexes is still continuing the importance in the reduction and fixation of CO_2 to organic molecules.

Appendix

General Experiment

All common measurements including electrochemical, spectroscopic, and chemical identifications are summarized.

1. Electrochemical measurement

The electrochemical measurements were carried out in a glass cell equipped with a glassy carbon working electrode, a platinum auxiliary electrode, a Ag/AgCl reference electrode, and a nozzle for bubbling of N_2 or CO_2. Cyclic voltammograms were obtained by the use of a Hokuto Denko HA-301 poteitiostat, and Yokogawa Electric inc. 3077 X-Y recorder.

2. Infrared spectroscopy

IR spectra were recorded by Shimadzu FT-IR DR 8000 in resolution of 4 cm^{-1} in KBr disks and a constructing liquid cell.

3. GC, IP, and HPLC

Some chemical identifications were carried out by GC, IP (Isotachophoretic analyzer) and HPLC. CO, H_2, CH_3OH and some organic materials and CO_2 were separated with GC, using a molecular shieve 13X column for CO and H_2, a Gaschropak 54 for CH_3OH and some organic materials and CO_2, in which Ar or He as carrier gas were achieved at 40°C for gases and at 120 ~ 150 °C for organic compounds. Organic acids were separated with IP and LC according to literature methods.[35]

5. NMR measurement

^1H- and ^{13}C-NMR were measured with JEOL-EX270 in a 5mm diameter-glass tube at room temperature.

6. Other measurements

Elemental analyses and FAB mass spectra were carried out at the chemical material center for Institute for Molecular Science.

References

(1) Recent reviews:

a) Leitner, W., *Angew. Chem. Int. Ed. Engl.* **1995**, *34*, 2207-2221. b) Pandey, Krishna K., *Coord. Chem. Rev.* **1995**, *140*, 37-114. c) Jessop, P.G.; Ikariya, T.; Noyori, R., *Science* **1995**, *269*, 1065-9.

(2) Inoue, S.; Yamazaki, N., Ed., *Organic and Bio-organic hemistry of Carbon Dioxide*, Kodansh: Tokyo, 1982.

(3) Behr, A., *Angew. Chem. Int. Ed. Engl.* **1988**, *27*, 661.

(4) Photochemical reduction of CO_2:

(a) Ishitani, O.; George, M. W.; Ibusuki, T.; Johnson, F. P. A.; Koike, K.; Nozaki, K.; Pac, C.; Turner, J. J.; Westwell, J. R. *Inorg. Chem.* **1994**, 33, 4712. (b) Matsuoka, S.; Yamamoto, K.; Ogata, T.; Kusaba, M.; Nakashima, N.; Fujita, E.; Yanagida, S. *J. Am. Chem. Soc.* **1993**, 115, 601. (c) Calzaferri, G.; Haedener, K.; Li, J. *J. Photochem. Photobiol., A* **1992**, 64, 259. (d) Kimura, E.; Bu, X.; Shinomiya, M.; Wada, S.; Maruyama, S. *Inorg. Chem.* **1992**, 31, 4542, and references therein. a) Ogata, T.; Yamamoto, Y.; Wada, Y.; Murakoshi, K.; Kusaba, M.; Nakashima, N.; Ishida, A.; Takamuku, S.; Yanagida, S., *J. Phys. Chem.* **1995**, *99*, 11916-22. b) Yanagida, S.; Ogata, T., *Kagaku Kogyo* **1995**, *46*, 635-9. c) Yanagida, S.; Ogata, T., *Kagaku to Seibutsu* **1995** *33*, 341-4.

(5) Sullivan, B.P., Ed. *Electrochemical and Electrocatalytic reduction of Carbon Dioxide*, Elsevier: Amsterdam, 1993.

(6) Inoue, S.; Izumii, K.; Tanaka, K., Ed. *Carbon Dioxide*, Tokyo Kagaku Dojin; Tokyo, 1994, p4.

(7) (a) Steffey, B. D.; Miedaner, A.; Maciejewski-Farmer, M. L.; Bernatis, P. R.; Herring, A. M.; Allured, V. S.; Carperos, V.; DuBois, D. L. *Organometallics* **1994**, 13, 4844. (b) Fujita, E.; Haff, J.; Sanzenbacher, R.; Elias, H. *Inorg. Chem.* **1994**, 33, 4627. (c) Chardon-Noblat, S.; Collomb-Dunand-Sauthier, M.-N.; Deronzier, A.; Ziessel, R.; Zsoldos, D. *Inorg. Chem.* **1994**, 33, 4410. (d)

Kimura, E.; Wada, S.; Shionoya, M.; Okazaki, Y. *Inorg. Chem.* **1994**, 33, 770. (e) Collomb-Dunand-Sauthier, M. N.; Deronzier, A.; Ziessel, R. *J. Chem. Soc., Chem. Commun.* **1994**, 189. (f) Haines, R. J.; Wittrig, R. E.; Kubiak, C. P. *Inorg. Chem.* **1994**, 33, 4723. (g) Collomb-Dunand-Sauthier, M.-N.; Deronzier, A.; Ziessel, R. *Inorg. Chem.* **1994**, 33, 2961. (h) Halmann, M. M., Ed. *Chemical Fixation of Carbon Dioxide*; CRC Press: London, 1993, p67. (i) Arana, C.; Keshavarz, M.; Potts, K. T.; Abruna, H. D. *Inorg. Chim. Acta* **1994**, 225, 285. (j) Szymaszek, A.; Pruchnik, F. *Rhodium Express* **1994**, 5, 18. (k) Ogura, K.; Sugihara, H.; Yano, J.; Higasa, M. *J. Electrochem. Soc.* **1994**, 141, 419. (l) Christensen, P.; Hamnett, A.; Muir, A. V. G.; Timney, J. A.; Higgins, Simon *J. Chem. Soc., Faraday Trans.* **1994**, 90, 459. (m) Kolodsick, K. J.; Schrier, P. W.; Walton, R. A. *Polyhedron* **1994**, 13, 457. (n) Bhugun, Iqbal; Lexa, Doris; Saveant, Jean-Michel, *J. Am. Chem. Soc.* **1994**, 116, 5015 o) Nakajima, H.; Mizukawa, T.; Nagao, H.; Tanaka, K., *Chem. Lett..* **1995**, 251-2. p) Costamagna, J.; Canales, J.; Vargas, J.; Ferraudi, G., *Pure Appl. Chem.* **1995**, *67*, 1045-52. q) Ogura, K.; Nakayama, M., *Kagaku* . **1995**, *50*, 580-1. r) Christensen, P. A.; Higgins, S. J., *J. Electroanal. Chem.* **1995**, *387*, 127-32. s) Bagotzky, V. S.; *Osetrova, N. V., Russ. J. Electrochem. (Transl. of Elektrokhimiya)* **1995**, *31*, 409-25. t) Lam, K.-M.; Wong, K.-Y.; Yang, S.-M.; Che, C.-M., *J. Chem. Soc., Dalton Trans.* **1995**, 1103-7. u) Herring, A. M.; Steffey, B. D.; Miedaner, A.; Wander, S. A.; DuBois, D. L., *Inorg. Chem.* **1995**, *34*, 1100-9.

(8) Fischer, F.; Priziza, O.; *Ber. Dtsch. Chem. Ges.* **1914**, *47*, 256.

(9) (a) Freze, K. W. Jr.; Learch, S.; *J. Electrochem. Soc.* **1985**, *132*, 259. (b) Hori, Y.; Murata, A.; Takahashi, R.; Suzuki, S. *J.Chem.Soc.Chem.Comm.* **1988**, 17

(10) (a) Hori, Y.; Kikuchi, K.; Suzuki, S., *Chem. Lett.* **1985**, 1695 (b) Inoue, S.; Izumii, K.; Tanaka, K., Ed. *Carbon Dioxide*, Tokyo Kagaku Dojin; Tokyo, 1994, p44.

(11) Halmann, M., *Nature* **1978**, *275*, 115

(12) (a) Chandrasekaran, K.; Thomas, J.K.; Manassen, J., *Solar Energy* **1980**, *25*, 165. (b) Yamashita, H.; Kamada, N.; He, H.; Tanaka, K.; Ehara, S.; Anpo, M., *Chem. Lett.* **1994**, 855.

(13) (a) Beley, M.; Collin, J.-P.; Ruppert, R.; Sauvage, J.-P., *J. Chem. Soc. Comm.*, **1984** 1315. (b) Beley, M.; Collin, J.-P.; Ruppert, R.; Sauvage, J.-P., *J. Am. Chem. Soc.* **1986**, *108*, 7461.

(14) Kelly, C.A.; Mulazzani, Q.G.; Venturi, M.; Blinn, E.L.; Rodgers, A.J., *J. Am. Chem. Soc.* **1995**, *117*, 4911.

(15) Fujita, E.; Creuz, C.; Suitin, N.; Brunschwig, B. S.; *Inorg. Chem.* **1993**, *32*, 2657.

(16) (a) Ishida, H.; Katsuyuki, F.; Ohba, T.; Ohkubo, K.; Tanaka, T.; Terada, T.;Tanaka, T. *J. Chem. Soc., Dalton Trans.* **1990**, 2155. (b)Tanaka, K.; Morimoto, M.; Tanaka, T. *Chem. Lett.* **1983**, 901. (c) Pugh, J. R.; Bruce, M. R. M.; Sullivan, B. P.; Meyer, T. J., *Inorg.Chem.* **1991**, *30*, 86. (d) Sullivan, B. P.; Meyer, T. J. *J. Chem. Soc., Chem. Commun.*, **1984**, 1244.

(17) Ishida, H.; Tanaka, K.; Morimoto, M.; Tanaka, T. *Organometallics* **1986**, 5, 724.

(18) (a) Nagao, H. ; Mizukawa, T. ; Tanaka, K. *Inorg. Chem.* **1994**, 33, 3415. (b) Nagao, H.; Mizukawa,T.; Tanaka, K. *Chem. Lett.* **1993**, 955

(19) Bennett, M.; Rokicki, A., *Organometallics* **1985**, *4*, 180

(20) (a) Tanaka, H.; Tzeng, B.C.; Nagao, H.; Peng, S.M.; Tanaka, K. *Organometallics* **1992**, 11, 3171. (b) Tanaka, K.; Tzeng, B.-C.; Nagao, H.; Peng, S.-M.; Tanaka, K. *Inorg. Chem.* **1993**, 32, 1508.

(21) Nakamoto, K.; Margoshes, M.; Rundle, R. E., *J. Am. Chem. Soc.* **1956**, *77*, 6480.

(22) (a) Collomb-Dunand-Sauthier, M.-N.; Deronzier, A.; Ziessel, R., *J. Chem. Soc. Chem. Comm.* **1994**, 189. (b) Collomb-Dunand-Sauthier, M.-N.; Deronzier, A.; Ziessel, R., *J. Orgmet. Chem.* **1993**,*444*, 191.

(23) Eggelston, D. S.; Goldsby, K. A.; Hodgson, D. J.; Meyer, T. J., *Inorg.Chem.* **1985**, *24*, 4573.

(24) (a) Calabresa, J. C.; Herskovitz,T.; Kinney, J. B., *J. Am. Chem. Soc.* **1988**, *105*, 5914. (b) Gambarotta,S.; Francesco, A.; Floriani, C.; Zanazzi, P. F., *J. Am. Chem. Soc.* **1982**, *104*, 5082. (c) Sakamoto, M.; Shimizu, I.; Yamamoto, A., *Organometallics* **1994**, *13*, 407.

(25) (a) Gibson, D. H.; Mehta, J. M.; Ye, M. ; Richardson, J. F.; Mashuta, M. S., *Organometallics* **1994**, *13*, 1070 (b) Pinkes, J. R.; Steffey, B. D.; Vites, J. C.; Cutler, A. R., *Organomatallics* **1994**, *13*, 21. (c) Vites, J. C.; Steffey, B. D.; Giuseppetti-Dery, M. E.; Cutler, A. R., *Organometallics* **1991**, *10*, 2827. (d) Gibson, D. H.; Ye, M.; Richardson, J. F., *J. Am. Chem. Soc.* **1992**, *114*, 9716.

(26) Lee, G. L.; Maher, J. M.; Cooper, N. J., *J. Am. Chem. Soc.* **1987**, *109* , 2956.

(27) Lawson, H. J.; Atwood, J. T., *J. Am. Chem. Soc.* **1988**, *108*, 3680.

(28) Dickson, M. K.; Dixit, N.; Roundhill, D. M., *Inorg. Chem.* **1983**, *22*, 3130.

(29) (a) Gladysz, J. A., *Adv. Orgmet. Chem.* **1982**, *20*, 1 (b) Wong, W.-K.; Tam, W.; Strouse C. E.; Gladysz, J.A., *J. Chem. Soc. Chem. Comm.* **1979**, 530 (c) Casey, C. P.; Andrews, M. A.; Rinz, J.E., *J. Am. Chem. Soc.* **1979**, *101*, 741 (d) Casey, C.P.; Andrews, M. A.; McAlister, D.R., *J. Am. Chem. Soc.* **1979**, *101*, 3371 (e) Tam, W.; Wong, W.-K.; Gladysz, J. A., *J. Am. Chem. Soc.* **1979**, *101*, 1589

(30) (a) Tam, W.; Lin, G. Y.; Wong, W.-K.; Kiel, W. A.; Wong, V.K.; Gladysz, J. A., *J. Am. Chem. Soc.* **1982**, *104*, 141 (b) Casey, C. P.; Andrew, M. A.; McAlister, D. R.; Rinz, J. E., *J. Am. Chem. Soc.* **1980**, *102*, 1927 (c) Casey, C.P.; Newmann, S. M., *J. Am. Chem. Soc.* **1978**, *100*, 2544, and references therein.

(31) (a) Gladysz, J. A.; Tam, W., *J. Am. Chem. Soc.* **1978**, *100*, 2545 (b) Tam, W.; Marsi, M.; Gladysz, J. A., *Inorg. Chem.* **1983**, *22*, 1413

(32) (a) Caballol, R.; Sanchez M., E.; Barthelat, J., C. *J. Phys. Chem.* ,**1987**, 91, 1328. (b) Jegat, C.; Fouassier, M.; Tranquille, M.; Mascetti, J.; Tommasi, I.; Aresta, M.; Ingold, F.; Dedieu, A. *Inorg.Chem.*, **1993** ,32, 1279. (c) Jegat, C.; Fouassier,

M.; Mascetti, J. *Inorg.Chem.*, **1991**, 30, 1521. (d) Jegat, C.; Fouassier, M.; Tranquille, M.; Mascetti, J. *Inorg.Chem.*, **1991**, 30, 1529.

(33) Kelly, J.,M.; O'Connell, C.,M. *J.Chem.Soc.Dalton Trans.*, **1986**, 253.

(34) (a) Hartley, F. R.; Patai, S., Ed. *The Chemistry of the metal-carbon bond ; Volume 1* ; John Wiley & Sons; Chichester, 1982, and references therein. (b) Nakamoto, K., *Infrared and Raman Spedtra of Inorganic and Coordination Compounds*; Wiley Interscience: New York, 1986, and references therein.

(35) GL science, *General Catalog No. 25*: Tokyo, 1994.

Acknowledgment

I would like to express my sincere gratitude to Professor Koji Tanaka of Institute for Molecular Science for his guidance throughout this work and to Dr. Hirotaka Nagao of Sophia University for his invaluable discussion and help.

I wish to thank Professor Sadao Yoshikawa in Kogaku-in University for his relevant suggestion in my college life in Keio University.

I wish to thank Pofessor Kunitake in Kyushu University for his help in my graduate life and to give the chance for coming to IMS.

I wish to thank Dr. Kiyoshi Tsuge and Dr. Masato Kurihara for their great help in the preparation of this paper.

I wish to thank Mr. Hiroshi Nakajima, Dr. Yoshinori Kushi, Dr. Hide Kambayashi, Dr. Nobutoshi Komeda, Mr. Tetsunori Mizukawa in Tanaka's Laboratory and Mr. Fujita in Kyushu University for their helpful advice and encouragement.

And thanks are also extended to all the members of the Coordination Chemistry Laboratories in Institute for Molecular Science.

Finally, I would like to express my thanks to my parents for their kindness.

Kiyotsuna Toyohara